Lucas F. M. da Silva
Raul D. S. G. Campilho

Advances in Numerical Modelling of Adhesive Joints

SpringerBriefs in Applied Sciences
and Technology · Computational Mechanics

Lucas F. M. da Silva · Raul D. S. G. Campilho

Advances in Numerical Modelling of Adhesive Joints

Springer

Lucas F. M. da Silva
Departamento de Engenharia Mecânica
Faculdade de Engenharia da
Universidade do Porto
Rua Dr. Roberto Frias
4200-465 Porto
Portugal
e-mail: lucas@fe.up.pt

Raul D. S. G. Campilho
Departamento de Engenharia Mecânica
Instituto Superior de Engenharia do Porto
Rua Dr. António Bernardino
  de Almeida 431
4200-072 Porto
Portugal
e-mail: raulcampilho@gmail.com

Cover design: eStudio Calamar, Berlin/Figueres

Printed on acid-free paper

Contents

Advances in Numerical Modelling
of Adhesive Joints

Abstract The analysis of adhesively bonded joints started in 1938 with the closed-form model of Volkersen. The equilibrium equation of a single lap joint led to a simple governing differential equation with a simple algebraic equation. However, if there is yielding of the adhesive and/or the adherends and substantial peeling is present, a more complex model is necessary. The more complete is an analysis, the more complicated it becomes and the more difficult it is to obtain a simple and effective solution. The finite element (FE) method, the boundary element (BE) method and the finite difference (FD) method are the three major numerical methods for solving differential equations in science and engineering. These methods have also been applied to adhesive joints, especially the FE method. This book deals with the most recent numerical modelling of adhesive joints. Advances in damage mechanics and extended finite element method are described in the context of the FE method with examples of application. The classical continuum mechanics and fracture mechanics approach are also introduced. The BE method and the FD method are also discussed with indication of the cases they are most adapted to. There is not at the moment a numerical technique that can solve any problem and the analyst needs to be aware of the limitations involved in each case.

Keywords Adhesive joints · Finite element method · Continuum mechanics · Fracture mechanics · Damage mechanics · Extended finite element method · Boundary element method · Finite difference method

1 Introduction

Adhesive bonding is a material joining process in which an adhesive, placed between the adherend surfaces, solidifies to produce an adhesive bond. Adhesively bonded joints are an increasing alternative to mechanical joints in engineering

applications and provide many advantages over conventional mechanical fasteners. Among these advantages are lower structural weight, lower fabrication cost, and improved damage tolerance. The application of adhesively bonded joints in structural components made of fibre reinforced composites has increased significantly in recent years. The traditional fasteners usually result in the cutting of fibres and hence the introduction of stress concentrations, both of which reduce structural integrity. By contrast, bonded joints are more continuous and have potential advantages of strength-to-weight ratio, design flexibility and ease of fabrication. In fact, adhesive bonding has found applications in various areas from high technology industries such as aeronautics, aerospace, electronics, and automotive to traditional industries such as construction, sports and packaging. There are several reference books dealing with adhesive joints such as those of Adams et al. (1997), Kinloch (1987) and more recently that of da Silva et al. (2011).

Bonded joints are frequently expected to sustain static or cyclic loads for considerable periods of time without any adverse effect on the load-bearing capacity of the structure. A lack of suitable material models and failure criteria has resulted in a tendency to 'overdesign' adhesive joints. Safety considerations often require that adhesively bonded structures, particularly those employed in primary load-bearing applications, include mechanical fasteners (e.g. bolts) as an additional safety precaution. These practices result in heavier and more costly components. The development of reliable design and predictive methodologies can be expected to result in more efficient use of adhesives. In order to design structural joints in engineering structures, it is necessary to be able to analyse them. This means to determine stresses and strains under a given loading, and to predict the probable points of failure. There are two basic mathematical approaches for the analyses of adhesively bonded joints: closed-form analyses (analytical methods) and numerical methods (i.e. finite element or FE analyses). Differential equations are derived by applying a physical principle such as conservation of mass, momentum or energy. These equations govern the kinematic and mechanical behaviour of general bodies. The analysis of adhesively bonded joints started 70 years ago with the simple closed-from model of Volkersen (1938) that considers the adhesive and adherends as elastic, and that the adhesive deforms only in shear. The equilibrium equation of a single lap joint led to a simple governing differential equation with a simple algebraic equation. However, the analysis of adhesive joints can be highly complex if composite adherends are used, the adhesive deforms plastically or if there is an adhesive fillet. In those cases, several differential equations of high complexity might be obtained (non-linear and non-homogeneous). For those cases, numerical methods are more adequate. The FE method, the boundary element (BE) method and the finite difference (FD) method are the three major numerical methods for solving partial differential equations in science and engineering. The FE is by far the most common technique used in the context of adhesively bonded joints. Adams et al. are among the first to have used the FE method for analyzing adhesive joint stresses (Adams and Peppiatt 1974; Crocombe and Adams 1981; Adams and Harris 1984; Adams et al. 1986; Adams and Davies 2002). One of the first reasons for the use of the FE method was to

assess the influence of the spew fillet. The joint rotation and the adherends and adhesive plasticity are other aspects that are easier to treat with a FE analysis. The study of Adams and Harris (1984) is one of the first FE analyses taking into account these three aspects. The use of the BE method is still very limited in the analysis of adhesive joints. The FD method is especially used for solving complex governing differential equations in closed-form models. The three numerical techniques are treated in three separate sections. The book was prepared for engineers and scientists that have already some background in adhesive joints and numerical modelling. A brief description of each numerical method is given and the most recent advances made concerning the analysis of adhesive joints are discussed. The FE is obviously the one treated in more detail due to its importance, and several approaches to failure analysis are accounted for: continuum mechanics, fracture mechanics and the more recent damage mechanics and extended finite element method (XFEM). Examples of application of damage mechanics and XFEM are given to illustrate the most recent advances in numerical modelling of adhesively bonded joints.

2 Finite Element Method

The FE method is a numerical analysis procedure that provides an approximate solution to problems in various fields of engineering. Ashcroft (2011) gives a description of the method applied to adhesive joints. The FE method is based on the idea of building a complicated object with simple blocks or dividing a complicated object into small and manageable pieces. The first efforts to use piecewise continuous functions defined over triangular domains appeared in applied mathematics literature with the work of Courant (1943). Advances in the aerospace industry and the development of computers in the 1950s and 1960s saw further development and computerization of these methods (Turner et al. 1956). This was the direct pre-cursor of nearly all current commercial FE analysis methods. The term FE was introduced by Clough (1960). Zienkiewicz and Cheung (1967) describe the applicability of the method to general field applications. In the 1980s, generalised software packages designed to run on powerful computers were developed and improved techniques for the analysis of non-linear problems were established. The FE method is now used in practically all fields of engineering analysis such as structural, heat transfer, material transport (such as diffusion), fluid mechanics and electro-magnetics. Recent FE programs offer the possibility to multi-physics problems (coupling of different analysis classes, such as thermo-structural or hygro-thermo-structural problems).

To predict the joint strength, one must have the stress distribution and a suitable failure criterion. The stress distribution can be obtained by a FE analysis or a closed-form model. For complex geometries and elaborate material models, the FE method is preferable. One of the simplest failure models is that based on a stress or strain limit state, i.e. based on a continuum mechanics approach. Fracture

mechanics principles can also be used within a FE analysis. This can be based on either the stress intensity factor or energy approaches. An extension to this approach is damage modelling with cohesive zone elements or continuum elements, which also allows to account for damage of a material ahead of a crack. This technique is a combination of a continuum mechanics and fracture mechanics approach. Another method for modelling cracks in materials is the XFEM, which uses enriched shape functions to represent a discontinuous displacement field. The main advantage of XFEM is that the crack may initiate at any point in the material and propagate based on loading conditions. No remeshing is required as the crack can grow within an element, and it does not need to follow element boundaries. All these approaches (continuum mechanics, fracture mechanics, damage modelling and XFEM) are described in this section with examples of application, especially for the most advanced methods of damage modelling and XFEM. However, a brief description of the FE method is first given with simple guidelines for modelling adhesive joints.

2.1 Simple Description

Basically, this method involves the discretization of a structure in various sub domains, known as elements, joined at their nodes. Each node has a limited number of degrees of freedom (dof). Hence, the continuum is now represented by a finite number of dof, determined by the number of elements, the number of nodes per element and the number of dof per node. In an element, the field quantity or behaviour of the model (for example displacements, δ, in stress analyses) is interpolated from the values of the field quantity at the nodes. Connecting the elements by the nodes, the field quantity can be interpolated over the whole structure. The most common formulation method in FE analysis is the variational method. This method involves the solution of a governing partial differential equation (for example the equilibrium equations in elasticity problems), by determining the conditions that make a functional stationary, i.e., maximum or minimum. In elasticity problems, the functional used is the total potential energy of the structure. The optimal values of the field quantity are those that minimise the total energy of the system, satisfying internal compatibility and essential boundary conditions. The process of minimisation creates a system of algebraic equations for the field quantity at the nodes. The matrix symbolism used for that system of equations is

$$\mathbf{K\delta = F}, \tag{1}$$

where $\mathbf{\delta}$ is a vector with the values of the field quantity at the nodes (values of δ for example), $\mathbf{F}$ is a vector of known loads (for example forces in elasticity problems) and $\mathbf{K}$ is a matrix of known constants that represents the property of the elements. In elasticity problems, $\mathbf{K}$ is the stiffness matrix. In stress analyses, to simulate a

given loading on the model, boundary conditions and loads or values of δ are applied and the output values of δ are obtained from Eq. 1. However, the stiffness matrix **K** in Eq. 1 contains integrals that generally cannot be solved algebraically. Instead, a numerical integration scheme (such as Gauss quadrature) has to be used to determine the stiffness matrix. In general, the integrals can be computed by sampling from a number of points (Gauss points) and multiplying by an appropriate value or weighting factor. As the number of Gauss points increases, more accurate integration results are typically obtained. However, using too many Gauss points would require more computational resources and the results may not improve. The numerical solution of Eq. 1 gives the δ values, which in turn allow the calculation of strains and stresses along the whole structure. For more information on the FE method, the reference books of Cook (1995) for a first introduction and that of Zienkiewics and Taylor (2001) for a more detailed description are recommended.

The FE method allows studying any type of geometry, i.e., it can take into account variations in the adherends shape and the adhesive fillet, which is very difficult or impossible with the closed-form analyses. Another important advantage of the method is that it enables to calculate all the stress and strain components of a structure for more realistic strength predictions. However, in general parametric FE studies (e.g. study of a geometrical parameter such as the adhesive thickness, t_A) are more difficult than with closed-form models because they generally involve creating a new model for each new configuration.

The commercial FE programs permit to easily include geometric non-linearities such as those occurring in the single lap joint. There are also a variety of material models from linear elastic elastic to visco-plastic. To determine the initial yielding and subsequent plastic deformation in a bonded joint, a yielding model needs to be included for the adhesive and possibly for the adherend. For metallic substrates, the von Mises yield criterion may be applied. For composite adherends, yielding seldom occurs and failure criteria are used instead. In the case of adhesives and polymeric adherends, a yielding model that takes into account the hydrostatic pressure is generally required such as that proposed by Raghava et al. (1973). Failure is discussed in more detail in the following sections.

As seen above, the domain or structure is divided in elements leading to a mesh. Stress concentrations need a fine mesh to capture the stress gradients. In the particular case of stress singularities, mesh refinements may lead to convergence problems since the stress tends to infinity as finer elements are used. Elasto-plastic analyses or fracture mechanics concepts are advised in those cases, as discussed in the coming sections. A pre-processor is used to generate the geometry and the mesh. It is advised to apply the boundary conditions and the loads so that the mesh can be easily modified without altering the boundary conditions, to reduce the meshing effort. The geometry should be modelled with precision using at the same time any symmetry that reduces the size of the model and the number of calculations. The boundary conditions should simulate the reality as closely as possible. The most common boundary conditions for single lap joints are those represented in Fig. 1, which simulate gripping and loading in a testing machine. When double
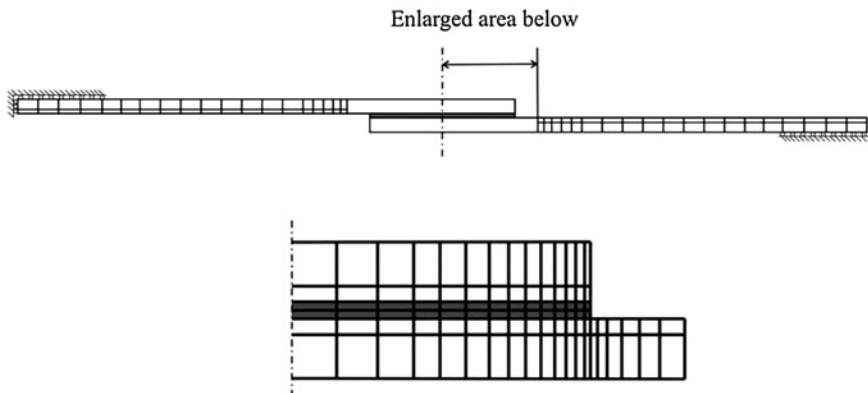
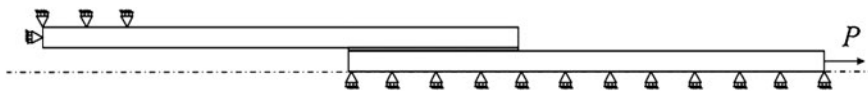Fig. 1 Finite element mesh and boundary conditions for a single lap joint

Fig. 2 Boundary conditions for a double lap joint

lap joints are analysed, half of the joint is sufficient for analysis due to symmetry, as shown in Fig. 2.

Various factors should be taken into account when preparing a mesh for a bonded joint, such as the mesh density and the type of element. The choice of elements (for example simple beams and continuum solid elements) has an important effect on the final results. Each type of element has advantages and disadvantages depending on the application. Continuum solid elements are most suited for linear analyses and also for complex non-linear problems involving plasticity and large deformations. An adhesively bonded joint can be modelled in two dimensions (2D) (Figs. 1 and 2) or three dimensions (3D). The 2D continuous elements include plane stress, plane strain and generalised plane strain. The plane stress elements are used when one of the dimensions of the body is very small in relation to the others. This situation occurs in plates where the stresses in the thickness direction are considered nil. The plane strain elements are used when the width is much larger than the thickness. This is the case of a single lap joint where the strains in the width direction are considered nil. In the case of the generalised plane strain elements, two parallel rigid planes exist that can only move away or closer to each other, which permits to account for the transversal strains. Continuous 3D elements suppress the approximation introduced by the plane stress or plane strain conditions. Despite a 3D analysis giving more accurate results than 2D analyses, the time and effort of a 3D analysis are often not justified.
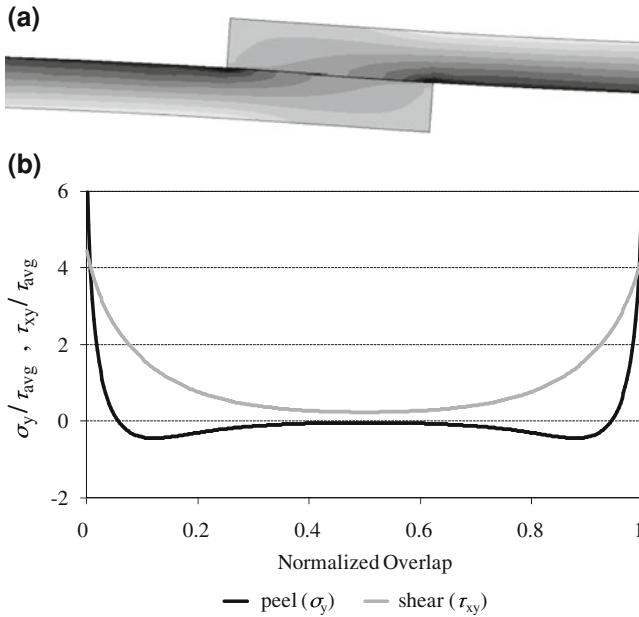
Fig. 3 Deformed shape of a single lap joint at the overlap (**a**) and normalized peel and shear stress distributions in the adhesive bond along the overlap (**b**) (Campilho 2009)

In adhesively bonded joints, a 2D analysis in plane strain conditions is often preferred. Despite 3D effects such as the lateral deformation (Adams and Peppiatt 1973) and the anticlastic bending (Adams and Davies 1996; Gonçalves et al. 2002), various studies have shown that 2D analyses give accurate enough results (Adams et al. 1997; Adams and Davies 2002). The elements are often isoparametric quadratic elements of eight nodes. Isoparametric triangular elements of six nodes are also used, especially in areas that need mesh refinement. Generally, a first coarse mesh is modelled and the mesh is refined progressively (increasing the number of elements by decreasing their size). A reduction of the element size increases the stress and strain levels until a point where there is practically no change, in which a converged mesh is attained. In the case the model contains a singularity, which is common in adhesive joints, there is no convergence and the values tend to infinity as the mesh is refined. After the process step where the calculations are made by the computer, the results are analysed in the postprocess step. The first thing to do is to check if the imposed loading and boundary conditions create a logical deformed shape. The continuity of the stress contours must also be checked to minimise any discontinuity.

Figure 3 illustrates the 2D deformed shape of a single lap joint (a) and the peel and shear stress distributions in the adhesive bond along the overlap, normalized by the average shear stress in the bond (b) for a joint with carbon-epoxy
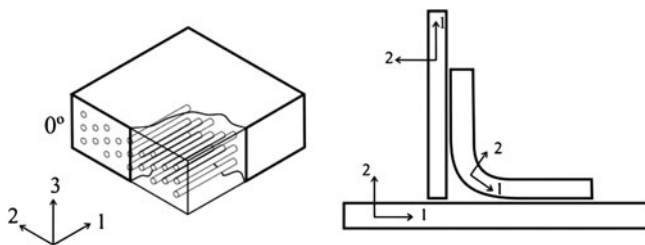
Fig. 4 Local coordinates in the case of laminated composites

adherends and a ductile adhesive bond (Campilho 2009). In the areas where the stress is relatively uniform, a coarser mesh can be used to reduce the computation time. An example of a mesh is given in Fig. 1. The mesh is usually refined at the ends of the overlap where stress concentrations exist due to the sharp geometry change. The adherends mesh is also refined along the overlap. The commercial programs have pre-processors which facilitate the mesh generation of complicated shapes.

The modelling of laminated composite materials requires the definition of local coordinates to guarantee that the orientation of the layers is coincident with the model orientation (Fig. 4). For curved sections, the orientation of the system must be coincident with the laminate orientation.

The numerical problem can be solved using implicit or explicit mathematical codes. The implicit code is used for solving a great variety of linear and non-linear problems and it is based on the resolution of Eq. 1. The solution is considered acceptable when the difference between the two members of the equation is lower than a value (residue) that is determined by the user. Therefore, the process requires an iterative procedure for a given solution in each load increment. The explicit code is adequate for short transient dynamic events such as impact loadings, and is also very efficient for highly non-linear problems. The explicit method is particularly useful for modelling ductile adhesives that exhibit high failure deformations. It needs very small increments in static analyses so that the kinetic energy is always negligible. The term convergence is used to indicate that the process used to solve the equations system converges, and the solution at the end of an increment is a solution that by definition converged. If a solution has not been found for a given increment, the method reduces the size of the increment and solves again the equation. If a too small increment is reached without convergence, it is considered that the analysis method and the model have not converged. Convergence problems are generally associated to materials that have an unstable behaviour and occur frequently in non-linear problems. The non-convergence is also less common in loadings applied by a specified value of δ that by a force.

2.2 *Continuum Mechanics Approach*

In the continuum mechanics approach, the maximum values of stress, strain or strain energy, predicted by the FE analyses, are usually used in the failure criterion and are compared with the corresponding material allowable values. Initially, the maximum principal stresses were proposed for very brittle materials whose failure mode is at right angles to the direction of maximum principal stress. This criterion ignores all the other principal stresses, even though they are not nil. Establishing the failure modes in lap joints bonded with brittle adhesives, Adams et al. (1997) have extensively used this criterion to predict joint strength with success. However, because of the singularity of stresses at re-entrant corners of joints, the stresses depend on the mesh size used and how close to the singular points the stresses are taken. Values of stresses calculated at Gauss points near the singularity or extrapolation of Gauss point values to the singularity were, in fact, used. Therefore, care must be taken when using this criterion. Although the criterion is sensitive to the mesh size used, the physical insight into the failure process is very clear, as the maximum principal stress is the most responsible for the failure of joints bonded with brittle adhesives. However, it should be noted that the adherend corners are usually not sharp in practice. There is, in general, a small amount of rounding at the adherend corner due to the production process. This may affect the stress distributions in the region of the adherend corner and, therefore, the joint strength, because stresses in this area are very sensitive to the change in the geometry. One consequence of the adherend rounding is the non-existence of the singularity, which facilitates the application of a stress or strain limit criterion. Adams and Harris (1987) theoretically and experimentally demonstrated that the strength of single lap joints with rounded adherends with a toughened adhesive increased substantially compared with joints with sharp adherend corners. More recently, Zhao et al. (2011a, b) have also studied the effect of adherend rounding (Fig. 5). An example of stress distribution is given in Fig. 6 as a function of the degree of rounding, showing that the stress singularity vanishes with a small degree of rounding.

Von Mises proposed a yield criterion, which states that a material yields under multi-axial stresses when its distortion energy reaches a critical value, that is

$$\sigma_{VM}^2 = (\sigma_1 - \sigma_2)^2 + (\sigma_2 - \sigma_3)^2 + (\sigma_3 - \sigma_1)^2 = \text{constant}, \tag{2}$$

where σ_i $(i = 1, 2, 3)$ are the principal stresses. Such a criterion has been used by Ikegami et al. (1990) to study the strength of scarf joints between glass fibre composites and metals. It should be noted that this criterion is more applicable to material yielding than strength.

Shear stresses have been extensively used to predict lap joint strength, especially in closed-form analyses, considering a limiting maximum shear stress equal to the bulk adhesive shear strength. These are also described here for a complete description of the continuum mechanics approach. Greenwood (1969) used the
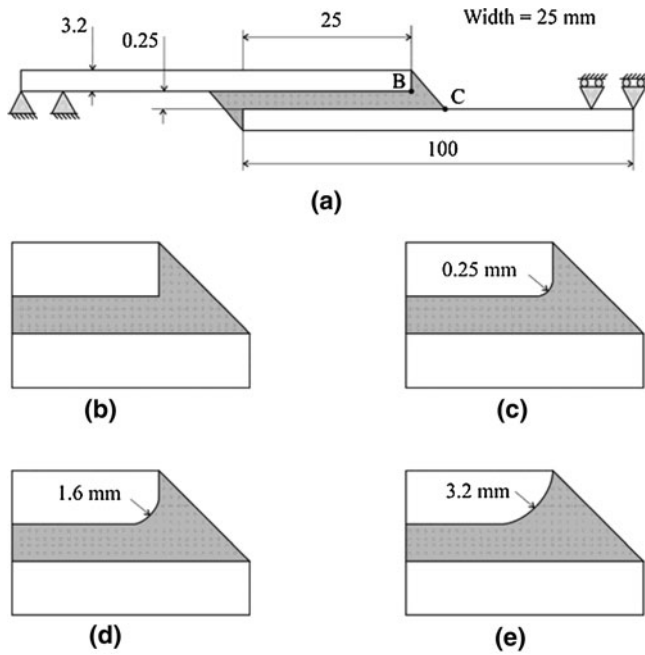
Fig. 5 Aluminium/epoxy single lap joints with different degrees of rounding (Zhao et al. 2011a)
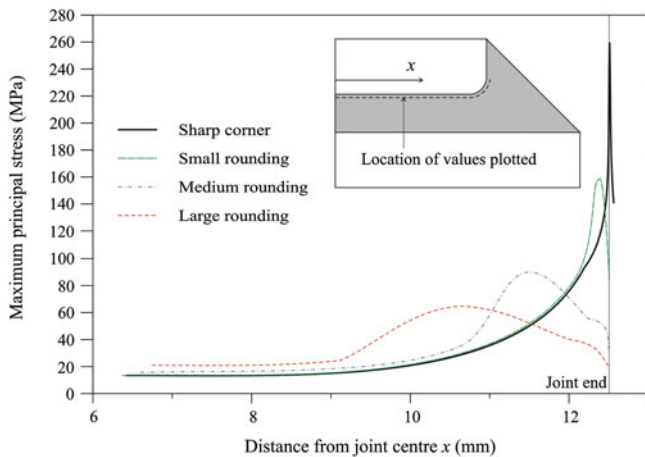
Fig. 6 Maximum principal stresses in the adhesive with a 20 kN applied load, close to the unloaded adherend (Zhao et al. 2011a)

maximum shear stress calculated by Goland and Reissner's analysis (Goland and Reissner 1944) to predict joint strength. The Engineering Sciences Data Unit (ESDU 1979) implemented this criterion into a commercial package. More recently, John et al. (1991) used shear stresses together with a critical distance to

predict the strength of double lap joints. Lee and Lee (1992) also used the maximum shear stress in tubular joints. da Silva et al. (2009a, b) showed for single lap joints that this criterion is only valid for brittle adhesives and short overlaps. This approach ignores the normal stresses existing in lap joints and therefore it overestimates the joint strength.

When ductile adhesives are used, criteria based on stresses are not appropriate because joints can still endure large loads after adhesive yielding. For ductile adhesives, Adams and Harris (1984) used the maximum principal strain as failure criterion for predicting the joint strength. This criterion can also predict the failure mode. However, it is equally sensitive to the mesh size, as previously discussed for the maximum principal stress approach.

Hart-Smith (1973) proposed that the maximum shear strain might be used as a failure criterion when plastic deformation was apparent. da Silva et al. (2009c) implemented this criterion and others into a commercial package. Other analyses go beyond that of Hart-Smith, which allows both shear and peel contributions to plasticity such as that by Adams and Mallick (1992). ESDU (1979) also implemented the maximum shear strain criterion in their commercial program. da Silva et al. (2009a, b) have shown, for single lap joints, that the maximum shear strain criterion is very accurate for ductile adhesives.

Clarke and McGregor (1993) predicted failure when the maximum principal stress exceeded the maximum uniaxial stress for a bulk adhesive over a certain length normal to the direction of the maximum principal stresses. No justification was given for the choice of zone size. It was noted that the sensitivity to changes in local joint geometry, such as radius of the adherend corner, was reasonably low for this criterion. Crocombe (1989) studied the failure of cracked and uncracked specimens under various modes of loading and used a critical peel stress at a distance from the singularity with some success. An alternative method was also proposed to use an effective stress, matched to the uniaxial bulk strength, at a distance. However, it was found for the latter criterion that the critical distance at which it should be applied varied with different modes of loading because of the change in the plastic zone size. No general criterion for a given adhesive was presented. Kinloch and Williams (1980) and Kinloch and Young (1983) also considered some cracked specimens, and applied failure criteria at critical distances with some success, but the work was not extended to consider un-cracked continua. There is no real physical justification for these criteria applied at a distance, and many of them are dependent on parameters such as t_A, which means that no general criterion of failure is available within these methods.

The strain energy is the area under the stress–strain (σ–ε) curve. Therefore, both stress and strain criteria can be related to strain energy. However, it should be noted that criteria based on strain energy take account of all the stress and strain components. As a result, they are more suitable as a failure criterion than either stresses or strains alone. Plastic energy density has also been used as a failure criterion (Adams and Harris 1987), being similar to the total strain energy criterion but it only takes the plastic part of the deformation into account. Zhao et al. (2011b) applied a criterion whereby if the average plastic energy density over a

certain distance within the single lap joint reached a critical value, then the joint was deemed to have failed. The specific energy is not so sensitive to the size of the integration zone, as it is 'averaged' over an area (2D analyses) or volume (3D analyses). It is common knowledge that the accuracy of the FE approach is more reliable when it is interpreted as an average, rather than in a pointwise sense. The integration region is usually chosen as a whole element for numerical convenience. In Zhao et al. (2011b), the value of t_A was used for integration and the predictions compared very well with the experimental results for a ductile adhesive.

In the analysis of lap joints, Crocombe (1989) found that, for largely ductile adhesives, the whole overlap yielded before failure. A new failure criterion was then proposed based on the yielding of adhesive in the whole overlap. Once a path of yielding was found in the overlap with a given load, the joint was thought to be failed. Such a criterion is useful for very ductile adhesives in which the adhesive bond cannot support any larger load once it yields globally. However, it should be noted that the adhesives need to be extremely ductile (more than 20% of failure strain in shear) for the whole adhesive bond to yield before final failure (Adams et al. 1997; da Silva et al. 2008; da Silva et al. 2009d). Also, this criterion is only applicable to lap joints. Unfortunately, for certain geometric conditions joints tend to fail before the whole adhesive bond yields.

It should be realized that all the above criteria are applicable to continuous structures only. They run into difficulty when defects occur or more than one material is present, since stresses or strains are not well defined at the singular points. As a result, new criteria or modified versions of the above criteria need to be developed.

2.3 Fracture Mechanics Approach

Continuum mechanics assumes that the structure and its material are continuous. Defects or two materials with re-entrant corners obviously are not consistent with such an assumption. Consequently, continuum mechanics gives no solution at these singular points resulting in stress or strain singularities. Cracks are the most common defects in structures, for which fracture mechanics has been developed. In fracture mechanics, it is well accepted that stresses calculated by using continuum mechanics are singular (infinite) at the crack tip. The reason why singularities exist is explained as follows. Figure 7 shows stresses around the tip of a sharp crack in an infinitely large plate given by continuum mechanics. Physically, the y-stresses, σ_y, at the crack tip A must be finite (instead of infinite as theory predicts). However, σ_y stresses into the crack and away from the tip of the crack (shown as B in Fig. 7) are nil because of the free surfaces. Consequently, a discontinuity of σ_y is apparent at point A unless σ_y is zero there. Such a stress distribution cannot be accommodated in continuum mechanics, which requires all the stresses to be continuous. As a result, stresses at the crack tip are not defined (being infinite).

Fig. 7 Stress discontinuity around (**a**) a crack tip and (**b**) a re-entrant corner
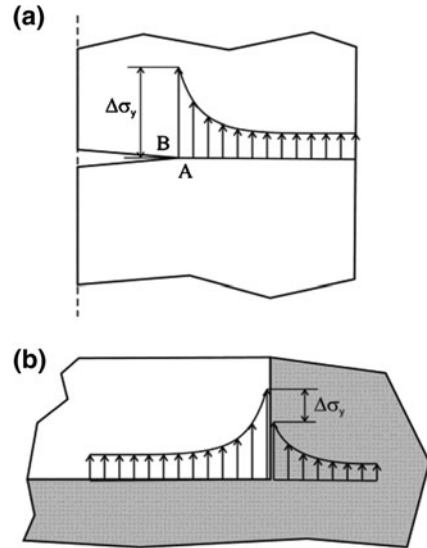
With current theories on mechanics, such a singularity always exists when the crack angle is <180°. This result was found by Williams (1959) for stress singularities in a wedged notch. This argument is also applicable to the stress singularity in two materials bonded together with a re-entrant corner. Actually, the stress discontinuity still exists, although the free surfaces do not exist.

For ductile materials, a large amount of material yielding occurs and the crack may propagate stably before final failure. Thus, linear elastic fracture mechanics (LEFM) does not work anymore for such materials. The HRR (Hutchinson Rice Rosengreen) solution developed by Hutchinson (1968) and by Rice and Rosengren (1968) has, however, been extensively used in ductile fracture. Another important parameter governing failure is the so-called crack tip opening displacement (Dugdale 1960). However, a strain singularity still exists for ductile materials, even though the stress singularity has disappeared.

Fracture mechanics has been successfully applied to many engineering problems in recent years. The damage tolerance design concept, originally adopted in the aircraft industry, was based mainly on the well-established concept of LEFM, and it has gradually gained ground in other engineering fields. Many studies dealing with adhesive joints use the strain energy release rate, G, and respective critical value or fracture toughness, G^c (Fernlund and Spelt 1991; O'Brien et al. 2003; Cheuk et al. 2005; Shahin and Taheri 2008) instead of stress intensity factors because these are not easily determinable when the crack grows at or near to an interface. However, the fracture of adhesive joints inherently takes place under mixed mode because of the varying properties between different materials and the complex stress system. Failure criteria for mixed mode fracture can be developed in a way analogous to the classical failure criteria, although the fracture surface (or envelope) concept must be introduced. Various mathematical surface functions
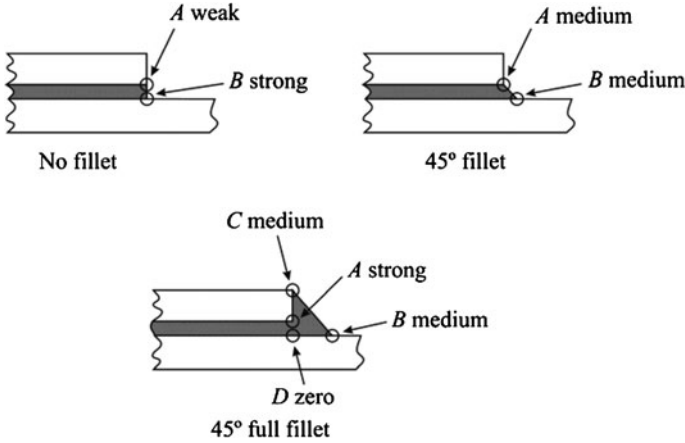
Fig. 8 Singularities in adhesive lap joints with different spew fillet geometry

have been proposed to fit the experimental results, such as the 3D criterion (Dillard et al. 2009):

$$\left(\frac{G_n}{G_n^c}\right)^{\alpha}+\left(\frac{G_s}{G_s^c}\right)^{\beta}+\left(\frac{G_t}{G_t^c}\right)^{\gamma}=1, \tag{3}$$

where G_n, G_s and G_t are the values of G under pure tension, shear and tearing modes, respectively, and G_n^c, G_s^c and G_t^c the respective values of G^c. The linear energetic criterion ($\alpha = \beta = \gamma = 1$) and the quadratic one ($\alpha = \beta = \gamma = 2$) are the most used. The law parameters may be chosen to best fit the experimental data, or they may be prescribed based on some assumed relationship. Alternate forms for fracture envelope criteria have also been proposed (Kinloch 1987; Hashemi et al. 1989; Charalambides et al. 1992). In all cases, the failure surface can be made to match experimental results very closely, by including additional constants. Constructing such a surface will require an increasing number of independent material parameters, which must all be best fitted by experiments. Apart from the amount of experimental work involved, this purely mathematical surface fitting method does not help much to understand the physical failure mechanism of mixed mode fractures. Although fracture mechanics is mainly used for dealing with sharp cracks, angular wedged notches are also of practical importance, as shown in Fig. 8 for the case of adhesive joints.

The use of a generalized stress intensity factor, analogous to the stress intensity factor in classical fracture mechanics, to predict fracture initiation for bonded joints at the interface corners has also been investigated (Xu et al. 1999). Groth (1988) assumed that initiation of fracture occurs when the generalized stress intensity factor reaches its critical value, initially tuned experimentally. Gleich et al. (2001) carried out a similar study by calculating the singularity strength and intensity for a range of t_A values. These approaches work well for the joints that

were used to determine the critical stress intensity factor but their application is questionable for extrapolation to other types of geometries. Fracture mechanics can thus be used to predict joint strength or residual strength if there is a crack tip or a known and calibrated singularity (Clarke and McGregor 1993).

When materials deform plastically, the LEFM concepts have to be extended into elasto-plastic fracture mechanics. The J-integral proposed by Rice and Rosengren (1968) is suited to deal with these problems. The analytical definition of the J-integral is given by Rice as an energy line integral

$$J = \int_C w \, \mathrm{d}x_2 - T_j \frac{\partial u_j}{\partial x_1} \, \mathrm{d}S, \tag{4}$$

where C denotes a curve surrounding the crack tip, the variable S indicates the arclength, w is the energy density, T_j is the traction vector, u_j is the displacement vector and $x_1 - x_2$ is the coordinate system. The integral path can be arbitrary provided that it travels from one of the crack surfaces to another counter-clockwise and it encloses the crack tip. The J-integral approach has been used by a variety of researchers to predict the joint strength of cracked adhesive joints with good results (Fernlund et al. 1994; Choupani 2008; Sørensen and Jacobsen 2003; Banea et al. 2010). Nonetheless, for ductile adhesives the value of G^c is not independent of the joint geometry (Kinloch and Shaw 1981; Hunston et al. 1984). This is mainly because the adherends restrict the development of the yield zone in the adhesive bond, making G^c a function of joint geometry. Chen et al. (2011a) have shown that the vectorial J-integral is interface length dependent for a bonded bi-material system, as shown in Fig. 9.

Paths 8, 9 and 10 correspond to the same interface length (10.8 mm). The two components of the vector J were considered in the analysis. The classical introduction of the J-integral by Rice focused the attention on the J_1 component which is responsible for controlling the forward propagation of the crack. However, in the context of multi axial loading and crack turning it is more appropriate to consider both components of the vector J-integral, since more exhaustive information is provided for the application of various crack path determination criteria.

The major advantage of the path-independence of the J-integral in homogeneous materials disappears due to the interface length dependence and practice of using far field stresses and strains to calculate J is no longer possible. Under these conditions, the J-integral must be extrapolated against interface length to a point so that a great deal of mesh refinement is required. In real joints, the bondline is usually very thin and the two interfaces with the adherends will interact with each other. The interference of different singular sources so closely sited (thin bondlines) makes numerical extrapolation very difficult. If an integral path includes both interfaces, some singular effects will offset each other and the accuracy is then doubtful. Therefore, the parameter J may not be used as a strength criterion for joints without a pre-crack. Moreover, failure modes are extremely complicated in the area of stress or strain concentrations. Therefore, if fracture mechanics is to be used for ductile adhesives, the process will be prohibitive: first it needs to be

Fig. 9 Elastic *J*-integral 1 and 2 against path length for a two-material bond under tension. **a** Bi-material model; **b** integral J_2 as a function of the path length; **c** Integral J_1 as a function of the path length (Chen et al. 2011a)
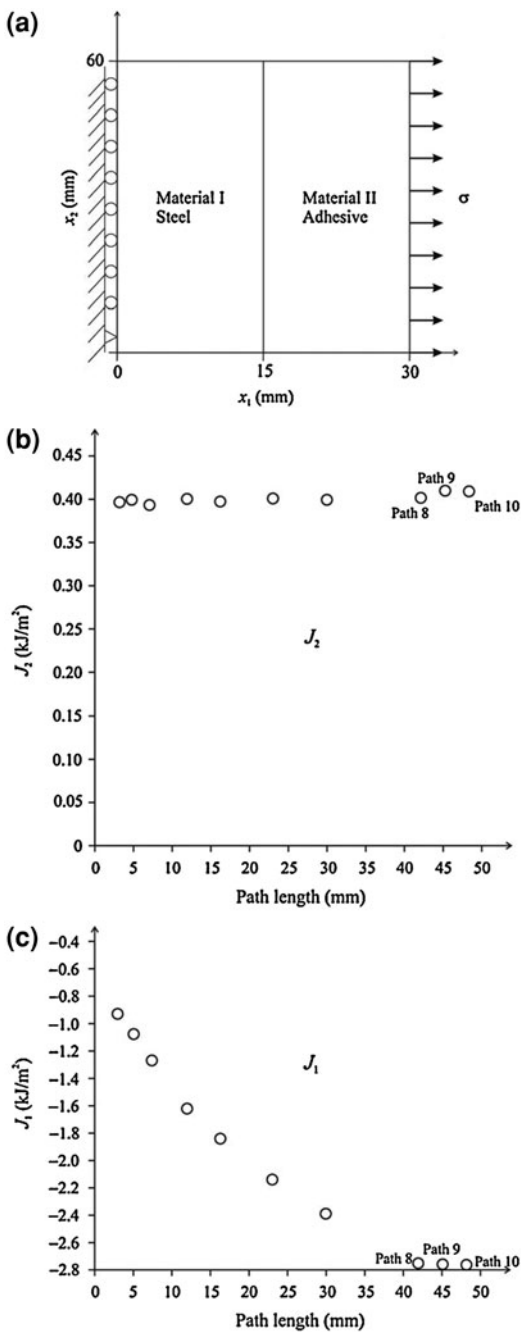
determined when and where a crack with a reasonable size initiates. Then, this crack has to propagate stably and be arrested. Next, a new crack at another place may initiate and propagate into an unstable one, causing catastrophic failure. This process is very difficult to simulate because the crack sizes and positions are very difficult to determine. Furthermore, such a process will involve a large amount of computing time with very fine mesh, and the mesh shifting and releasing involved in crack propagation will be very difficult to perform.

2.4 Damage Mechanics

Advanced modelling techniques are required that comprise accurate failure predictions, surpassing the aforementioned limitations associated to the continuum and fracture mechanics approaches, to effectively model damage evolution within a material or structure with bonded components (Liljedahl et al. 2006). Structural damage during loading can be found in the form of micro-cracks over a finite volume or interfacial region between bonded components, such that load transfer is locally reduced, globally resulting on a drop of applied load for a given value of δ applied to the structure. Figure 10 reports on a typical uni-axial σ–ε diagram up to failure for a ductile material or structure. A FE model built solely with solid continuum elements comprising the elastic and plastic constitutive behaviours of each one of the materials wrongly gives as modelling output the abcd$'$ curve because of generalised plasticization without damage evolution, while a damage and failure based model can actually provide the real abcd curve, by allowing damage to grow through the simulation of material stiffness degradation between point c (damage onset) and point d (complete failure).

Damage mechanics permits the simulation of step-by-step damage and fracture at a pre-defined crack path or arbitrarily within a finite region up to complete structural failure (Duan et al. 2004). However, this is still an innovative field under intense development, regarding more accurate modelling techniques, reliable and simple parameter determination methods, increase of robustness and elimination of convergence issues (Liljedahl et al. 2006), and it is also under heavy implementation in commercial FE software packages such as Abaqus® (Campilho et al. 2011a). The available techniques for damage modelling can be separated into local or continuum approaches. In the local approach, damage is confined to a zero volume line or a surface, allowing the simulation of an interfacial failure between materials, e.g. between the adhesive bond and the adherend (Yang et al. 2001), the interlaminar failure of stacked composites (Turon et al. 2007a) or the interface between solid phases of materials (Chandra et al., 2002). By the continuum approach, the damage is modelled over a finite region, within solid finite elements of structures to simulate a bulk failure (Song et al. 2006) or along an adhesive bond to model a cohesive fracture of the adhesive bond (Kafkalidis and Thouless 2002). The use of cohesive zone models (CZM's) coupled to conventional FE analyses is the most widespread method of predicting static or fatigue damage uptake in

Fig. 10 Typical uni-axial $\sigma-\varepsilon$ response of a ductile material or structure
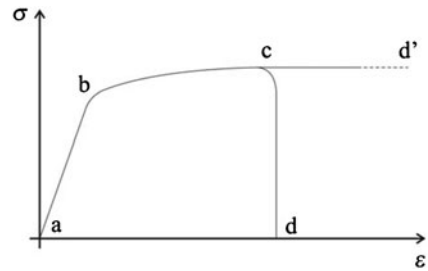
structures (Tvergaard and Hutchinson 1992, Tvergaard and Hutchinson 1993, Wei and Hutchinson 1997, Wei and Hutchinson 1999, Yang et al. 1999, Yang et al. 2000, Cavalli and Thouless 2001, Yang and Thouless 2001, Campilho et al. 2005, Campilho et al. 2007). CZM's are based on the concepts of stress and fracture mechanics, and can be fitted into the local or continuum approach, since they can either be considered to model the interfacial fracture behaviour of equally or differently oriented plies in stacked composites or the adhesive/adherend interface to simulate adhesive failures (local approach), or on the other hand to simulate a thin bulk layer of a constant thickness material (continuum approach). Under the continuum assumption, thin adhesive bonds to join structural members are a large field of application of CZM's (Campilho et al. 2008a), but the single row of cohesive elements used to model the bulk strip of adhesive makes it impossible to differentiate thickness-wise effects or concentrations of stresses towards the interface (Magalhães et al. 2005), providing an equivalent behaviour of the bond. Differences exist regarding the definition of the CZM laws, namely in which concerns their initial stiffness, between the local approach modelling (the initial stiffness can use the penalty function method) and continuum CZM modelling (the initial stiffness must accurately reproduce the deformation behaviour of the thin material strip). These issues will be addressed in detail in Sect. 2.4.1 and "Triangular Cohesive Zone Model". As CZM modelling is nowadays largely preponderant for researchers and designers, both in terms of modelling developments and validation/application studies of these methodologies and, additionally, it is very much alike between the local or continuum formulations, the damage mechanics section (Sect. 2.4) is separated into CZM modelling and alternative approaches to CZM modelling, the former with much more detail due to the aforementioned reasons, and the latter comprising alternative continuum damage modelling (ACDM) techniques to CZM formulations, equally tested in recent years under the scope of bonded structures.

2.4.1 Cohesive Zone Modelling

Although the computer implementation of LEFM techniques endured great success some decades ago, they are restricted to small-scale yielding beyond the crack tip. Since for modern toughened adhesives the plastic zones developing along the adhesive bond can be larger than the adherends thickness, t_P (Ji et al. 2010),
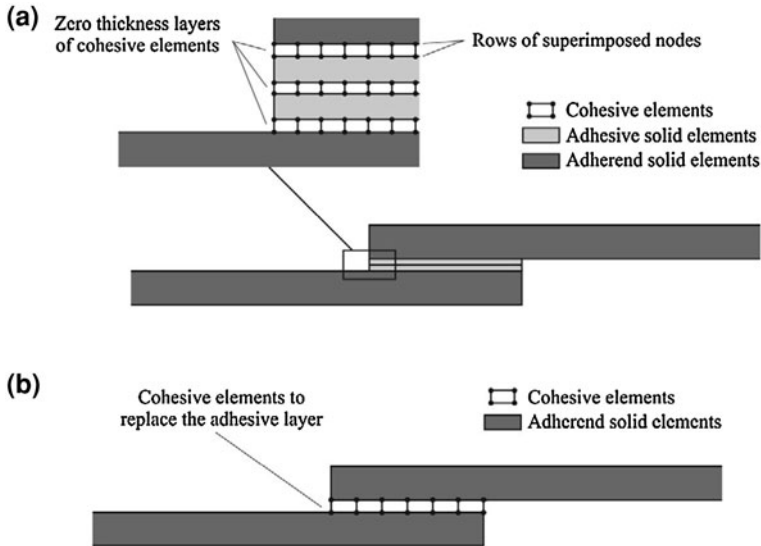
Fig. 11 Cohesive elements to simulate zero thickness failure paths—local approach (**a**) and to model a thin adhesive bond between the adherends—continuum approach (**b**) in an adhesive bond

a large effort was undertaken beginning in the late 1950s/early 1960s by the independent studies of Barenblatt (1959, 1962) and Dugdale (1960). The concept of cohesive zone was proposed by these authors to describe damage under static loads at the cohesive process zone ahead of the apparent crack tip. CZM's were largely refined and tested since then to simulate crack initiation and propagation in cohesive and interfacial failure problems or composite delaminations. CZM's are based on spring (Cui and Wisnom 1993; Lammerant and Verpoest 1996) or more typically cohesive elements (Mi et al. 1998; Petrossian and Wisnom 1998; Feraren and Jensen 2004), connecting 2D or 3D solid elements of structures. An important feature of CZM's is that they can be easily incorporated in conventional FE softwares to model the fracture behaviour in various materials, including adhesively bonded joints (Ji et al. 2010). CZM's are based on the assumption that one or multiple fracture interfaces/regions can be artificially introduced in structures, in which damage growth is allowed by the introduction of a possible discontinuity in the displacement field. The technique consists on the establishment of traction–separation laws (addressed as CZM laws) to model interfaces or finite regions.

The CZM laws are established between paired nodes of cohesive elements, and they can be used to connect superimposed nodes of elements representing different materials or different plies in composites, to simulate a zero thickness interface (local approach; Fig. 11a; Pardoen et al. 2005), or they can be applied directly between two non-contacting materials to simulate a thin strip of finite thickness between them, e.g. to simulate an adhesive bond (continuum approach; Fig. 11b; Xie and Waas 2006).

A few works on CZM techniques use the local approach (Campilho et al. 2005, Liljedahl et al. 2006, Turon et al., 2007a). With this methodology, the plastic dissipations of the adhesive bond are simulated by the solid finite elements, whilst the applicability of cohesive elements is restricted to damage growth simulation (Fig. 11a). The CZM laws usually present an extremely high initial stiffness (penalty function method), not to change the structures global stiffness. Placement of the cohesive elements at different growth planes in the transverse direction of the adhesive bond is also feasible, capturing the respective stress gradients and concentration towards the singular regions (Campilho et al. 2005). In the local approach for bonded joints simulation, the adhesive is modelled as an elasto-plastic continuum by solid FE elements (Pardoen et al. 2005) and the "intrinsic fracture energy" is considered for the CZM laws instead of G^c, relating to the required dissipation of energy to create a new surface, while the plastic dissipations of ductile materials take place at the solid elements representative of the adhesive bond (Liljedahl et al. 2006). Thus, G^c is the sum of these two energy components, increasing by inclusion of the plastic dissipation of materials in the models. Under these assumptions, damage growth is ruled by the work of separation of the fracture surfaces instead of G^c, due to the dissipated energy by the continuum elements. The effects of external and internal constraints on the plastic dissipations of an adhesive bond are thus accountable for in the local approach. On the other hand, compared to the continuum approach, to be described in the following, more parameters and computations are needed (Ji et al. 2010).

CZM's have also been used to simulate the behaviour of adhesive bonds by a continuum approach (Fig. 11b), by the replacement of the entire adhesive bond by a single row of cohesive elements with the representative behaviour of the adhesive bond (Kafkalidis and Thouless 2002; Campilho et al. 2008a). The initial stiffness of the cohesive elements, unlike for the local approach, represents the adhesive bond stiffness in each mode of loading, and the global behaviours of the adherends are fully correlated by these elements. Due to the evident simplicity of this approach, it has been widely used in the damage growth simulation of bonded joints, giving accurate results providing that accurate calibrations are undertaken for the CZM laws (Campilho et al. 2009a). Despite the computationally efficiency of continuum CZM modelling of bonded joints, few limitations exist: (1) the physical meaning of the fracture process was somehow lost, because real cohesive separations are usually accompanied with localized plastic behaviours across the adhesive interlayer, even for brittle adhesives, represented with this method by averaged equivalent properties and (2) CZM's become dependent of the structure geometry, more specifically on t_P and t_A, because these largely affect the size of the fracture process zone (FPZ) and plasticity around the crack tip, thus making the CZM laws dependent of these parameters (Ji et al. 2010).

From this discussion, it is evident that CZM's provide a macroscopic reproduction of damage along a given path, disregarding the microscopic phenomena on the origin of failure, by the establishment of a traction-relative displacement $(t - \delta)$ response between paired nodes on opposite faces of the pre-defined crack path, by specification of large scale parameters ruling the crack growth process such as G_n^c,

Fig. 12 Triangular CZM law (adapted from Abaqus® Documentation 2009)
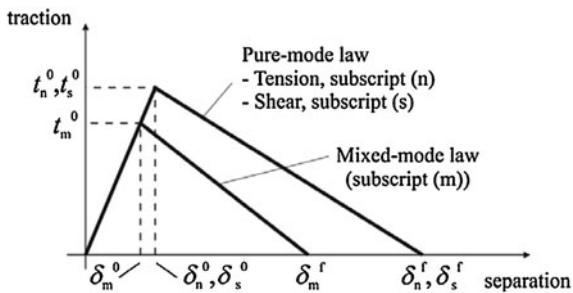
G_s^c or G_t^c (Zhao et al. 2011b). CZM's thus simulate strength evolution and subsequent softening up to complete failure, to account for the gradual degradation of material properties. The traction–separation laws are typically represented by linear relations at each one of the loading stages (Yang and Thouless 2001), although one or more stages can be defined differently for a more accurate representation of the materials behaviour. Figure 12 represents the 2D triangular CZM model actually implemented in Abaqus® for static damage growth, which is described here in detail. The 3D version is similar, but it also includes the tearing component. More details on the 3D CZM implemented in Abaqus® can be found in the work of Campilho et al. (2011b) or in Abaqus® Documentation (2009).

Regarding the nomenclature used throughout this work, the subscripts n and s relate to pure normal (tension) and shear behaviours, respectively. t_n and t_s are the corresponding current stresses, and δ_n and δ_s the current values of δ. CZM's require the knowledge of G_n and G_s along the fracture paths and respective values of G_n^c and G_s^c. Additionally, the cohesive strengths must be defined (t_n^0 for tension and t_s^0 for shear), relating to the onset of damage, i.e., cancelling of the elastic behaviour and initiation of stress softening. δ_n^0 and δ_s^0 are the peak strength displacements, and δ_n^f and δ_s^f the failure displacements. The values of δ_n^f and δ_s^f are defined by G_n^c or G_s^c, respectively, as these represent the area under the CZM laws. As for the mixed mode CZM law (Fig. 12), t_m^0 is the mixed mode cohesive strength, δ_m^0 the corresponding displacement, and δ_m^f the mixed mode failure displacement.

Under pure mode loading, the respective t-δ response attains its peak at the cohesive strength (t_n^0 or t_s^0), corresponding to damage initiation by the induced reduction of stiffness of the cohesive element. Softening follows and, when the values of t are completely cancelled, the crack propagates up to the adjacent set of paired nodes in the failure path, permitting the gradual debonding between crack faces. Under mixed loading (i.e., when two or three modes of loading are simultaneously present), stress and/or energetic criteria are often used to combine the pure mode laws, thus simulating the typical mixed mode behaviour inherent to bonded assemblies. By the mentioned principles, the complete failure response of structures can be simulated (Zhu et al. 2009). For the estimation of the cohesive law parameters, a few data reduction techniques, described further in detail, are available (e.g. the property determination technique, the direct method and the

inverse method) that enclose varying degrees of complexity and expected accuracy of the results (Sørensen and Jacobsen 2003; Li et al. 2005a; Liljedahl et al. 2006).

A CZM thus extends the concepts of continuum mechanics described in Sect. 2.2 by including a zone of discontinuity when the pre-defined CZM path is fulfilled, using characteristic parameters of the continuum mechanics approaches for the onset of damage and energy parameters of fracture approaches for propagation (Banea and da Silva 2009; Chen et al. 2011b). This allows CZM's to be of much more general utility than conventional fracture mechanics, because of the simulation of onset and non-self-similar growth of damage without user intervention, and non-dependence on an initial flaw, unlike conventional fracture mechanics approaches. Compared to continuum mechanics approaches, CZM's are mesh independent provided that sufficient integration points are simultaneously under softening at the crack front (Campilho et al. 2009b; Campilho et al. 2011a). Actually, when the mixed mode softening initiates at a given set of paired nodes, material degradation initiates, leading to a stress reduction and consequent stress redistribution to the neighbouring sets of nodes. If this is performed smoothly by sufficiently small load increments, then a stable propagation takes place, avoiding any mesh influence. CZM's have been largely used in recent years to simulate the behaviour of structures up to failure, as they allow to include in the numerical models multiple failure possibilities, within different bulk regions of materials or between materials interfaces, e.g. at the adhesive bonding interfaces. The knowledge of the loci of damage occurring in a structure is not required as an input parameter, as the CZM globally searches damage initiation sites at specified failure paths satisfying the established criteria. However, cohesive elements must exist at the planes where damage is prone to occur, which, in several applications, can be difficult to know in advance. Although a large amount of CZM failure paths may be introduced in a structure to simulated different fractures (Campilho et al. 2009a), it is not feasible to introduce cohesive elements between every field element, even in a moderate size mesh. However, an important feature in bonded assemblies is that damage propagation is restricted to well defined planes, i.e., at or near the adhesive/adherend interfaces between the adhesive and the adherends, or cohesively in the adhesive bond, which allows overcoming this limitation (Campilho et al. 2008a). Several CZM law shapes have been presented in the literature, depending on the nature of the material or interface to be simulated. The triangular, exponential and trapezoidal shapes, as shown in Fig. 13, are the most commonly used for strength prediction of typical materials. For the represented trapezoidal CZM, δ_n^s and δ_s^s are the stress softening onset displacements.

Selection of the Cohesive Law Shape

The shape of the CZM laws can be adjusted to conform to the behaviour of the thin material strip or interface they are simulating. Developed models over the years include triangular (Alfano and Crisfield 2001), linear-parabolic (Allix and Corigliano 1996), polynomial (Chen 2002), exponential (Chandra et al. 2002) and
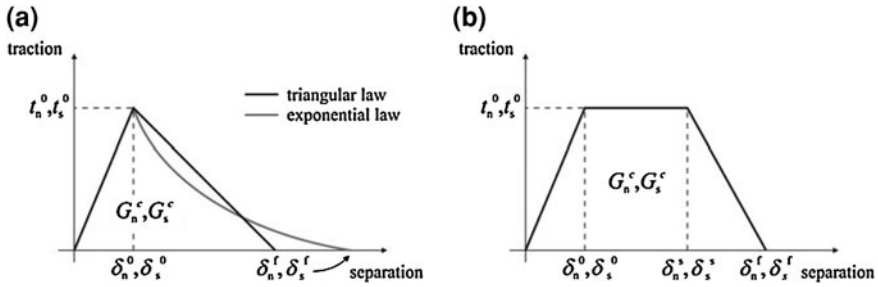
Fig. 13 Different shapes of pure mode CZM laws: triangular or exponential (**a**) and trapezoidal (**b**)

trapezoidal laws (Kafkalidis and Thouless 2002). Thus, CZM's can be adapted to simulate ductile adhesive bonds, which can be modelled with trapezoidal laws (Campilho et al. 2008a, 2009a). It was recently made possible to define the precise CZM shape by advanced techniques, although this is always a difficult task to be performed by experimental procedures. As a result, the CZM is often assumed or simplified based on the perceived knowledge of the materials/interfaces to be simulated (Kafkalidis and Thouless 2002). Notwithstanding this fact, varying published results gave predictions within acceptable errors even for small variations to the optimal CZM parameters and shapes (Liljedahl et al. 2006).

On the other hand, the effect of the CZM law shape significantly varies depending on the structure geometry and behaviour of the materials. These issues became evident in the experimental and FE study of Pinto et al. (2009), which predicted the tensile strength of single lap joints between adherends with similar and dissimilar materials and values of t_P, bonded with the adhesive 3 M DP-8005®. The authors concluded that for stiffer adherends, the precise shape of the cohesive law is fundamental for the accuracy of the results and load–displacement (P–δ) response of the structure, since peel loads are minimized and the joint is mainly loaded by shear. Due to the large longitudinal stiffness, differential deformation effects are minimized as well, which results on identical shear loading along the adhesive bond. As a result, the P–δ curve precisely follows the shape of the CZM law. Compliant adherends give rise to substantial shear and peel peak stress gradients along the adhesive bond, diluting the miscalculation of current stresses over the entire overlap. The results of Ridha et al. (2010) also emphasized on the CZM shape influence, by modelling a thin adhesive bond of a high elongation epoxy adhesive FM® 300 M (Cytec) in scarf repairs on composite panels. Linear, exponential and trapezoidal softening was considered to model plasticity of the adhesive, with the use of linear softening resulting in under predictions of the repairs strength by nearly 20%, because of premature softening at the bond edges after t_m^0 (Fig. 12) that is not consistent with the actual behaviour of the adhesive.

In which regards to the suitability of the CZM laws for adhesive bonds, a trapezoidal law is often preferred for ductile adhesives (Feraren and Jensen 2004;

Campilho et al. 2010), especially when extremely stiff components are bonded, due to the practically absence of differential deformation effects in these components (Alfano 2006, Pinto et al. 2009). A triangular CZM is commonly selected for brittle materials that do not undergo plasticization after yielding (Campilho et al. 2011a), and also for the intralaminar fracture of composite adherends in bonded structures, due to their intrinsic brittleness (Xie et al. 2006).

For the selection of the most appropriate CZM law shape for a given application, the material/interfacial behaviour should always be the leading decision factor. Nonetheless, the CZM law shape also influences the iterative solving procedure and the time required to attain the solution of a given engineering problem. Actually, larger convergence difficulties are expected for trapezoidal rather than triangular CZM laws, mainly because of a more abrupt change in the cohesive elements stiffness during stress softening. Actually, for a specified value of G_n^c or G_s^c, the larger the value of δ_n^s or δ_s^s of the trapezoidal law (Fig. 13b), the larger is the variation to the triangular descending slope. In summary, the selection of CZM law cannot be separated from any of these issues.

Triangular Cohesive Zone Model

The triangular CZM law, described in detail in this section, is the most commonly used due to its simplicity, reduced number of parameters to be determined, and generally acceptable results for most real conditions (Liljedahl et al. 2006). However, generically speaking, the shape of the cohesive laws can be adjusted to conform to the behaviour of the material or interface they are simulating for more precise results (Campilho et al. 2009a). The current section describes the static triangular 2D CZM implemented in Abaqus® v6.10 (Fig. 12). Different shape CZM's are based on this formulation, typically differing on the softening simulation.

Fatigue CZM's are also invariably based on the described formulation in this section but, as no software implementation is yet available and different approaches have been proposed, these are characterized in "Fatigue Applications of Cohesive Zone Models", which specifies fatigue CZM's in detail. Under pure mode, damage propagation occurs at a specific set of paired nodes when the values of t_n or t_s are released in the respective CZM law. Under mixed mode, stress and energetic criteria are often used to combine tension and shear (Campilho et al. 2008a).

Cohesive elements are assumed to be under one direct component of strain (tension) and one transverse shear strain, which are computed directly from the element kinematics. The membrane strains are assumed as zero, which is appropriate for thin and compliant bonds between stiff adherends. Undamaged strength evolution is defined by a constitutive matrix relating the current stresses and strains in tension and shear across the cohesive elements (subscripts n and s, respectively) (Abaqus® Documentation 2009)

$$\mathbf{t} = \left\{ \begin{array}{c} t_n \\ t_s \end{array} \right\} = \left[\begin{array}{cc} K_{nn} & K_{ns} \\ K_{ns} & K_{ss} \end{array} \right] \cdot \left\{ \begin{array}{c} \varepsilon_n \\ \varepsilon_s \end{array} \right\} = \mathbf{K_{COH}}\boldsymbol{\varepsilon}. \tag{5}$$

The matrix $\mathbf{K_{COH}}$ contains the stiffness parameters of the adhesive bond, whose definition depends on whether the local or continuum approach is being used. In the local approach, used to simulate zero thickness fractures, the $\mathbf{K_{COH}}$ parameters are chosen as an extremely large value (penalty function method) for the cohesive elements not to interfere with the structure deformations, given that this task is to be performed solely by the continuum FE elements (Campilho et al. 2005). For continuum CZM modelling of bulk thin strips and more specifically for adhesive bonds, a suitable approximation is provided with $K_{nn} = E$, $K_{ss} = G$, $K_{ns} = 0$ (Abaqus® Documentation 2009); E and G are the longitudinal and transverse elastic moduli, respective. Under these conditions, the model response for the adhesive bond accurately reproduces its deformation behaviour. A few user implemented models in the literature (Campilho et al. 2008a) specify Eq. 5 directly in terms of $\mathbf{t}$–$\boldsymbol{\delta}$ relationship; $\boldsymbol{\delta}$ representing the vector of relative displacements including δ_n and δ_s. With this formulation, K_{nn} and K_{ss} are defined as the ratio between E or G and t_A.

Damage initiation under mixed mode conditions can be specified by different criteria. In this description, the quadratic nominal stress criterion for the initiation of damage is presented, previously tested for accuracy (Campilho et al. 2009a), expressed as (Abaqus® Documentation, 2009)

$$\left\{ \frac{\langle t_n \rangle}{t_n^0} \right\}^2 + \left\{ \frac{t_s}{t_s^0} \right\}^2 = 1. \tag{6}$$

$\langle \rangle$ are the Macaulay brackets, emphasizing that a purely compressive stress state does not initiate damage (Jing et al. 2009). After t_m^0 is attained (Fig. 12) by the fulfilment of Eq. 6, the material stiffness initiates a softening process. This is simulated by the energy being released in a cohesive zone ahead of the crack tip (FPZ). This region is where the material undergoes damage by different ways (Pereira and de Morais 2003), e.g. micro-cracking, extensive plasticity and fibre bridging (e.g. for composite adherends). Numerically, this is implemented by a damage parameter whose values vary from zero (undamaged) to unity (complete loss of stiffness) as the material deteriorates. Complete separation (δ_m^f in Fig. 12) are predicted by a linear power law form of the required energies for failure in the pure modes (Abaqus® Documentation 2009)

$$\frac{G_n}{G_n^c} + \frac{G_s}{G_s^c} = 1. \tag{7}$$

Convergence Issues

The use of CZM's for static or fatigue strength prediction is intrinsically linked to convergence issues that may occur in the incremental iterative process in which the load step is divided into, at the time of reaching to the solution of the system of equations expressed in Eq. 1. As previously specified in Sect. 2.1, in a given increment, solution is attained when the iterative procedure gives an error between the left and right sides of the fundamental equation under a software pre-defined or used-defined value (Abaqus® Documentation 2009).

Usually, the main factors contributing to convergence difficulties are the propagation of damage by CZM formulations (which depend on the CZM law shape) and respective instability, the consideration of plastic constitutive behaviours for the solid elements, the adhesive plasticity, the adherends stiffness, the orthotropic nature of composite materials, coarse meshes at or near stress concentration/damage propagation sites and structural geometries with large stress concentrations, singular regions or intersecting cracks (Hamitouche et al. 2008), more specifically if two or more of these features exist concurrently within an analysis. In FE models, the increments usually run smoothly up to damage uptake by the cohesive elements along the failure paths, after which convergence problems appear due to the abrupt variation of K (Eq. 1) between consecutive increments.

Obviously that, as it was previously mentioned, trapezoidal laws give more convergence problems because of the more abrupt change in the cohesive elements stiffness during softening. Gradual softening and reduction of the mesh size at the fracture regions can or not be enough to surpass difficulties and attain total separation. Convergence problems may also occur during unstable crack propagation, when the available value of G is higher than the respective G^c (Abaqus® Documentation 2009), which can be prevented by smaller step incrementations. Isotropic plasticity in the adherends or orthotropic elasticity for composite adherends creates larger difficulties during CZM damage growth and, under these conditions, elastic-perfectly plastic approximations or approximation to isotropic equivalent properties, respectively, can assist to a smoother fracture without compromising the results. On the same line of the adherends plasticity, compliant adherends such as polymers usually endure significant deformations and element distortions near the damage propagation sites, with the respective difficulty to reduce the iterative errors during crack growth for implicit solving techniques such as in Abaqus®/Standard. There is not an ultimate solution to improve convergence for this scenario, although the local reduction of the mesh size or use of geometric non-linearities in the FE software may help. Concerning the adhesive behaviour, brittle adhesives turn the CZM softening process more abrupt, notwithstanding the CZM law shape that, added to the smaller FPZ's at the crack tip, result in larger convergence difficulties. Depending on the bonded system, the increase of G_n^c and/or G_s^c is sometimes enough to achieve surface separation, although a small over prediction of the structural strength is naturally associated (up to 10% in single lap joints for 100% increase of G_n^c and G_s^c; Campilho et al. 2011c). All of the

other issues, such as coarse meshing, singularities or intersecting cracks are partially solved by a bigger mesh refinement.

Transversely to all of these scenarios, the reduction of the cohesive elements initial stiffness up to t_n^0 or t_n^0 is equally a possibility for the reduction of convergence problems by the reduction of the adjacent elements distortion and stress concentrations. However, this must be performed in such a manner that the structure's overall stiffness is not compromised (for both local and continuum approaches) and, additionally for adhesive bonds modelled by a continuum CZM, bearing in mind that the constitutive behaviour of the bond is being altered. Interpenetration of the crack faces can also occur for small stiffness values and should be prevented as well (Khoramishad et al. 2010). Following extensive studies, the value of 10^6 N/mm^3 was recommended by Gonçalves et al. (2000) for a triangular static CZM (local approach modelling) for an accurate convergence and minimization of convergence difficulties during the nonlinear procedure. Nonetheless, values down to 5×10^4 N/mm^3 were used without compromising the global behaviour of bonded repairs on composite structures (Campilho et al. 2008b). Smaller values are not recommended on account of the stiffness accuracy issues and numerical ill-conditioning problems (Khoramishad et al. 2010).

Apart from the proposed solutions, FE software packages usually hold a few techniques to aid the iterative process. Abaqus®, as an example, gives the user three main possibilities (Abaqus® Documentation 2009): (1) viscous regularization, (2) automatic stabilization and (3) non-default solution controls.

Using viscous regularization in Abaqus®/Standard improves the convergence of fracture problems, by implementation of viscous regularization within the constitutive equations, which allows stresses to be outside the limits of the CZM laws. A small value for the viscosity parameter, compared to the characteristic time increment, usually improves the convergence rate of simulations during the softening regime, without compromising the accuracy of the results.

Consideration of automatic stabilization is another possibility to improve convergence for unstable problems (e.g., due to buckling or material softening). If the instability is localized, a local transfer of strain energy takes place from one part of the model to the neighbouring regions, and global solution methods may not work (Abaqus® Documentation 2009). These difficulties have to be solved either dynamically or with the introduction of (artificial) damping. Abaqus®/Standard uses an automatic algorithm for the stabilization of locally unstable quasi-static problems by the automatic addition of volume-proportional damping to the model.

The use of non-default solution controls consists on the user modification of the nonlinear equation solution accuracy and time increment adjustment, to actively affect the incremental solving procedure and solver parameters to force convergence. However, caution is required, since if less strict convergence criteria are imposed, results may be accepted as converged although they are not sufficiently close to the exact system solution. The line search algorithm is also within the scope of solution controls, allowing the detection of divergent equilibrium iterations in strongly nonlinear problems solved by the Newton algorithms of
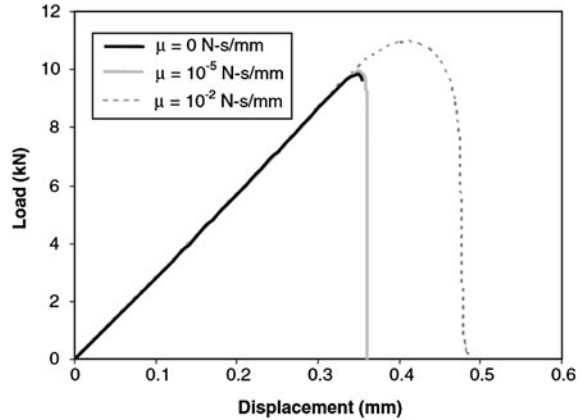
Abaqus®/Standard. A scale factor is then applied to the computed solution correction, which helps to prevent divergence.

The work of Khoramishad et al. (2010), relating to the development of a fatigue CZM for single lap joints, included a preliminary study on the viscous regularization technique of Abaqus® as a requirement for the attainment of static failure, for further progress to the fatigue damage implementation. The authors emphasized on the necessity of not changing the overall structural response by the inclusion of viscous damping in the models. As a result, the optimal value of this parameter was found by a parametric study with decreasing levels of implemented viscous damping coefficient, μ (Fig. 14).

Figure 14 shows the result of a non-optimized value of μ (10^{-2} N.s/mm), as the response of the bonded joints are largely affected, and the final optimized results by consideration of $\mu = 10^{-5}$ N.s/mm, since this quantity allowed surpassing the divergent behaviour of the solution although it did not change the overall results.

Determination of the Cohesive Parameters

CZM analyses offer a powerful means to account for the largely nonlinear fracture behaviour of modern adhesively bonded joints, but the CZM parameters require careful calibrations by experimental data and respective validation in order to accurately simulate the failure process (DuBois 2004; Carlberger and Stigh 2010). Despite this fact, standardized methods for the definition of t_n^0 and t_s^0 are not yet available (Lee et al. 2010). In recent years, many works were published regarding the definition of the CZM parameters (G_n^c, G_s^c, t_n^0 and t_s^0) and a few data reduction techniques are currently available (e.g. the property determination technique, the direct method and the inverse method) that enclose varying degrees of complexity and expected accuracy of the results. The few of these works that validated with mixed mode experiments the estimated pure mode CZM's typically made use of

double-cantilever beam (DCB), end-notched flexure (ENF) or single lap specimens, generally with good results (Kafkalidis and Thouless 2002; Zhu et al. 2009).

The property determination method, consisting on the isolated definition of all the cohesive law parameters by suitable tests, is particularly critical if bulk tests are used, owing to reported deviations between the bulk and thin adhesive bond cohesive properties (Andersson and Stigh 2004). This is caused by the strain constraining effect of the adherends in bonded assemblies, and also by the typical mixed mode crack propagation in adhesive bonds (Andersson and Stigh 2004; Högberg and Stigh 2006; Högberg et al. 2007; Leffler et al. 2007). Actually, in bulk materials cracks tend to grow perpendicularly to the direction of maximum principal stress (Chai 1992). In thin bonds, cracks are forced to follow the bond length path since, as the adhesive is typically weaker and more compliant than the components to be joined, failure is often cohesive within the adhesive (Zou et al. 2004; Campilho 2005). The inverse method consists on the trial and error fitting analysis to experimental data on bonded joints, such as the $P–\delta$ curve, allowing tuning of the simplified shape CZM laws for particular conditions. For the property determination technique and the inverse method, a simplified parameterized shape is often selected (e.g. bilinear or trilinear) for the CZM, based on an assumption made by the user depending on the material behaviour to be simulated (Campilho et al. 2009a). On the other hand, in the direct method the precise shape of the CZM laws is easily defined, since it computes the CZM laws of an adhesive bond from the measured data of fracture characterization tests (Pandya and Williams 2000) by differentiation of the $G_n–\delta_n$ or $G_s–\delta_s$ curves. However, for subsequent use by FE strength prediction techniques, it is common practice to build a simplified approximation for easier implementation.

Notwithstanding the parameter identification method, deviations are expected to occur between the quantitative prediction of the cohesive parameters and the real behaviour of the adhesive bond (Leffler et al. 2007; Pinto et al. 2009). Contrarily to the property determination method, the inverse and direct methods provide more accurate estimations as the adhesive can be characterized under identical adherend restraining conditions to real applications, giving accurate estimations (Pardoen et al. 2005). However, the direct method is still considered to give the most accurate results, since it provides the precise shape of the CZM laws, while the inverse method parameters are based on previously assumed CZM shapes. Concerning the CZM parameters, G^c is usually the key parameter to be determined, because of the role that it plays on the overall results. For its estimation, the LEFM-based methods are usually easier to apply, although these can only be used for brittle or moderately ductile adhesives. For adhesives that endure extensive plasticization, LEFM techniques are rendered unfeasible, and the J-integral method emerges as a viable alternative. However, it is more complicated to apply, as generally additional data is required from the tests, such as the adherends rotation during loading.

Disregarding the parameter determination method, the CZM parameters invariably depend on t_A and t_P, which emphasizes the importance of the t_A and t_P consistency between the fracture tests and the structures to be simulated (Bascom

Fig. 15 DCB (**a**) and ENF
(**b**) tests for fracture
characterization of thin
adhesive bonds
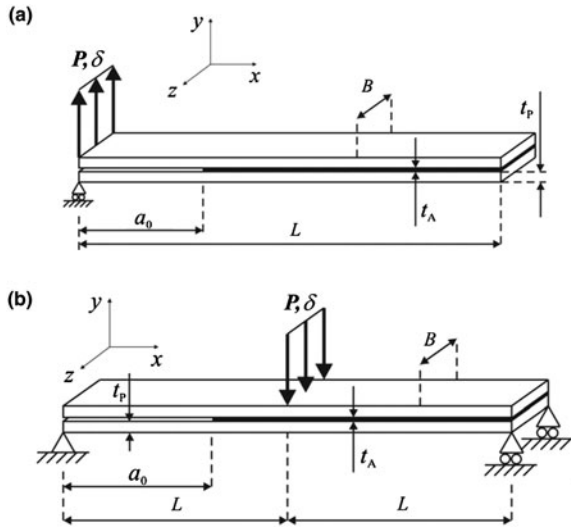
and Cottington 1976; Chai 1986a, b; Andersson and Stigh 2004; Leffler
et al. 2007).

Fracture Characterization Methods

The values of G_n^c and G_s^c are estimated by standardized test methods for all of the
three data reduction methods. Additionally, the inverse and direct methods, also
take advantage of the P–δ results of the fracture tests for the accurate derivation of
the CZM laws in each mode of loading. The DCB test for tension (Fig. 15a) and
the ENF test for shear (Fig. 15b) are the most widespread test methods (B is the
specimen width, a_0 the initial crack length and L the specimen length; DCB test, or
half-length; ENF test).

Several works are available for fracture characterization in tension by the DCB
test (Bader et al. 2000; Ducept et al. 2000; Nairn 2000; Andersson and Stigh 2004;
Hojo et al. 2006). The main advantages of this test method include its simplicity
and the possibility to obtain G_n^c mathematically using the beam theory (Yoshihara
2007). However, some issues must be taken into account for an accurate estima-
tion. In fact, unstable crack propagation was experimentally detected by Bader
et al. (2000) and Ducept et al. (2000), which hinders a clear crack length
(a) monitoring during the test. In other cases, in the DCB test of adhesively bonded
structures, the crack tip may not be clearly visible depending on the adhesive. This
can induce non-negligible errors on the derivative of the compliance ($C = \delta/
P$) relatively to a used in the compliance calibration method (CCM). On the other
hand, the energy dissipated at the FPZ can be large for ductile adhesives, implying
that beam theory-based methods without any corrections will underestimate G_n^c.
A few methods are available that allow the direct extraction of G_n^c, accounting for
the FPZ effects and not requiring the crack length measurement during propagation

(Tamuzs et al. 2003; Biel and Stigh 2008; de Moura et al. 2008). Blackman et al. (2003) considered tapered double-cantilever beam (TDCB) and peel tests instead to assess G_n^c of an adhesive layer and to study fracture of adhesively bonded joints.

Fracture characterization in shear is still not well addressed owing to some inherent features of the most popular tests: ENF, end-loaded split (ELS) and four-point end-notched flexure (4ENF). Actually, the ELS test involves clamping one of the specimen edges, constituting a source of variability and increasing the complexity of data reduction (Blackman et al. 2005). On the other hand, the 4ENF test requires a complex setup and presents some problems related to large friction effects (Schuecker and Davidson 2000). Therefore, the ENF test is the most suited for shear fracture characterization of adhesively bonded structures (Leffler et al. 2007). However, problems related to unstable crack growth and to crack monitoring during propagation are yet not fully solved. In addition, the classical data reduction schemes, based on beam theory analysis and compliance calibration, require the monitoring of a during propagation. Added to these issues, a quite extensive FPZ develops ahead of the crack tip for ductile adhesives, which affects the measurement of G_s^c. Consequently, its influence should be taken into account, which does not occur when the real value of a is used in the selected data reduction scheme. To overcome these limitations, data reduction schemes for the measurement of G_s^c that are only based on the specimens compliance are also available (de Moura et al. 2009).

An important issue to account for when using the direct or inverse methods for the estimation of the CZM laws is to match as possible the values of t_P, lay-up (for stacked composite laminates) and t_A between the fracture tests and the bonded structures to be simulated (Campilho 2009), since the cohesive parameters of the adhesive bond largely depend on the adherends restraining to the adhesive bond. Pardoen et al. (2005) performed a parametric study of the effect of t_P on the values of G_n^c, using TDCB and compact tension (CT) fracture tests. It was shown that the increased bending of thin adherends promoted plasticity in the adhesive bond, greatly increasing G_n^c. Actually, the large transverse deflection of thin adherends is associated with large root rotation and substantial shear stresses, which tend to promote plastic yielding in the adhesive, increasing plastic strains as well. Additionally, extra plastic dissipation associated with the bending of the adhesive bond develops around the crack tip.

Particular attention should also be paid to match t_A between the fracture characterization tests and the real structures to be simulated, as previously mentioned in "Determination of the Cohesive Parameters". In fact, adhesives in the form of thin bonds behave differently than as a bulk material (Andersson and Stigh 2004), because of the strain constraining effects of the adherends and the respective typical mixed mode crack propagation (Högberg and Stigh 2006, Leffler et al. 2007). Different studies reported on an obvious dependence of G^c of adhesive bonds with t_A (Bascom et al. 1975; Bascom and Cottingham 1976; Hunston et al. 1989; Bell and Kinloch 1997; Lee et al. 2003; Lee et al. 2004). Typically, the value of G^c of a thin adhesive bond increases with t_A up to a peak value, bigger than the bulk quantity (Kinloch 1987; Chai 1988; Crews et al. 1988). After, G^c decreases

Fig. 16 Location of the CZM elements in the single strap repairs (Campilho et al. 2008a)
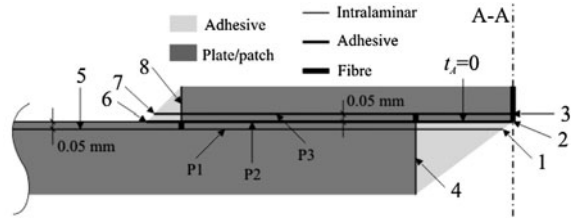
with t_A to a steady-state value, corresponding to G^c of the bulk adhesive (Ikeda et al. 2000; Duan et al. 2002, 2003). This tendency is consistent with the works of Yan et al. (2001a, b), which studied the influence of t_A on the fracture properties of DCB and CT joints with aluminium adherends and a rubber-modified epoxy adhesive. Using a large deformation FE technique and the peak loads measured in the experiments, the critical value of the J-integral was calculated for different values of t_A. Biel (2005) also emphasized on the bigger values of G^c near the optimal value of t_A than as a bulk. This was due to the predominantly state of prescribed deformation at the region where the crack could propagate, which enlarged the FPZ. Actually, with tough engineering adhesives, near the optimal value of t_A the FPZ typically extends several times larger than the value of t_A, and substantially longer than in bulk adhesives, resulting on bigger values of G^c.

Property Determination Method

In the property determination method, at least one of the CZM law parameters is approximated by consideration of bulk adhesive properties (Pinto et al. 2009). Campilho et al. (2008a) evaluated the tensile strength of bonded single strap repairs on laminated composites as a function of the overlap length and the patch thickness. A FE analysis including a trapezoidal CZM was used to simulate a thin ductile adhesive bond of Araldite® 420 (Hunstman) by the continuum approach. In the authors work, t_n^0 and δ_n^s were obtained from the σ–ε curve of the bulk adhesive, substantiated by previous evidence (Andersson and Stigh 2004) that t_n^0 is of the same order of magnitude of the tensile strength measured in bulk tests, and that δ_n^0 and δ_n^s do not significantly influence the numerical results (Yang et al. 1999). On the other hand, t_s^0 was derived from t_n^0 by the von Mises yield criterion for bulk isotropic materials and, owing to its less influence on the results (Yang et al. 1999), δ_n^s was defined considering a similar softening slope to the tension CZM law (Carlberger and Stigh 2007). The values of G_n^c and G_s^c were estimated from DCB and ENF tests, respectively. The interlaminar, intralaminar and fibre failure properties of the composite were obtained from previous works, considering triangular CZM laws (local approach). Different fracture paths were equated (Fig. 16; A–A represents the line of symmetry for the FE simulations), in order to account for different failure modes. A reasonable agreement was found for the

stiffness and failure load/displacement, despite the aforementioned CZM parameter approximations.

Nonetheless, for an evaluation of the effect of the described approximations on the predictions, a sensitivity analysis was also performed by the authors, showing that δ_n^s and δ_s^s of the adhesive bond CZM laws do not change the failure mode of the repairs nor do they affect the failure load. Accounting for the observed failures, at lines P1 and P3 (interlaminar failure of the composite), the shear interlaminar CZM parameters showed a larger influence on the strength than the tension ones.

Pinto et al. (2009) tested a trapezoidal CZM with a continuum formulation to model a $t_A = 0.2$ mm adhesive bond (3 M DP-8005®) for the estimation of the tensile strength of single lap joints between adherends with different values of t_A and materials (polyethylene, polypropylene, glass-epoxy and carbon-epoxy composites). The FE analysis was carried out in Abaqus®, with user developed CZM elements implemented in a sub routine. For the tensile CZM law, t_n^0 and δ_n^s (Fig. 13b) were assumed to be equal to the corresponding bulk quantities. Although the authors did emphasize on possible miscalculations arising from this procedure, this course of action was substantiated by previous results (Andersson and Stigh 2004). G_n^c was estimated from DCB tests using the ASTM D3433-99 (2005) standard. The value of δ_n^s was approximated by the product of the average failure strain obtained in the adhesive bulk tests with t_A, as this parameter does not significantly influence the FE results (Yang et al. 1999).

Oppositely to this course of action, the CZM parameters in shear loading were obtained with an inverse method (the basic principles of this technique are described in detail in "Inverse Method"), considering the block-shear test method (ASTM D4501-01 (2009). The block shear test was adopted since the adhesive layer is mainly loaded in shear, while normal stresses are minimized. The FE simulations captured fairly accurately the experimental behaviour of the joints, in terms of stiffness, and maximum load and the corresponding value of δ for all of the geometry and material configurations tested.

Direct Method

By the direct method, the complete CZM law and respective shape for a given material strip or interface can be precisely estimated by the differentiation of the $G_n–\delta_n$ or $G_s–\delta_s$ curves. A few works currently exist on the direct parameter determination of adhesive bonds (Sørensen 2002; Zhu et al. 2009) and fiber-reinforced composites (Sørensen and Jacobsen 2003). Andersson and Stigh (2004) used a direct method to determine the continuum CZM parameters in tension of a ductile adhesive bond of Dow Betamate® XW1044-3 in a DCB test configuration, after approximation of the $G_n–\delta_n$ data to a series of exponential functions to reduce errors in the measured data. The results showed that the $t_n–\delta_n$ relationship can be divided in three parts. Initially t_n increases proportionally to δ_n (linear elastic behaviour of the adhesive), until a limit stress is achieved. A plateau region followed, corresponding to the development of plasticity in the adhesive.

Fig. 17 G_n–δ_n and G_s–δ_s relations for the adhesive Dow Betamate® XW1044-3 and $t_A = 0.2$ mm (Carlberger and Stigh 2010)
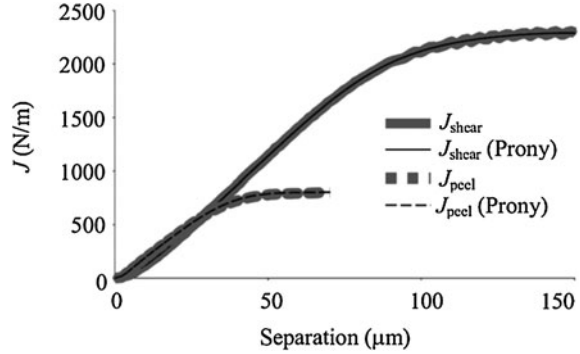
The curve ended with a parabolic softening region, giving an approximate trapezoidal shape.

Högberg and Stigh (2006) proposed a direct integration scheme to capture the CZM laws (continuum approach) of an adhesive bond by a mixed-mode DCB specimen, which consisted on the differentiation of the J-integral vs. δ_n (tension CZM law) or δ_s (shear CZM law). The J-integral was derived from the test data by a developed formulation that required the adherends rotation at the loading point, θ. Results showed that substantial differences exist between pure tensile and shear CZM laws, and that ten evenly distributed mode mixities can catch the mixed mode constitutive behaviour of an adhesive system for any load and geometry conditions.

In the work of Carlberger and Stigh (2010), the continuum CZM laws of a thin bond of a ductile adhesive (Dow Betamate® XW1044-3) were determined in tension and shear using the DCB and ENF test configurations, respectively, considering $0.1 \leq t_A \leq 1.6$ mm. The values of G_n and G_s were derived by a J-integral formulation to accurately capture the large plastic straining effects present at the crack tip of the ductile adhesive (Yan et al. 2001a, b). Actually, the J-integral is a viable means to capture the adhesive nonlinearity for a monotonic loading process, i.e., if no unloading occurs. The cohesive laws were derived by a direct method that used a least square adaption of a Prony-series to the G_n/G_s versus δ_n/δ_s data, to avoid errors on the measured data resulting from direct differentiation of the experimental results. Although the J-integral solutions for this purpose have its advantages, the respective formulae require additional data to the P–δ data available from the tests than LEFM techniques. Actually, on one hand, for G_n determination by the DCB test method, the applied force, P, and θ are necessary parameters to be defined as functions of δ_n. On the other hand, for shear characterization by the ENF test method, the simultaneous measurement of the applied force, P, and shear sliding at the tip of the adhesive bond, δ_s, are required. With this data, by direct application of formulae derived in the authors work, the evolution of G_n and G_s (in the authors work addressed as J) with the deformation of the adhesive bond could be established (Fig. 17).

Fig. 18 CZM laws in tension for the adhesive Dow Betamate® XW1044-3 and $0.1 \leq t_A \leq 1.6$ mm (Carlberger and Stigh 2010)
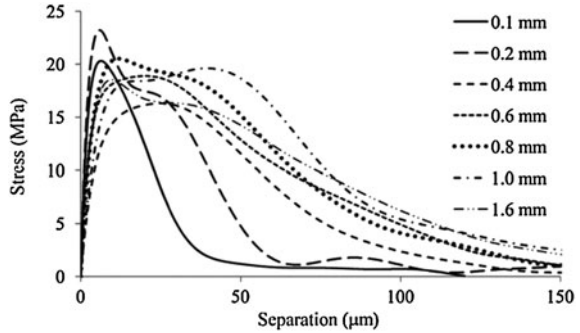
Differentiation of the Prony-series adaptions of G_n or G_s relatively to the relative displacements, δ_n or δ_s, gives the full cohesive law up to failure, provided that the curves of Fig. 17 are obtained up to a steady-state value (Zhu et al. 2009).

Figure 18 shows the averaged CZM laws in tension for each value of t_A, considering 5–8 specimens for each condition. The obtained results clearly show the transition between approximate triangular CZM laws for small values of t_A to trapezoidal laws for bigger values. This is obviously related to an increase of G_n^c, because of larger FPZ developments in the adhesive bond (Choi et al. 2004; Duan et al. 2004). Figure 19 represents the shear CZM laws for t_A values between 0.1 and 1.0 mm, averaged over at least two specimens. The reported results are qualitatively consistent with the tension data, i.e., a CZM shape dependence with t_A, with an approximate triangular shape for $t_A = 0.1$ mm and modification to a trapezoidal shape for bigger values of t_A. However, above $t_A = 0.2$ mm the value of G_s^c is virtually unaffected. The value of t_s^0 slightly diminished with t_A because of minor reductions of the effective strain rate with increasing values of t_A (Carlberger et al. 2009).

It was thus concluded that the CZM shapes and respective parameters significantly vary with t_A, ranging from a rough triangular shape for the smaller values of t_A to a trapezoidal shape for bigger values of t_A.

The continuum CZM analysis of Ji et al. (2010) addressed the influence of t_A on t_n^0 and G_n^c for a brittle epoxy adhesive (Loctite® Hysol 9460), by using the DCB specimen and the direct method for parameter identification. The analysis methodology relied on the measurement of G_n^c by the analytical J-integral method proposed by Andersson and Stigh (2004), requiring the measurement of θ. Figure 20 shows the testing setup for the measurement of G_n.

The testing machine was set to collect the load, load–point displacement (with linear transducers placed at the crack tip) and, for the measurement of θ, two digital inclinometers with a $0.01°$ precision were attached at the free end of each adherend. A charge-coupled device (CCD) camera with a resolution of 3.7×3.7 µm/pixel was also used during the experiments, adjusted perpendicularly to one of the DCB specimen side edges. The camera focused at the crack tip and it collected images, which were input in an image processing toolkit for the estimation of δ_n at the crack tip, necessary for correlation with the load and θ for

Fig. 19 CZM laws in shear for the adhesive Dow Betamate® XW1044-3 and $0.1 \leq t_A \leq 1.0$ mm (Carlberger and Stigh 2010)
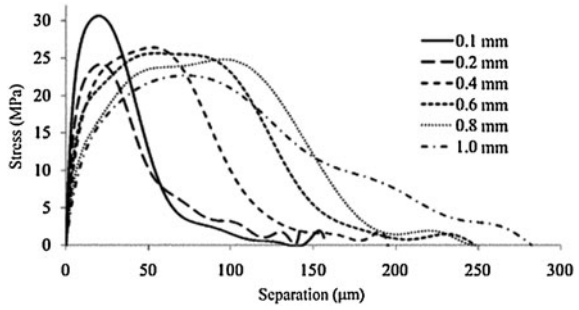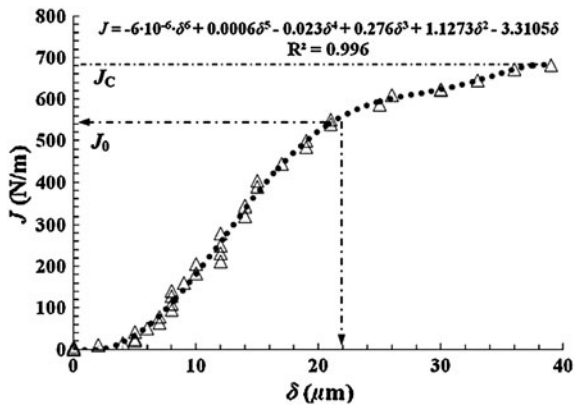

Fig. 20 DCB specimen in the testing machine with inclinometers attached to the adherends and camera for measurement of θ and δ_n, respectively (Ji et al. 2010)


Fig. 21 Relationship between G_n and δ_n for $t_A = 0.2$ mm (Ji et al. 2010)

the definition of G_n. The t_n–δ_n cohesive laws were quickly obtained by differentiation of the G_n–δ_n data (Sørensen 2002; Zou et al. 2009). Figure 21 reports on a typical G_n–δ_n relationship for $t_A = 0.2$ mm and respective 6th degree polynomial function for differentiation and respective estimation of the CZM law.

Representative CZM laws for the adhesive layer are depicted in Fig. 22, showing some interesting variations, such as the previously mentioned increase of G_n^c with t_A, perceptible by the increase of area under the t_n–δ_n curve (Carlberger and Stigh 2010). A reduction of t_n^0 was also found with bigger values of t_A. Another

Fig. 22 Representative CZM law shapes in tension loading for $0.09 \leq t_A \leq 1.0$ mm (Ji et al. 2010)
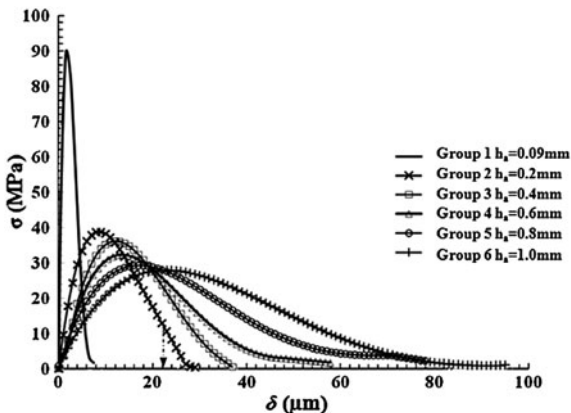
important finding was related to the value of $t_n^0 = 88$ MPa found for $t_A = 0.09$ mm, compared to the bulk strength of 30.3 MPa. However, for increasing values of t_A the estimated t_n^0 values quickly approached the bulk strength of the adhesive (Fig. 22). The authors concluded that the *J*-integral method for the evaluation of G_n^c and the direct method for the CZM law calculation give accurate and calibrated CZM law parameters for specific geometry and material conditions.

Inverse Method

The inverse method consists on an iterative curve fitting procedure between experimentally measured data and the respective FE predictions, considering a precise description of the experimental geometry and approximate cohesive laws, established based on the typical behaviour of the material to be simulated (Banea et al. 2011). The inverse characterization of adhesive bonds should be applied individually for each tested specimen to account for slight geometry variations between specimens (Campilho et al. 2009a). By this technique, the value of G_n^c or G_s^c, which corresponds to the steady-state value of G_n or G_s during crack propagation in the respective *R*-curve built from the fracture characterization test data, is input in the FE model. To completely define the CZM law, approximate bulk values can be used for t_n^0 or t_s^0 (Fig. 12) for the initiation of the trial and error iterative process (Campilho 2009). Tuning of the cohesive parameters is performed by a few numerical iterations until an accurate prediction of the experimental data is achieved. Examples of reliable experimental data for the iterative fitting procedure are the *R*-curve (Flinn et al. 1993), the crack opening profile (Mello and Liechti 2006), and more commonly the *P*–δ curve (Li et al. 2005b).

In the work of Campilho (2009), an inverse fitting methodology was considered for the definition of a shear CZM law by the ENF test (continuum approach) for a ductile epoxy adhesive bond (Hunstman Araldite® 2015) with $t_A = 0.2$ mm. Notwithstanding the crack measurement difficulties arising from crack growth
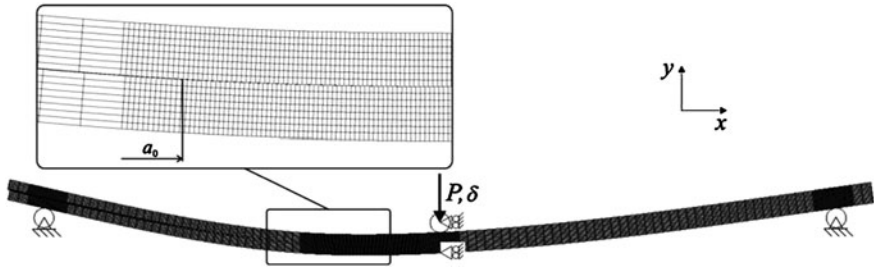
Fig. 23 Deformed shape of the ENF specimen during propagation, with boundary and loading conditions (Campilho 2009)

without opening (Blackman et al. 2005), the use of correction fluid along the crack growth path allowed a precise estimation of the current crack length by an imaging procedure, consisting on image recording during the tests with 5 s intervals using a 10 MPixel digital camera. Estimation of G_s^c was made possible by correlation of P–δ–a by the time elapsed from the test initiation. The testing time of each P–δ data point was calculated from the current value of δ and the loading rate. The correspondence to the values of a was established knowing the testing time of each picture. G_s^c was estimated by three methods: the CCM, the corrected beam theory (CBT) and the compliance-based beam method (CBBM), this last one not requiring the measurement of a during crack propagation as it computes G_s^c only using the experimental compliance. Data reduction by the three methods for five tested specimens showed similar CCM and CBBM results, and smaller values of CBT. The FE analysis faithfully represented each specimen geometry and measured value of a_0. A user defined continuum-based trapezoidal CZM formulation (Campilho et al. 2008a), coupled to Abaqus®, was considered to account for the adhesive ductility. Despite this fact, in terms of spatial modelling, the cohesive elements had zero thickness (Fig. 23).

The CBBM values of G_s^c, corresponding to the steady-state value of the respective R-curves, were used as input in the FE models. The remaining cohesive parameters (t_s^0 and δ_s^s) were estimated by fitting the experimental and numerical P–δ curves of each specimen. Figure 24 shows the experimental and FE P–δ curves for one tested specimen after the fitting procedure.

Figure 25 shows the average shear CZM law and respective values of G_s^c (J_{IIc}), t_s^0 ($\sigma_{u,II}$), δ_s^s ($\delta_{2,II}$) and δ_s^f ($\delta_{u,II}$), and also the CZM laws range after individual application of the inverse fitting principles to five experimental P–δ curves.

The manual fitting allowed a clear insight on the influence of the CZM parameters on the FE P–δ curves shape. G_s^c, which is the input value in the simulations, mainly influences the peak load. Higher values of t_s^0 increase the peak load and the specimen stiffness up this value, leading to a more abrupt post-peak load reduction. Finally, δ_s^s plays an important role on the roundness of the P–δ curve near the peak value. These findings indicated that a unique solution for the shear CZM law of the adhesive could be guaranteed by the inverse technique.

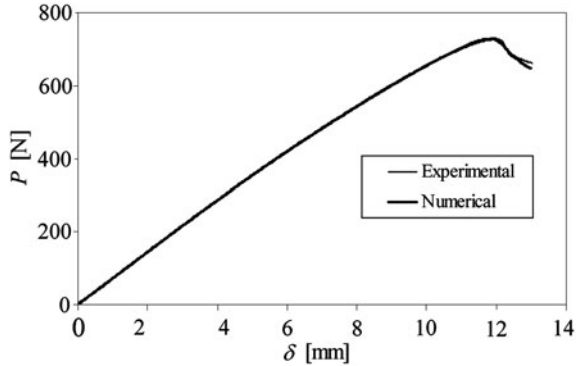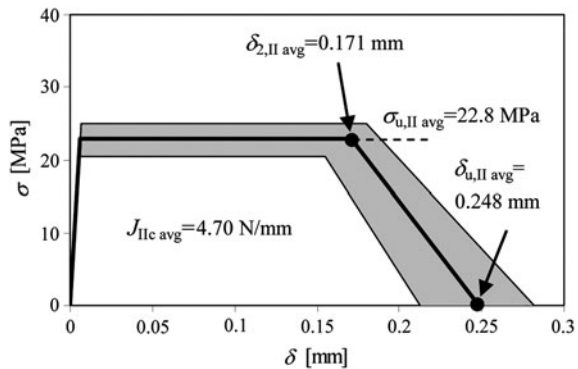**Fig. 24** Experimental and FE P–δ curves comparison for one tested specimen (Campilho 2009)

Fig. 25 Average shear CZM law and deviation after application of the inverse fitting principles to five specimens (Campilho 2009)

Lee et al. (2010) proposed a systematic procedure to estimate the local CZM parameters of an adhesive bond, using single-leg bending (SLB) mixed mode tests with tension or shear as the dominant modes, for the extrapolation of the pure mode laws, thus simplifying the inverse fitting technique. SLB specimens with co-cured adherends (upper carbon fibre reinforced composite adherend and lower steel adherend) were tested under different mode mixities, due to the allowance of controlling this parameter by changing the specimens geometry, for validation of the obtained pure tension and shear data. All fractured specimens showed a cohesive failure of the bond, with evidence of adhesive and fibres on the bonding surface of the steel adherends. Measurement of G^c was carried out from the test data, and the mode mixity was defined from the classical beam theory. Linear extrapolation of the measured data for both tension and shear mode dominant tests allowed the definition G_n^c and G_s^c, as depicted in Fig. 26. The mode decompositions resulted in $G_n^c = 140$ N/m and $G_s^c = 280$ N/m for pure tension and shear, respectively, within the range of typical values for epoxy matrices.

A mixed mode CZM was considered for the reproduction of the test results, built using triangular CZM laws for pure tension and shear, and whose criteria for stress softening and complete separation are consistent with those of Eqs. 6 and 7,

Fig. 26 Linear extrapolation of G_n^c and G_s^c from the mixed mode test results (Lee et al. 2010)
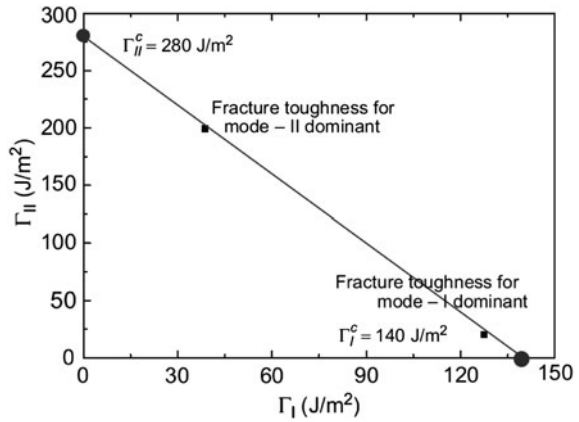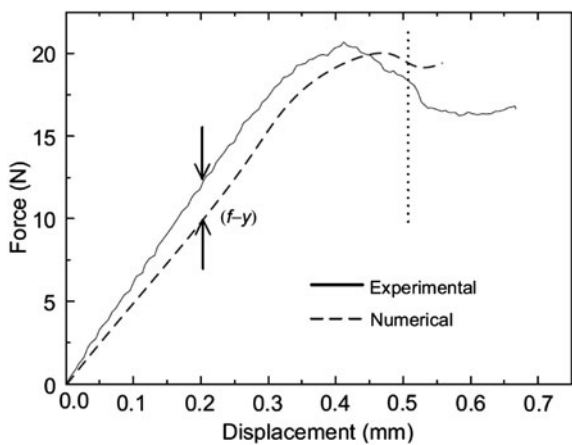

Fig. 27 Error defined by the KM, by comparison of the FE and experimental data (Lee et al. 2010)

respectively. Definition of the missing cohesive parameters (K_{nn}, K_{ss}, t_n^0 and t_s^0) used the design of experiments (DoE) and kriging metamodel (KM) techniques.

The DoE was built considering the aforementioned parameters to be determined as the DoE design variables, and setting the variable levels and required sampling rates for the experiments by the central composite method. As a result of the analysis, the quantity of 50 simulations was considered as the minimum number of experiments to obtain the four parameters. The KM, by allowing a mathematical basis between the system inputs (sampling points of the cohesive parameters) and outputs (errors between the simulation results and experimental data), allows attaining an optimized solution by minimization of the error ($f - y$ in Fig. 27).

An error function was defined as the load difference between the FE and experimental P–δ curves, at different pre-established values of δ within the test range (the vertical dashed line in Fig. 27 relates to the limit of the evaluation region). The CZM parameters to be defined in pure tension and shear were then
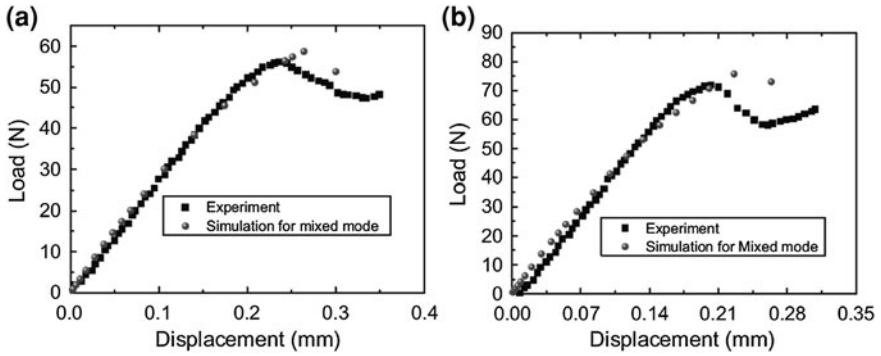
Fig. 28 P–δ curves for SLB specimens with varying mode mixities: composite adherend thickness of 1.28 (**a**) and 1.48 mm (**b**) (Lee et al. 2010)

estimated by a nonlinear optimization algorithm, the sequential quadratic programming algorithm, for minimization of the experimental/FE deviation. The obtained values of CZM parameters in each pure mode of loading were considered to built the pure tension and shear CZM laws, and were regarded as the optimized values to describe the co-cured SLB tests under the mixed mode tension or shear dominant modes, although applicable to pure modes or different mode mixities. Validation of the proposed CZM laws was carried out by consideration of two intermediate mode mixities (modification of the composite adherend thickness to 1.28 and 1.48 mm), by comparison of the test results and FE simulations with the previously defined parameters for the dominant modes mixities. Comparison of the FE and test P–δ curves is provided in Fig. 28, giving maximum errors of nearly 5% for both modelling conditions.

The mode mixities for the two reported conditions were superimposed on the plot of Fig. 26, further reinforcing the linear extrapolation assumption of G_n^c and G_s^c, as the new data fitted perfectly on the proposed linear relationship. From the global results, the authors concluded that the proposed procedure accurately described the fracture behaviour of mixed mode joints, showing the advantage of non-requirement of two separate tests as it is usually performed (e.g., DCB for tension and ENF for shear characterization).

Static Applications of Cohesive Zone Models

The majority of CZM studies relate to static applications. Concerning bonded joints, Yang et al. (1999) used a CZM, within the continuum framework, to simulate a pure tensile fracture in bonded DCB and T-peel joints, not specifying the adhesive used. A trapezoidal CZM law was employed to simulate the adhesive bond behaviour (Fig. 29).

The authors concluded that G_n^c (Γ_0 in Fig. 29) and t_n^0 (σ_c in Fig. 29) are the dominant parameters in the FE analyses, while the two shape parameters δ_n^0/δ_n^f

Fig. 29 Trapezoidal
traction–separation law in
tension of Yang et al. (1999)

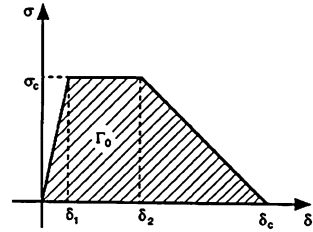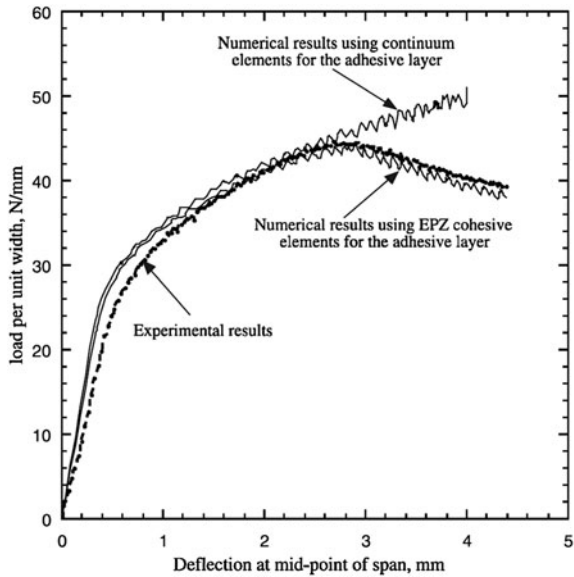**Fig. 30** Experimental and
numerical load–deflection
plot for the ENF test (Yang
et al. 2001)

(δ_1/δ_c in Fig. 29) and δ_n^s/δ_n^f (δ_2/δ_c in Fig. 29) have a marginal influence on the results. As a result, the shape parameters were arbitrarily fixed at $\delta_n^0/\delta_n^f = 0.15$ and $\delta_n^s/\delta_n^f = 0.5$, while G_n^c and t_n^0 were fitted by an inverse method between the experimental and FE data of the DCB specimens. By testing the proposed CZM law at varying conditions, the authors assumed that it could be used to predict the tensile fracture of different test geometries.

The same authors considered an identical trapezoidal CZM law (Fig. 29) for elastic–plastic crack growth modelling in shear by the continuum approach of a $t_A = 0.4$ mm ductile adhesive bond of Ciba® XD4600, considering the ENF test (Yang et al. 2001). The value of G_s^c was determined with a trial and error inverse procedure, by comparing the experimental and FE data for one particular set of dimensions. The two shape parameters, δ_s^0/δ_s^f and δ_s^s/δ_s^f, were arbitrarily equalled to 0.15 and 0.5, respectively, because of numerical evidence that their effect on the fracture process was not significant.

t_s^0 was estimated by the assumption that in the ENF tests performed, the local strains at the crack tip were approximately 40%. Using the shear stress–shear strain $(\tau - \gamma)$ experimental curve of the adhesive obtained by torsion tests of adhesively-bonded butt joints, the value of $t_s^0 = 35$ MPa was found for $\gamma = 40\%$, and thus it was used in the subsequent analyses. Fitting of the experimental and FE $P–\delta$ curves for one specimen is presented in Fig. 30. Results from a FEM calculation using only the continuum properties of the adhesive bond with no failure criterion were superimposed in Fig. 30, showing that the deformation behaviour of the specimen is only accurately captured until crack initiation, rendering the results invalid for crack propagation. The obtained values of G_s^c and t_s^0 were used to simulate fracture in ENF specimens with different values of t_P, and an excellent correlation to equivalent experiments was found. Therefore, the proposed CZM law was considered appropriate for the selected value of t_A and strain rate of the ENF tests. The authors also emphasized on the large difference of the CZM parameters for tension and shear loadings, justifying the use of mode dependent CZM relations to analyze the mixed mode fracture of bonded structures.

Yang and Thouless (2001) simulated the mixed mode fracture of plastically deforming asymmetric T-peel specimens and single lap joints using a mode-dependent CZM to simulate the adhesive bond (Ciba® XD4600), equally by a continuum modelling approach. Tension and shear fracture parameters obtained from previous works were combined with mixed mode propagation criteria to provide quantitative predictions of the deformation and fracture load of bonded structures under a mixed mode loading. Tension and shear CZM laws, previously developed for this adhesive in the works of Yang et al. (1999), (2001), respectively, were used without modification with an energetic propagation criterion similar to that of Eq. 7. Since experimentally both evaluated geometries undergo adhesive failures, the shear CZM parameters from the work of Yang et al. (2001) were used, since in this work adhesive failures also occurred in the ENF specimens tested. However, tension CZM parameters from the work of Yang et al. (1999) were not considered to be reliable, as they related to cohesive failures. Consequently, these were determined by the wedge test on adhesively bonded DCB specimens. Interfacial crack growth was induced placing a Teflon® strip prior to specimen curing.

For the T-peel specimens, the FE results matched well the experiments in terms of $\sigma–\delta$ curve, strains and rotations, extent of fracture and asymmetry of bending (Fig. 31). For the single lap joints, the FE simulations accurately predicted the load-deformation behaviour of the joints, capturing the influence of t_P on the fracture loads and strains. All relevant features of the deformed shapes, loads, displacements and crack propagation were well captured by the simulations.

Kafkalidis and Thouless (2002) performed a FE analysis of symmetric and asymmetric single lap joints using a continuum CZM approach that included the adhesive plasticity by means of trapezoidal CZM laws. The CZM laws, propagation criterion and analysis procedure were similar to those of Yang and Thouless (2001). Using CZM parameters determined for the particular combination of materials used, the FE predictions for different bonded shapes (varying the overlap length and t_P) showed excellent agreement with the experimental observations.
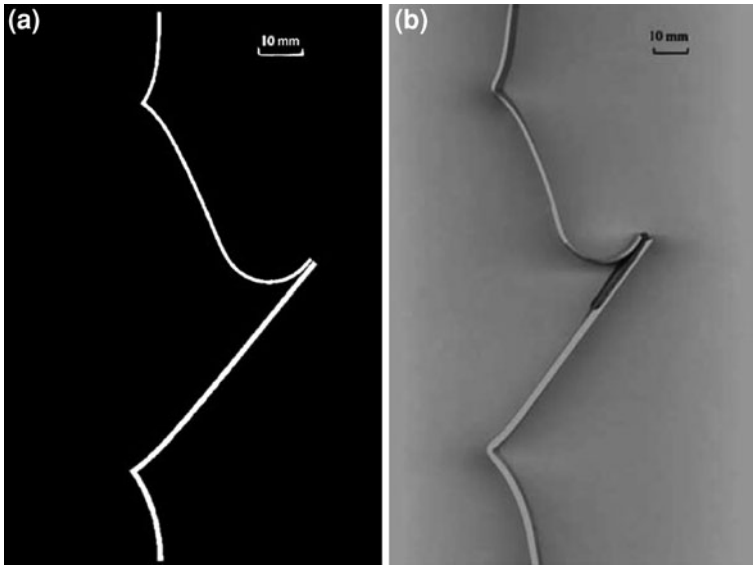
Fig. 31 Comparison between the FE predictions and experimental observations of an asymmetrical T-peel specimen (Yang and Thouless 2001)

Fig. 32 Experimental and FE single lap joint strength as a function of the overlap length for symmetric specimens (Kafkalidis and Thouless 2002)
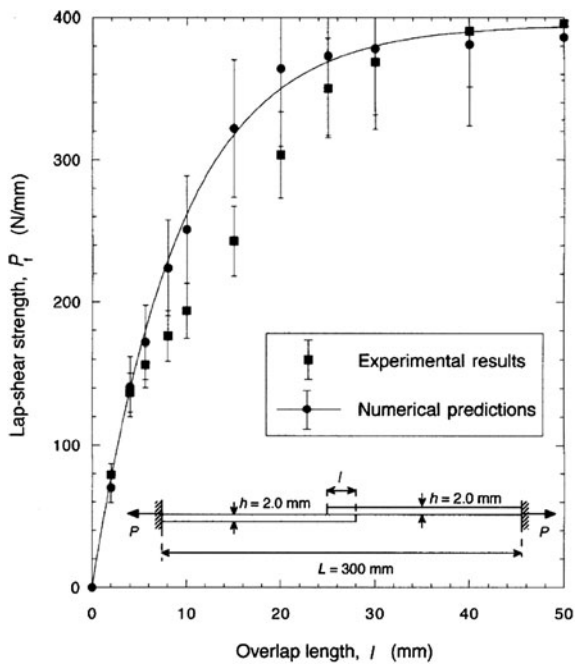
Fig. 33 FE deformation sequence and crack growth in an asymmetric single lap joint (Kafkalidis and Thouless 2002)
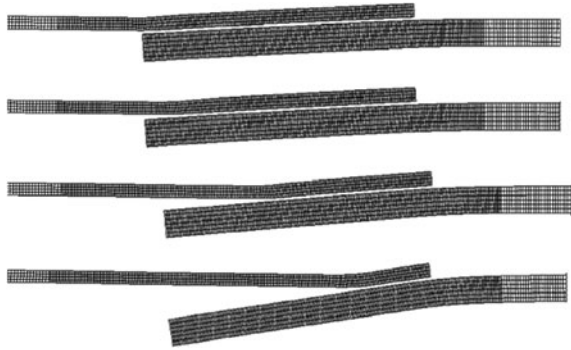
Figure 32 compares the measured and FE peak load values for a series of symmetric single lap joints with $t_P = 2.0$ mm aluminium adherends bonded with a $t_A = 0.25$ mm bond of Ciba® XD4600.

The slight discrepancies on the predicted strengths of Fig. 32 were justified by the sensitivity of the joint behaviour to the boundary conditions. In fact, the experimental configuration results in a slight misalignment of the grips, which was not accounted for in the simulations. Figure 33 shows the FE predictions for the sequence of deformation and crack growth in an asymmetric joint with a t_P ratio of two, which was consistent with the experimental behaviour. Overall, the FE models predicted accurately the failure loads, displacements and deformations of the joints.

A few parametric studies on bonded joints or repairs are also available that use CZM's for optimization of the geometry (Campilho et al. 2009b), or evaluation of geometrical modifications to the adherends or adhesive bond to increase their load bearing capabilities (Campilho et al. 2008b). The analysis of Karac et al. (2011) extends the typical applications of CZM's to rate dependent simulations (local approach), by using an implicit finite volume method coupled to the CZM analysis. In the work of Crocombe et al. (2006), a local CZM with a triangular shape was developed to predict the strength of environmentally degraded adhesively bonded single lap joints. Apart from the CZM parameters, the model included two moisture dependent fracture parameters, all of these experimentally calibrated by mixed-mode flexure (MMF) tests. The mechanical diffusion events were also implemented within Abaqus®, resulting on overall accurate predictions of the degraded strength of the joints.

Campilho et al. (2009a) experimentally tested carbon-epoxy scarf repairs in tension, using scarf angles between 2 and 45°, considering CZM's for the strength prediction. To account for the ductile behaviour of the adhesive (Huntsman Araldite® 2015), a trapezoidal CZM including the adhesive plasticity was used. The cohesive laws of the adhesive layer—continuum approach—and composite interlaminar and composite intralaminar (in the transverse and fibre direction)—local approach—necessary to replicate numerically the experimental failure paths, were previously characterized with DCB and ENF tests for tension and shear, respectively, using an inverse methodology. Validation of the proposed model

Fig. 34 Layout of cohesive elements with different CZM laws in the scarf repair FE models (Campilho et al. 2009a)

Fig. 35 Type B failure for a 3° scarf angle repair: experimental fracture surfaces (**a**) and FE prediction (distorted image for a clear visualization) (**b**) (Campilho et al. 2009a)

with experimental data was accomplished in terms of global stiffness, strength and corresponding value of δ, and failure mode. The layout of cohesive elements in the models is depicted in Fig. 34.

The adhesive representative elements were inserted along the scarf replacing the adhesive bond, the interlaminar elements were positioned between different oriented plies, the transverse intralaminar elements were used vertically in the 90° plies to simulate intralaminar matrix cracking, and the fibre elements were placed vertically in the 0° plies to simulate fibre cracking. Two distinct failure modes were experimentally observed: types A and B failures. Type A failure was observed for the repairs with 15°, 25° and 45° scarf angles, consisting on a cohesive failure of the adhesive. Type B failure occurred for the scarf angles of 2°, 3°, 6° and 9°, representing a mixed cohesive and interlaminar/intralaminar failure (Fig. 35). A detailed discussion for this failure mode modification was provided, based on a stress analysis of the repairs. The CZM simulations accurately reproduced the experimental fracture modes, and the failure mode modification
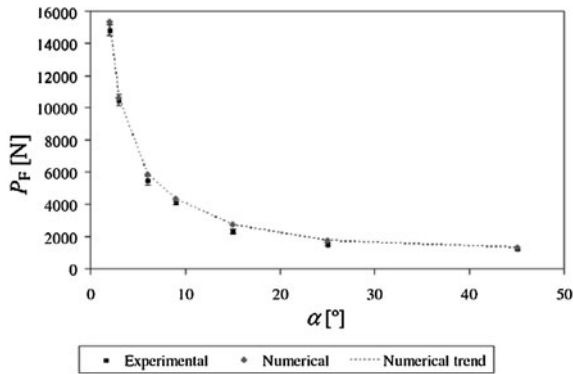
Fig. 36 Experimental and FE strength of the scarf repairs as a function of the scarf angle (Campilho et al. 2009a)
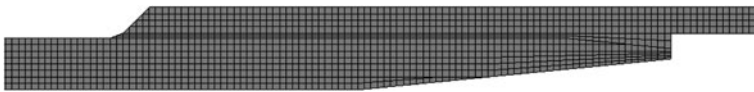

Fig. 37 Single strap repair combining a 45° fillet with adherend inner and outer chamfering (Campilho et al. 2009c)

between types A and B, showing the effectiveness of CZM modelling for static applications.

Figure 36 reports the strength results, showing an exponential increase with the reduction of the scarf angle, related to the increase of available shear area for load transfer between the adherends and the patch, accompanied by a reduction of peel stresses along the scarf length.

Generally, experimental and FE results showed a good agreement on the global elastic stiffness, strength and respective value of δ, although the latter exhibited some variations, which was imputed to difficulties on the attainment of the selected value of t_A during the fabrication of the specimens. On account of the described results, the authors concluded that CZM's can be successfully applied to predict the mechanical behaviour of bonded structures.

The FE study of Campilho et al. (2009c) addressed the tensile strength optimization of carbon-epoxy single and double strap bonded repairs by geometric modifications at the overlap. CZM's were considered for local modelling of the adhesive, i.e., to provide crack growth, whilst the ductile adhesive bond (Huntsman Araldite® 420) was modelled by solid FE elements. Validation of the procedure was initially accomplished with experimental results from the literature. The following techniques and respective combinations were tested: chamfering the patch outer and inner faces at the overlap ends, plug filling the adherends gap with adhesive, use of fillets of different shapes and dimensions at the patch ends, and chamfering of the outer and inner adherend edges. For single strap repairs, the 45° fillet (accounting for the entire patch thickness), and adherend inner and outer
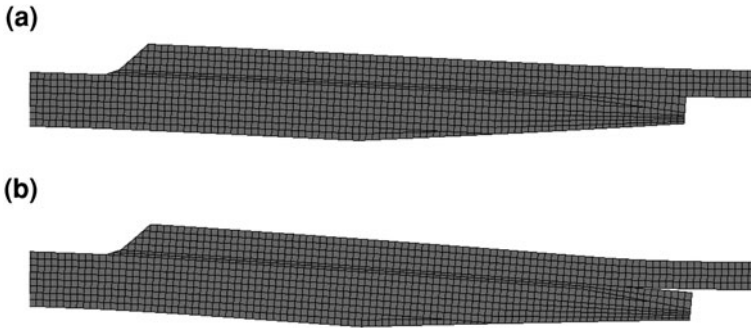
Fig. 38 Deformed configuration of the repairs for stiff (**a**) and compliant adherends (**b**) for the same value of prescribed load (Campilho et al. 2009c)

chamfering were the most effective solutions. By the combination of these three modifications (Fig. 37), an overall strength improvement of nearly 27% was attained.

For the double strap repairs, a 12% strength improvement was achieved by consideration of a 45° fillet and plug filling the adherends gap. Parametric studies were also performed regarding the adherend/patch lay-ups and the adherend gap effects on the predicted strength. For the single strap geometry, the adherends lay-up revealed a particular significance because of its influence on the repairs transverse flexure. Lay-ups with load-oriented plies at the adherend free surfaces were recommended on account of the reduction of peel stresses. Figure 38a reports to stiff and b to compliant adherends under a similar applied load, showing crack growth only for the compliant adherends repair because of higher peel stresses.

The double strap results showed a negligible perturbation on strength because of the adherends flexure elimination. On the other hand, the repairs were only affected by the adherends gap for values smaller than 5 mm. A progressive strength reduction was found below this value because of localized stress concentrations at the overlap edges. In the end, design principles were proposed for the strength improvement of adhesively bonded repairs on composite structures.

Fatigue Applications of Cohesive Zone Models

A large number of analytical and FE predictive techniques for the fatigue life in bonded joints have been proposed over the years. However, each one of these suffers from specific limitations in their functionality and applicability (Shenoy et al. 2010a). The fatigue strength prediction with CZM's is a recent possibility, under intense investigation in the last 5 years (Munoz et al. 2006; Turon et al. 2007a). Fatigue CZM's can be a valuable tool for the design of bonded joints by the safe-life prediction under various loading conditions. Implementation of

fatigue CZM's in FE softwares is also time and cost efficient, enabling designers to reduce experimental testing to a minimum (Khoramishad et al. 2010). Important issues possible to account for with fatigue CZM's are the accurate prediction of cyclic damage initiation, and the inclusion of fatigue life-time prediction, because under cyclic loads either one of these phases can be dominant depending on the specimens geometry, materials, load range and testing/loading conditions. However, the main advantage of CZM's for modelling fatigue crack growth is that damage initiates within un-cracked structures when the cyclic cohesive stresses exceed a pre-determined critical value (Moroni and Pirondi 2011).

With this purpose, the static formulation of CZM's, generically described in "Triangular Cohesive Zone Model", is adjusted to account for fatigue damage. In fact, for cyclic loadings, damage is not only dependent on the relative separations, δ_n and δ_s, but also on the load cycle count. An associated limitation to some fatigue CZM formulations is the geometry dependency, which restrict the applicability of the models to specific test specimens (Khoramishad et al. 2010). Regarding the CZM approach, continuum modelling is often selected for fatigue and, thus, this information will be neglected in the following references.

A few lines of analysis for fatigue applications are currently under development: (1) a cycle-by-cycle analysis for the damage progression (Roe and Siegmund 2003; Abdul-Baqi et al. 2005; Maiti and Geubelle 2005), (2) cyclic extrapolation techniques (Turon et al. 2007b) and (3) analysis based on the maximum fatigue load (Robinson et al. 2005; Tumino and Cappello 2007). The second and third approaches are less demanding in which regards to computational resources, whilst the former allows a more precise damage evolution to be implemented, predicting more accurately features such as crack growth retardation after overload (Roe and Siegmund 2003), although not being viable for high cycle fatigue (Khoramishad et al. 2010).

The cycle-by-cycle fatigue CZM (i.e., 1st approach) proposed by Maiti and Geubelle (2005) for crack growth in polymeric materials was upgraded from a static CZM identical to that of "Triangular Cohesive Zone Model", considering an evolution law relating the cohesive stiffness, the rate of crack opening displacement and the cyclic count from the onset of failure. The fatigue component relied on two parameters that were easily defined from the Paris curve, between the crack growth per cycle and the range of applied stress intensity factor. A different route was undertaken by Roe and Siegmund (2003), which simulated the crack growth at an interface by a fatigue CZM that incorporated a cycle-by-cycle simulation (thus, still within the scope of the described 1st approach) where damage was incremented according to the stress level attained in the previous cycle. In these two works, the main handicap was the fatigue parameters calibration, performed by experiment/FE comparisons, added to the aforementioned limitations related to the limited applicability to different geometries and high cycle fatigue.

The proposed fatigue CZM of Turon et al. (2007b), following the second described line of analysis for fatigue crack modelling of composites, does not require calibration of the fatigue parameters, solely requiring the static CZM parameters and the Paris-like law coefficients from fatigue crack growth tests.
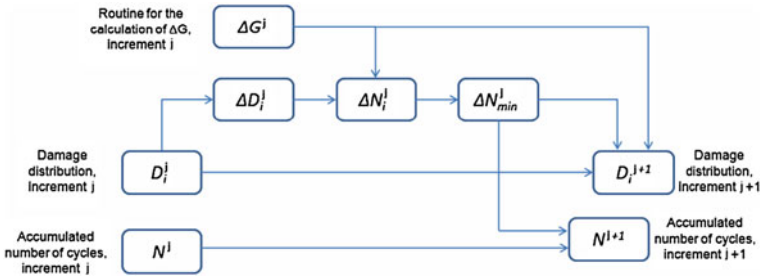
Fig. 39 Schematic representation of the algorithm used for the crack growth simulation (Moroni and Pirondi 2011)

However, the proposed formulation is restricted to test geometries in which G can be computed analytically and it is independent of a during the test, such as in the DCB test.

The work of Moroni and Pirondi (2011) followed the same principle to simulate fatigue crack growth in bonded joints with aluminium adherends (the adhesive was not specified). A fatigue CZM was implemented by the authors in Abaqus® based on the static formulation of "Triangular Cohesive Zone Model", more specifically in Eq. 6, for damage nucleation, whilst the Benzeggagh–Kenane (1996) criterion was considered for damage propagation, instead of the energetic criterion of Eq. 7. The crack growth rate was evaluated and implemented in the CZM with three Paris-like power laws proposed in the literature, but all of them expressed in terms of the current value of G: (1) the Kenane and Benzeggagh theory (Benzeggagh and Kenane 1996), in which the crack growth law parameters depend on the mixed mode ratio by two constitutive equations, (2) the model of Quaresimin and Ricotta (2006), requiring an equivalent G parameter, defined as the driving parameter for crack growth and making the crack growth law parameters independent of the mode mixity (consequently, they could be defined from a pure mode fatigue crack growth test and subsequently applied to varying mode mixity conditions) and (3) a simplification of the Wahab et al. (2002) model, which established the crack growth rate as a function of the tension and shear components (each one defined by the respective pure mode fatigue parameters).

The fatigue CZM algorithm (Fig. 39) was implemented in Abaqus® by user sub routines for each crack growth rate criteria. The cyclic load was initially divided in increments with a finite number of cycles. For each increment (defined as increment j), the number of accumulated cycles from the beginning of the analysis is expressed as N^j, and the respective damage for each integration point under analysis (i) is equal to D_i^j. After, an incremental damage within the analysis increment (ΔD_i^j) is established for each integration point from the smaller value between the increment needed to reach $D = 1$ (failure) and a user-defined value ΔD_{max}.

Fig. 40 CZM prediction and analytical comparison of *a* versus cycle count for the MMELS test and Paris-like law (1) (Moroni and Pirondi 2011)
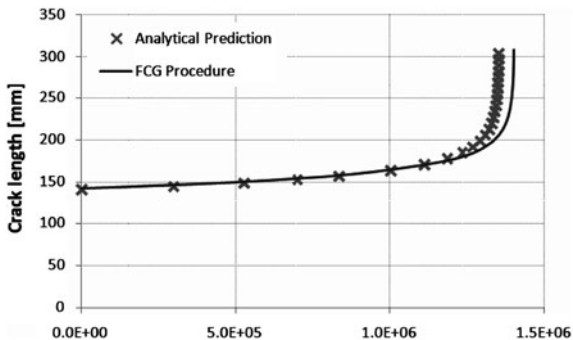
$$
\begin{aligned}
\Delta D_i^j = \Delta D_{\max} &\quad \text{if} \quad 1 - D_i^j > \Delta D_{\max} \\
\Delta D_i^j = 1 - D_i^j &\quad \text{if} \quad 1 - D_i^j < \Delta D_{\max}
\end{aligned}. \tag{8}
$$

Concurrently with ΔD_i^j, the user subroutine calculates ΔG as the *J*-integral over a path around the cohesive zone. To represent a cyclic loading between a minimum load $F_{\min}$ and a maximum load $F_{\max}$, the simulation is initially analysed with $F_{\max}$ and the respective maximum applied strain energy release rate $G_{\max}$ is defined. The value of ΔG is obtained using $R = F_{\min}/F_{\max}$ by

$$
\Delta G = \left(1 - R^2\right) G_{\max}. \tag{9}
$$

The number of cycles for the current increment, ΔN_i^j, is selected from the minimum value of all CZM element integration points ($\Delta N_{\min}^j$). The number of cycles (N^{j+1}) and the damage distribution (D^{j+1}) are finally updated and the analysis jumps to the next increment. The described model was tested by different geometries: in pure tension by the DCB specimen, in pure shear by the ELS test, and under mixed mode loading with a mixed mode ELS (MMELS) test. For the pure mode tests, the *a* versus cycle count predictions were extremely accurate and independent of the Paris-like law employed.

As for the mixed mode results by the MMELS test, the crack growth rate calculations differs between models (Fig. 40 shows results for model (1)). However, for all models the implemented algorithm was able to correctly model the crack growth prediction reported by the reference analytical models.

Robinson et al. (2005) followed the third line of analysis, by implementation of a cumulative damage model based on the maximum fatigue load within a static CZM. However, for the proposed formulation, the fatigue parameters were not independent of the mode mixity. As a result, these parameters required calibration for each testing conditions. A couple of years later, Tumino and Cappello (2007) partially solved this limitation by making the fatigue parameters dependent on the mode mixity. However, the proposed model became quite complicated because of

the numerous parameters of the fatigue model and cumbersome calibration process.

Khoramishad et al. (2010) developed a fatigue CZM for adhesively bonded joints with 2024-T3 aluminium adherends and the adhesive FM® 73 M OST (Cytec). The model was based on the maximum fatigue loading conditions (third line of analysis described) that are independent of the joint geometry, relying only on the adhesive system. Triangular damage laws were considered, and a strain-based fatigue damage model was developed and coupled to a static CZM for simulation of the fatigue influence on the structures behaviour. Two different configurations, bonded with FM® 73 M OST (Cytec) toughened epoxy film adhesive and with the same adhesive system, were experimentally tested—single lap joints in tension and laminated doublers in bending—giving different stress states and mode mixities. The development and calibration of the proposed fatigue model were carried out for the single lap joint tests, which was subsequently applied without any modification to the doublers in bending. Static tests were initially performed on both geometries for the definition of the static CZM parameters. The static CZM was tuned by an iterative technique to match the experimental responses, similar to that described in "Inverse Method". Whilst the static CZM principles were identical to those described in "Triangular Cohesive Zone Model", different criteria were considered for damage initiation and propagation: contrarily to Eq. 6, damage onset was predicted when either t_n or t_s exceeded the critical value (t_n^0 or t_s^0, respectively); contrasting to the linear energetic criterion for crack growth depicted in Eq. 7, the Benzeggagh–Kenane criterion was used, where η represents a material property.

$$G_n^c + \left(G_s^c - G_n^c\right) \cdot \left(\frac{G_s}{G_n + G_s}\right)^\eta = G_n + G_s. \tag{10}$$

Fatigue tests were subsequently carried out at 5 Hz and $R = 0.1$. For the assessment of damage evolution in the adhesive bond during fatigue loading, the back-face strain technique and in situ-microscopy were used. The back-face strain data was afterwards used for validation of the CZM by comparison to the predicted back-face strains. Fatigue damage simulation was implemented by degradation of the CZM response. A fatigue damage parameter was established, which evolved during the cyclic loading, based on the following damage evolution law

$$\frac{\Delta D}{\Delta N} = \begin{cases} \alpha(\varepsilon_{\max} - \varepsilon_{\text{th}})^\beta, & \varepsilon_{\max} > \varepsilon_{\text{th}} \\ 0, & \varepsilon_{\max} \leq \varepsilon_{\text{th}} \end{cases}, \tag{11}$$

with

$$\varepsilon_{\max} = \frac{\varepsilon_n}{2} + \sqrt{\left(\frac{\varepsilon_n}{2}\right)^2 + \left(\frac{\varepsilon_s}{2}\right)^2}. \tag{12}$$

ΔD is the increment of damage, ΔN is the cycle increment, $\varepsilon_{\max}$ is the maximum principal strain in the cohesive element (combination of the normal and shear

Fig. 41 Fatigue degradation of cohesive element properties (Khoramishad et al. 2010)
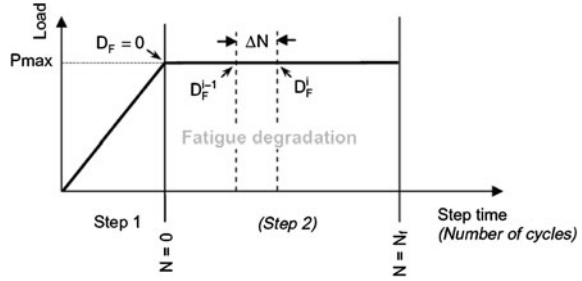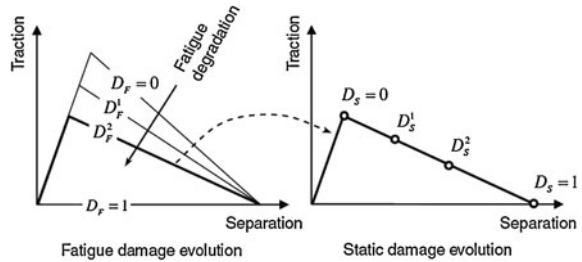

Fig. 42 Fatigue damage (D_F) and traction–separation response damage (D_S) parameters (Khoramishad et al. 2010)


components of strain, ε_n and ε_s), $\varepsilon_{\mathrm{th}}$ is the threshold strain (a critical value of $\varepsilon_{\max}$ below which no fatigue damage occurred) and α and β are material constants. Calibration against the test data was required for the parameters $\varepsilon_{\mathrm{th}}$, α and β. The defined number of fatigue cycles in each increment resulted in fatigue damage, which was established by the numerical integration of the cyclic damage rate of Eq. 11, depending on the cyclic count of the current increment and $\varepsilon_{\max}$. As specified in this equation, fatigue damage only occurs if $\varepsilon_{\max} > \varepsilon_{\mathrm{th}}$.

Implementation of the fatigue damage was carried out by artificial degradation of the CZM response through the reduction of t_n^0 and t_s^0 (Fig. 41). Fatigue crack growth was divided into two steps: (1) a static CZM analysis was carried out considering the maximum fatigue load, using the static damage variable D_S and providing the stress/strain state at the beginning of the fatigue test, and $\varepsilon_{\max}$ was calculated for all cohesive elements (Eq. 12); and (2) a cyclic damage variable (D_F; Fig. 41) was established at each integration point of the cohesive elements, which was numerically integrated according to Eq. 11 in each increment, corresponding to a specified value of ΔN. The values of t_n^0, t_s^0, G_n^c and G_s^c were then linearly reduced proportionally to D_F (Fig. 42). The increment-by-increment implementation of this process, with the individual calculation of ε and D_F until the structure no longer sustains the maximum fatigue load, gave the predicted fatigue life. An iterative data fitting approach was undertaken for the single lap joint results to determine appropriate fatigue model parameter values for the particular adhesive system selected for the tests.

Validation was performed against the bonded doublers in bending (Fig. 43), giving an accurate correlation to the experimental data. Further validation was

Fig. 43 Load-life fatigue data and respective FE predictions for the single lap tests and doublers in bending (Khoramishad et al. 2010)
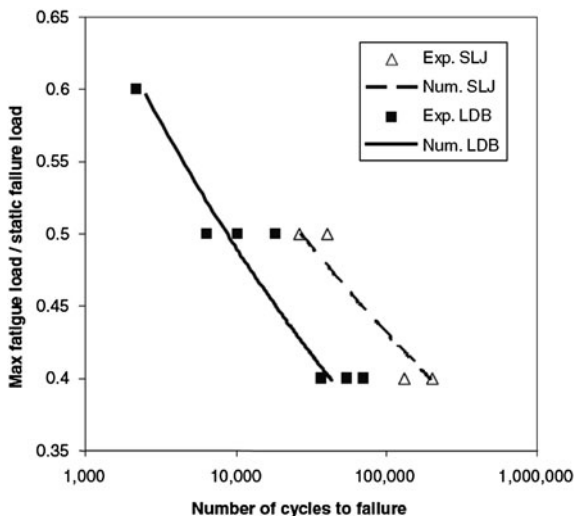
accomplished comparing the FE back-face strains with the test measurements from the undamaged state up to complete fatigue failure, equally giving a precise match.

2.4.2 Alternative Approaches to Cohesive Zone Modelling

This section describes ACDM techniques, i.e., other than CZM modelling, which can be categorized within the continuum framework if modelling finite volumes of material. In these methodologies, a damage parameter is established to modify the constitutive response of materials by the depreciation of stiffness or strength, e.g. for thin adhesive bonds (Khoramishad et al. 2010), or composite delaminations or matrix failure (Daudeville and Ladeveze 1993), to represent the severity of material damage during loading. This state variable can be used in a damage evolution law to model both pre-cracking damage uptake and crack growth. The damage variables can be categorized under two main groups: (1) variables that predict the amount of damage by the redefinition of the material constitutive properties but that do not directly relate to the damage mechanism, and (2) variables linked to the physical definition of a specific kind of damage, such as porosities or relative area of micro-cavities (Voyiadjis and Kattan, 2005). The second group for damage variables is based on macroscopic material properties whose evolution is governed by a state equation. In all cases, different damage mechanisms concurrently occurring in a material can be accounted for in the models, each of them by an independent damage variable. By ACDM, the growth of damage is defined as a function of the load for static modelling (Raghavan 2005) or the cyclic count for fatigue analyses (Wahab et al. 2001; Imanaka et al. 2003). Generic ACDM models for bulk materials are available in the literature (Lemaitre and Desmorat 2005), and respective modifications for particular kinds of

damage modelling, e.g. damage nucleation from voids and the formation of micro cracks (Gurson 1977; Tvergaard and Needleman 1984; Kattan and Voyiadjis 2005). ACDM's have also been used to numerically model scenarios of constant and variable amplitude fatigue (Bhattacharya and Ellingwood 1998). For bonded joints, little work is published in this field. Compared to fatigue CZM's, ACDM techniques do not provide a clear distinction between fatigue initiation and propagation phases, although they can give a basis for the predictive analysis (Khoramishad et al. 2010). Nonetheless, the evolution of damage prior to macro-crack growth can be simulated. On the other hand, damage modelling with fatigue CZM's is restricted to pre-defined crack paths and, on specific applications, ACDM's may be recommended if the damage is more widespread or the failure path is not known (Shenoy et al. 2010b).

Static Applications of Alternate Continuum Damage Mechanics

A few works are currently available using phenomenological ACDM techniques for static failure of structures, by the inclusion of one or more state variables affecting the macroscopic constitutive response of materials up to failure (Lemaitre and Chaboche 1985; Lemaitre 1986). The work of Sampaio et al. (2004) focused on the static strength prediction of butt adhesive joints of aluminium adherends bonded with a thin epoxy adhesive bond (Dow® DH331) by an analytical ACDM model accounting for the value of t_A. The model combined a relatively straight-forward mathematical background with the possibility to describe complex non-linear mechanical behaviour of bonded joints, including strain softening and size effects. The model was built on the assumption of two elastic bars (aluminium adherends) and a damageable bar to model the adhesive bond, considering an approximation of the 3D fracture behaviour to a 1D and equivalent ACDM model with a one-material homogeneous bar. An energy based formulation was estab-lished as a function of the axial strain, ε, and an auxiliary damage variable, D, was associated with the dissipative mechanism of failure to account for the reduction of elastic energy. To account for t_A effects in bonded joints, a quadratic energy function was defined based on previous experimental evidence. For validation of the model, the predicted values of failure stress were plotted against experimental data for different values of t_A, giving accurate representations of the tests and a decreasing strength of the butt joints with t_A up to a bulk representative constant value.

Hua et al. (2008) proposed a mesh-independent ACDM model for strength prediction of adhesively bonded joints under environmental degradation. Joints bonded with a ductile adhesive (Hysol® EA9321) were studied for different sce-narios of environmental degradation. This was performed by introducing a dis-placement-based damage parameter into the constitutive equation of damaged materials that was moisture-dependent, calibrated using the MMF test on aged specimens. The damage parameter allowed a linear function of the material response in the absence of damage to be established, giving a depreciated value of

Fig. 44 Failure progress for MY750 adhesive/steel single lap joints; (**a**) schematic failure step by step obtained numerically; (**b**) crack patch observed in the experiments (Chen et al. 2011b)
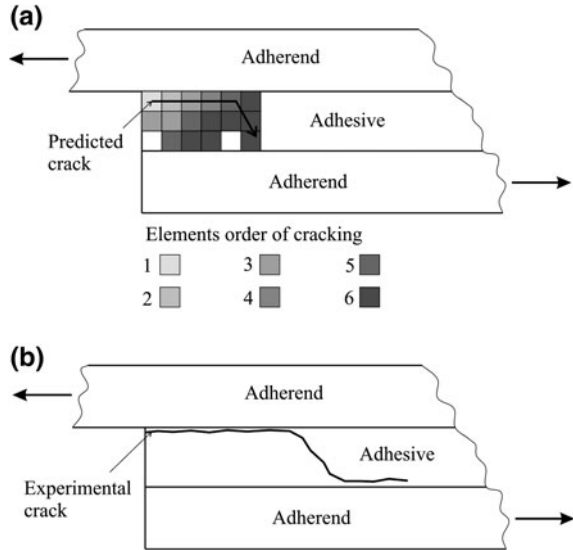
the actual stresses, depending on the equivalent plastic displacement rather than strain, to ensure mesh independent results. The implementation of this concept required the definition of an equivalent length, linked to each solid element integration point. The equivalent plastic displacement was calculated from the energy to rupture as the fracture work of the yield stress after the onset of damage.

The ACDM used by Hua et al. (2008) is currently implemented in Abaqus® (Abaqus® Documentation 2009), and it also included the required mechanical-diffusion models and the elastic–plastic response of the adhesive and adherends, both of these obtained from bulk tensile tests. For each one of the aging conditions, the respective damage parameter was then directly applied to model failure in single lap joints with aluminium and carbon-epoxy adherends, bonded with the same adhesive. A von Mises yield model was considered for the adhesive bond. The joint strength predictions and the respective damage propagation pattern matched well the experimental data, showing that the developed ACDM provided a means of predicting environmental degradation in ductile bonded joints, where failure is predominantly within the adhesive bond.

Chen et al. (2011b) used the average plastic strain energy to predict crack initiation and propagation in single lap joints, and also the failure load by an ACDM technique. Two adhesives were used, Ciba® MY750 (diglycidyl ether of bisphenol A) with hardeners HY906 (anhydride) and the same adhesive rubber-toughened with carboxyl terminated butadieneacryl (CTBN). These adhesives are designated by MY750 and CTBN, respectively, in the present description. This physical fracture process was simulated by a FE analysis as follows. When a converged solution was obtained after each applied load increment, a check was made to see whether the failure condition had been attained anywhere in the joint. Under these conditions, the values of E and Poisson's ratio (v) of the material

Table 1 Failure loads (in kiloNewton) for CTBN (ductile adhesive) bonded joints (Chen et al. 2011b)

Case	Exp. failure load	Standard deviation	Numerical failure load	Difference	Error (%)
cst	9.51	0.53	9.54	0.03	0.3
csftc	11.03	0.52	10.44	−0.59	−5.3
clt	11.80	0.25	12.00	0.20	1.7
clftc3	12.51	0.41	12.45	−0.06	−0.5
clftc1	15.65	1.51	15.00	−0.65	−4.2
cbt	8.76	0.73	10.08	1.32	15.1
cbftc	11.08	1.19	10.80	−0.28	−2.5

cst steel without fillet; csftc steel with fillet; clt 2L73 aluminium without fillet; clftc3 2L73 with defective fillet interface; clftc1 2L73 aluminium with small defect in fillet; cbt 2024 TB aluminium without fillet; cbftc 2024 TB aluminium with fillet

Fig. 45 Progressive damage algorithm of Liu and Wang (2007)
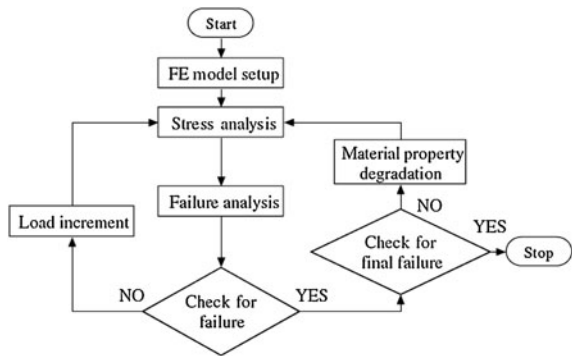
within the failed region were reset to zero (or near zero), such that it could deform almost freely without transferring any load. The stresses within this region were also reset to zero and then the whole system of equations (stiffness) was reassembled and solved. This FE model thus accounted for damage by voiding the cracked elements. All the checking and property depreciation were implemented in the FE program and done automatically. A new load increment was not applied until the damage process had stopped.

The comparison between experimental and FE predicted failure loads showed that the specific energy criterion used was fairly successful for fracture prediction, as shown in the example of Fig. 44, related to the MY750. All the FE fracture analyses were based on the most realistic conditions: all considered the large displacements theory; all materials were treated elasto-plastically based on their experimental σ–ε curve. The experimental failure loads compared very well with the experimental results with or without a fillet of adhesive as shown in Table 1 for the case of a ductile adhesive (CTBN).

The work of Liu and Wang (2007) presented an experimental and ACDM study of 3D double strap bonded repairs under a tensile load, using carbon-epoxy laminates and patches. A $[(0/90/ \pm 45/90/0)2]_S$ lay-up was considered for the laminate, and several quasi-isotropic lay-ups were tested for the patches. An epoxy

Fig. 46 Predicted strength versus experimental data of the double strap repairs (Liu and Wang 2007)
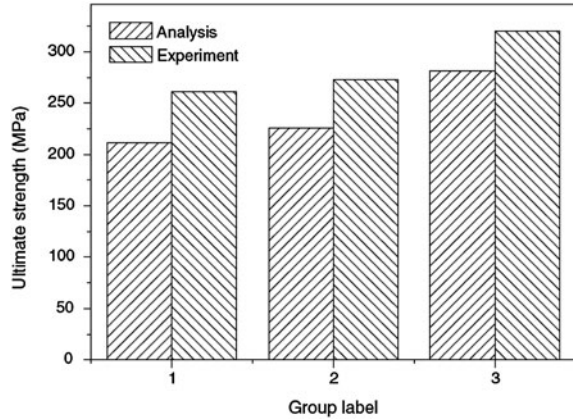
adhesive film with $t_A = 0.12$ mm was used. The implemented ACDM was based on the degradation of the continuum element properties when specified criteria were locally satisfied at a specified element. Different criteria were considered: (1) the Tsai-Wu criterion to predict fibre breakage and matrix cracking of the laminate and patches, (2) the Ye delamination criterion to detect delamination between plies and (3) the maximum shear stress criterion for adhesive bond failure. In the ACDM algorithm (Fig. 45), the analysis began with all material properties set to their initial values. Then, the failure criteria were applied to the structure in each incremental load step.

When each one of the criteria was attained at a specific element, the contribution of each stress component towards the failure index was assessed to identify which one contributes the most, allowing defining the dominant damage mechanism. The corresponding elastic properties, either of the composite or adhesive, were depreciated by multiplication with the stiffness reduction parameter, λ, which was previously estimated by extensive comparative studies, since it largely influences the strength and failure mechanism predicted by the ACDM. After the degradation procedure, the analysis then restarted without increment of load until no further damage was found in that step, or final failure of the structure was attained. A convergence study defined the optimal increment of load, corresponding to the best match between accuracy of the strength predictions and computational time to attain the solution.

Validation considered double strap repairs with different values of patch thickness and patch diameter, and three failure mode possibilities were introduced. In mode A, failure initiates in the adhesive bond, leading to patch debonding. The laminates then fractures transversely near the hole, causing catastrophic failure. In mode B, the patches fail to sustain the transmitted loads by the structure and split transversely. Almost simultaneously, the laminates fracture in an identical manner. Mode C failure is characterized by damage initiation at the singularity regions at the patch edges, growing to the laminate as transverse cracks.
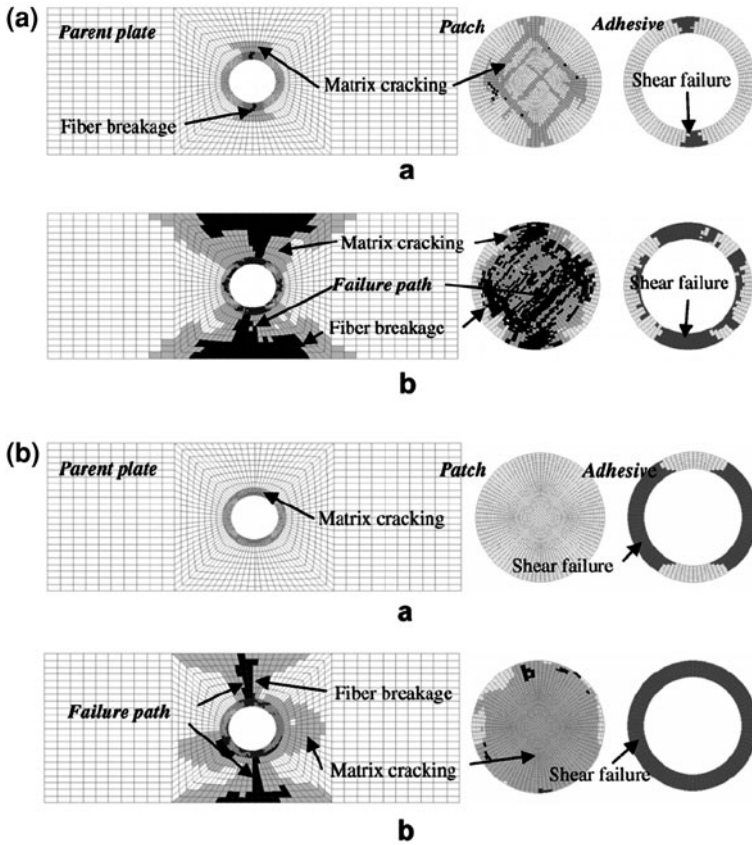
Fig. 47 ACDM failure process for group 1 (**a**) and group 2 (**b**) in two load stages (Liu and Wang 2007)

Figure 46 reports the good correspondence between the predicted strengths and the experiments (groups 1–3 relate to patch thickness of 0.3, 0.7 and 0.875 mm, respectively; patch diameter of 40 mm for groups 1 and 2, and 50 mm for group 3).

Group 1 specimens fractured experimentally by mode B, which was accurately captured by the numerical models (Fig. 47a), with almost simultaneous transverse fractures of the patch and laminate. This was substantiated by the reduced value of patch thickness and its inability to reinforce the laminate near the hole. Fracture for groups 2 and 3 corresponded to mode A, initiating in the adhesive bond, due to peel stress concentrations caused by the thicker patches. After losing the support of the patches, the laminate failed by transverse cracking initiating at the hole edges. This behaviour is consistent with the numerical analysis described earlier (Fig. 47b for group 2). From these results, it was possible to conclude that for the material and geometric parameters evaluated, the failure mode is ruled by the patch thickness. On the other hand, group 3 revealed the highest strength, justified by the

larger patch diameter. Since the average strength of groups 1 and 2 was similar, it is concluded that this parameter was ruled by the patch diameter. After validation of the ACDM methodology, the influence of several geometric parameters on the repairs strength and failure mode was further studied (patch diameter, patch thickness, patch lay-up and t_A), providing design principles for repairing bonded repairs of composite structures.

Fatigue Applications of Alternate Continuum Damage Mechanics

Fatigue ACDM applications are not as widespread as static implementations (Solana et al. 2010), although a few formulations were proposed recently. Wahab et al. (2001) compared fracture mechanics and ACDM approaches for fatigue life-time prediction of bonded double lap joints with carbon-epoxy adherends, showing that the proposed continuum model was more suited for constant amplitude fatigue than fracture mechanics. Variable amplitude fatigue was not addressed in this work, but there is ample evidence of damage or crack growth accelerations or decelerations occurring under variable amplitude due to load interaction effects, depending on the type of material (Shenoy et al. 2010b). Currently, scarce works are published on the effect of variable amplitude fatigue on bonded joints by ACDM.

Shenoy et al. (2010b) investigated the variable amplitude fatigue behaviour of single lap joints by ACDM, made of 7075 T6 aluminium adherends bonded with the epoxy adhesive film FM$^{®}$ 73 M (Cytec), considering various types of variable amplitude conditions. Significant load interaction effects were found by the application of the Palmgren–Miner law to the experimental data, showing that a smaller amount of fatigue cycles at higher fatigue loads gives a significant reduction in the fatigue life by accelerating damage growth. Two different lines of analysis were conducted for life prediction: fracture mechanics and ACDM. Two fracture mechanics-based techniques were tested, accounting for a different cycle counting procedure. Although these did not include load interaction effects, which could over predict the fatigue life if these were found to accelerate damage, the fracture mechanics results consistently under predicted the joints fatigue life for the entire range of fatigue spectra. This was because of the perceived inability of fracture mechanics models to account for the crack initiation phase that showed to be more dominant than the load interaction effects.

The ACDM approach used a relation between localised damage and plastic strain in an empirical continuum damage law, allowing modelling the initiation and propagation phases of the joints fatigue life, and also accounting for load history effects by the accumulation of incremental damage. The ACDM predicted the fatigue life within the experimental scatter, oppositely to the fracture mechanics techniques. However, further development of the formulation was proposed by the authors, concerning the form of the damage law used and respective implementation within the FE software. Nonetheless, the comparative analysis to the experiments made clear that ACDM techniques have great potential
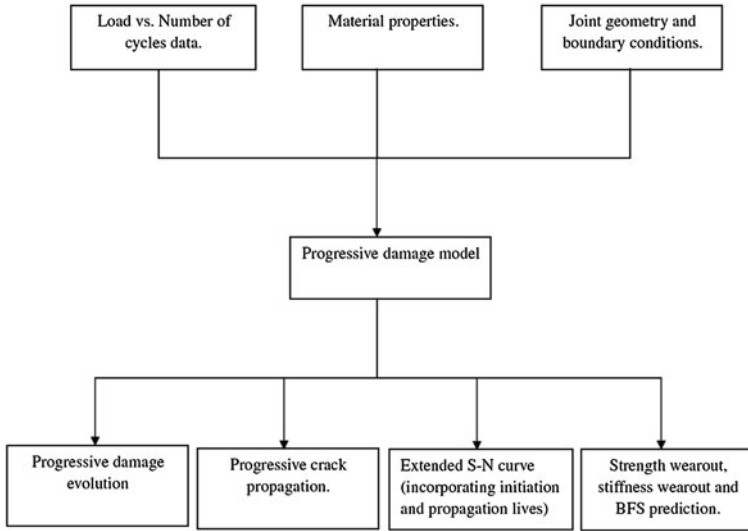
Fig. 48 Schematic representation of the proposed fatigue model (Shenoy et al. 2010a)

for predicting fatigue failure in bonded joints subjected to variable amplitude fatigue.

Shenoy et al. (2010a) presented a unified ACDM model to predict the fatigue failure of bonded joints, wherein the evolution of fatigue damage in the adhesive was defined by a power law function of the micro-plastic strain. Single lap joints were considered with 7075 T6 aluminium adherends and the adhesive Cytec FM$^{®}$ 73 M, including in the FE models the fillet radius emerging from the fabrication procedure. Fatigue testing was carried out at 5 Hz with $R = 0.1$. The ACDM was implemented by a sub routine in the MSC Marc FE software, aiming to propose a universal methodology that could be widely applicable.

In the described formulation, a single damage evolution law was implemented to predict all the main parameters characterising the fatigue life of bonded joints, i.e., the progressive evolution of damage, crack initiation and propagation lives, back-face strains up to failure, and strength and stiffness degradation. The fatigue model is schematically described in Fig. 48. The ACDM algorithm requires as input the material properties, joint geometry and boundary conditions, and a small number of test results for the fatigue life are also needed to estimate the damage evolution law parameters. A number of user implemented algorithms were then coupled to the FE analysis for the predictions. The rate of damage evolution was assumed to be a power law function of the localised equivalent plastic strain, i.e.:

$$\frac{dD}{dN} = m_1 (\varepsilon_P)^{m_2}, \tag{13}$$

where D stands for the damage variable ($D = 0$ for undamaged material; $D = 1$ for completely damaged material), N relates to the fatigue cyclic count, m_1 and m_2

are material parameters to be experimentally determined and ε_P is the localised equivalent plastic strain. ε_P was chosen for damage progression in the proposed approach to allow a means of inducing a set value of ε below which the structure does not sustain damage (wherever $\varepsilon_P = 0$). If the applied value of load is not high enough, the adhesive bond endures $\varepsilon_P = 0$ and, hence, no fatigue damage is accumulated because the load is below the endurance limit for the adhesive. Because of this, ε_P should be regarded as an endurance limit for a particular mesh, rather than an accurate measure of adhesive plasticity. Simulation of the damage evolution is performed by numerical integration of Eq. 13 over each element, which is followed by crack propagation when $D = 1$. By this algorithm, the number of cycles to failure can be calculated for different fatigue load conditions. A disadvantage of the methodology was related to the mesh dependency of the parameters m_1 and m_2, and necessity of adjustment for a particular mesh size, added to the requirement of optimization for the load range in which these parameters could be applied. On the other hand, modelling possibilities included the straightforward implementation of a visco-elastic/plastic constitutive model for the adhesive to simulate time dependent straining (potentially used to model the creep enhanced fatigue failure of bonded joints), and, since damage is calculated over every element, the non-uniformity of damage present in the adhesive can also be simulated.

For the fatigue life prediction, the load–life (L–N) curve was chosen, because in bonded joints the stress fields are extremely non-uniform and it is not possible to define a relation between the average shear stresses in lap joints and the respective maximum stresses. The total fatigue life, N_f, can thus be separated into crack initiation (N_i, number of cycles to crack onset) and propagation (N_p, number of crack propagation cycles at failure) stages as follows

$$N_f = N_i + N_p \qquad (14)$$

By this analysis, it is possible to divide N_f into these two components, showing the fatigue life proportion between crack initiation and propagation. For the strength and stiffness degradation, an association was made with the damage within the adhesive (Eq. 13). Thus, the strength reduction of a bonded structure owing to fatigue damage could be easily calculated by application of an increasing load until complete failure. Actually, once the adhesive was damaged or cracked, a series of increasing loads were applied until the model became unstable, indicating that the joint cannot bear further loads, thus giving an approximate strength for the joint. The progressive damage modelling algorithm can be summarized in eight steps as follows:

- *Step 1* a FE model of the bonded structure is built and the values of N and D are set to zero for all elements of the adhesive bond,
- *Step 2* a non-linear static analysis is performed and ε_P is calculated for all the elements in the adhesive bond,
- *Step 3* a check is made on whether the analysis converges. If yes go to *Step 4*, otherwise $N = N_f$ and the program is stopped,

Fig. 49 Crack growth prediction versus experimental results comparison for two values of maximum fatigue load and $R = 0.1$ (Shenoy et al. 2010a)
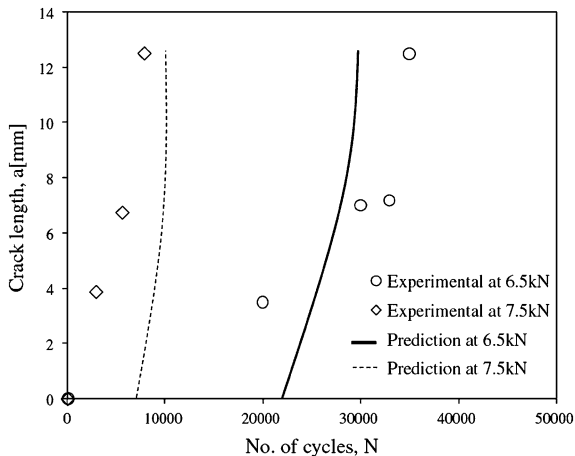
- *Step 4* the damage rate, *dD/dN*, is globally determined by Eq. 13,
- *Step 5* the updated value of D in each element is estimated using the damage rate calculated in the previous step as

$$D = D + \frac{dD}{dN} \cdot dN, \tag{15}$$

where *dN* corresponds to the number of cycles of the current load increment,

- *Step 6* a check is made if $D = 1$. If yes, the respective element is deleted, and the analysis jumps back to Step 2,
- *Step 7* if $D \neq 1$ in a given element the reduced element properties are calculated as

$$E = E_0 \cdot (1 - D), \tag{16}$$

$$\sigma_{yp} = \sigma_{yp0} \cdot (1 - D) \text{ and} \tag{17}$$

$$\beta = \beta_0 \cdot (1 - D). \tag{18}$$

E_0, σ_{yp0} and β_0 are the initial values of E, yield stress and plastic surface modifier constant for the parabolic Mohr–Coulomb model, respectively, and

- *Step 8* the updated value of N is calculated and the analysis jumps to *Step 2* and it is repeated.

A convergence test was conducted to this algorithm for determination of the optimum value of *dN* for each load increment, showing converged results for $dN \leq 100$, regarding the damage curve and the number of cycles to failure. Parameter calibration and ACDM model validation were carried out for single lap joints. Figure 49 reports to crack growth prediction versus experimental results comparison for two values of maximum fatigue load and $R = 0.1$. For a maximum fatigue load of 7.5 kN, the predicted values of *a* were slightly bigger than the

Fig. 50 Experimental/ACDM comparison of the extended life versus N curve, showing crack initiation and total fatigue life; and conventional fracture mechanics prediction for comparison (Shenoy et al. 2010a)
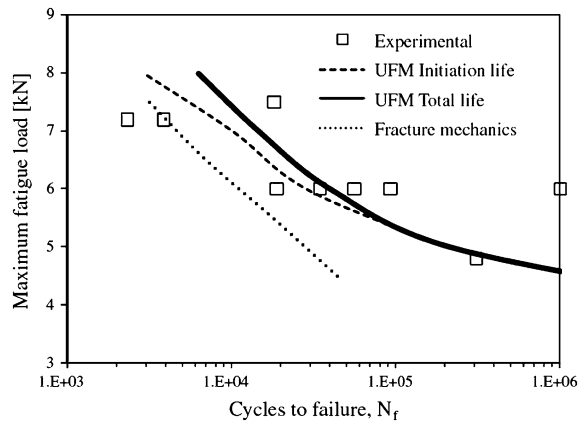
corresponding experiments, although with 6.5 kN the predictions are more accurate. For both scenarios the predicted crack growth rate was slightly higher than that of the experiments. Nonetheless, taking into account the elevated scatter characteristic of fatigue life data, both predictions were satisfactory.

Figure 50 depicts the total fatigue life calculated by ACDM (addressed as UFM in the figure's legend), showing a good correspondence with the experiments. By dividing the total life into initiation and propagation phases as represented in Eq. 14, evidence shows that the predicted proportion of initiation life increases with the reduction of fatigue load, which is entirely consistent with the current experiments and also with those from a previous work by the authors (Shenoy et al. 2009). The predicted crack propagation life using a conventional fracture mechanics approach, considering a Paris-like damage law, is superimposed to the data of Fig. 50. The fracture mechanics approach underestimated the fatigue life because it only predicted the propagation life. However, it was closer to the test data at higher fatigue loads, where the proportion of initiation life to total life is lower. The authors concluded that the proposed ACDM technique with proper parameter calibration is accurate in predicting variable amplitude fatigue strength, with the advantage of quick adaption to combination with creep fatigue. As previously discussed, changes in the nature of the damage law or damage parameter may be required for specific applications.

2.5 Extended Finite Element Method

The XFEM is a recent improvement of the FE method for modelling damage growth in structures. It uses damage laws for the prediction of fracture that are based on the bulk strength of the materials for the initiation of damage and strain for the assessment of failure (defined by G_n^c), rather than the values of t_n^0/t_s^0 or δ_n^0/δ_s^0 used for the CZM's. XFEM gains an advantage over CZM modelling as it does not

require the crack to follow a predefined path. Actually, cracks are allowed to grow freely within a bulk region of a material without the requirement of the mesh to match the geometry of the discontinuities neither remeshing near the crack (Mohammadi 2008). This method is an extension to FE modelling, whose fundamental features were firstly presented in the late 90s by Belytschko and Black (1999). The XFEM relies on the concept of partition of unity and it can be implemented in the traditional FE by the introduction of local enrichment functions for the nodal displacements near the crack to allow its growth and separation between the crack faces (Moës et al. 1999). Due to crack growth, the crack tip continuously changes its position and orientation depending on the loading conditions and structure geometry, simultaneously to the creation of the necessary enrichment functions for the nodal points of the finite elements around the crack path/tip.

Varying applications to this innovative technique were proposed to simulate different engineering problems. Sukumar et al. (2000) updated the method to 3D damage simulation. Modelling of intersecting cracks with multiple branches, multiple holes and cracks emanating from holes were addressed by Daux et al. (2000). The problem of cohesive propagation of cracks in concrete structures was studied by Moës and Belytschko (2002), considering three-point bending and four-point shear scaled specimens. More advanced features such as plasticity, contacting between bodies and geometrical non-linearities, which show a particular relevance for the simulation of fracture in structures, are already available within the scope of XFEM. The employment of plastic enrichments in XFEM modelling is accredited to Elguedj et al. (2006), which used a new enriched basis function to capture the singular fields in elasto-plastic fracture mechanics. Modelling of contact by the XFEM was firstly introduced by Dolbow et al. (2000) and afterwards adapted to frictional contact by Khoei and Nikbakht (2006). Fagerström and Larsson (2006) implemented geometrical nonlinearities within the XFEM. Fatigue applications for XFEM were proposed very recently (Xu and Yuan, 2009; Sabsabi et al. 2011), but these have not yet been applied to the mixed mode fracture of bonded joints. As a result, only static applications of XFEM applied to bonded joints will be considered.

2.5.1 Extended Finite Element Method Formulation

Although a few static implementations of the XFEM were developed in recent years for scenarios other than bonded joints, the generic Abaqus[®] embedded formulation will be described in this section (Abaqus[®] Documentation, 2009). The XFEM considers an initial linear elastic behavior of the materials, which is represented by an elastic constitutive matrix that relates stresses with the normal and shear separations of the cracked elements. Damage and failure are simulated in XFEM by suitable damage initiation criteria and damage laws between the real and phantom nodes of a cracked element (to be detailed further in this section). The damage initiation criteria can rely on the maximum principal stress or strain, while the traction–separation laws that simulate material degradation up to failure
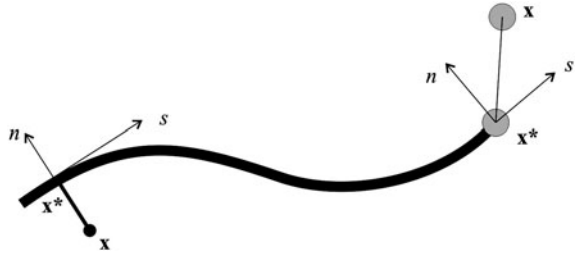
can be linear or exponential. Damage initiation is assessed by Abaqus® typically
by the maximum principal stresses or strains, calculated from the stress/strain state
at each integration point of the solid finite elements. The damage initiation
function (f) can be expressed as (Abaqus® Documentation, 2009)

$$f = \left\{ \frac{\langle \sigma_n \rangle}{\sigma_n^0} \right\}, \tag{19}$$

where σ_n relates to the maximum principal stress at an integration point and σ_n^0 to
the material strength in tension. The Macaulay brackets interpretation is identical
to that of Eq. 6, i.e., it is used to specify that a purely compressive stress state does
not induce damage. As an extension to the conventional FE technique, the XFEM
is based on the integration of enrichment functions in the FE formulation, which
allows modelling the displacement jump between crack faces that occurs during
the propagation of a crack. The fundamental expression of the displacement vector
u, including the displacements enrichment, is written as (Abaqus® Documentation
2009)

$$\mathbf{u} = \sum_{i=1}^{N} N_i(x) \left[\mathbf{u}_i + H(x)\mathbf{a}_i + \sum_{\alpha=1}^{4} F_\alpha(x) b_i^\alpha \right]. \tag{20}$$

$N_i(x)$ and $\mathbf{u}_i$ relate to the conventional FE technique, corresponding to the nodal
shape functions and nodal displacement vector linked to the continuous part of the
formulation, respectively. The second term between brackets, $H(x)\mathbf{a}_i$, is only active
in the nodes for which any relating shape function is cut by the crack and can be
expressed by the product of the nodal enriched degree of freedom vector including
the mentioned nodes, $\mathbf{a}_i$, with the associated discontinuous shape function, $H(x)$,
across the crack surfaces (Abaqus® Documentation, 2009)

$$H(x) = \begin{cases} 1 \text{ if } & (\mathbf{x} - \mathbf{x}*) \cdot \mathbf{n} \geq 0 \\ -1 & \text{otherwise} \end{cases}. \tag{21}$$

x is a sample Gauss integration point, **x*** is the point of the crack closest to **x**,
and **n** is the unit vector normal to the crack at **x*** (Fig. 51). Finally, the third term
is only to be considered in nodes whose shape function support is cut by the crack
tip and is given by the product of the nodal enriched degree of freedom vector of
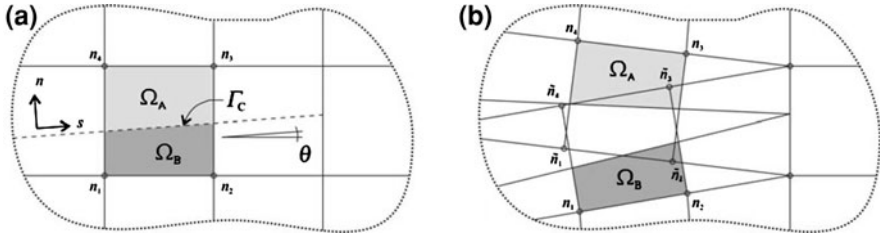
Fig. 52 Damage propagation in XFEM using the phantom nodes concept: before (**a**) and after partitioning (**b**) of a cracked element into sub elements. (Campilho et al. 2011d)

this set of nodes, b_i^α, and the associated elastic asymptotic crack-tip functions, $F_\alpha(x)$ (Sukumar and Prevost 2003). $F_\alpha(x)$ are only used in Abaqus® for stationary cracks, which is not the current scenario.

In the presence of damage propagation, a different approach is undertaken, based on the establishment of phantom nodes that subdivide elements cut by a crack and simulate separation between the newly created sub elements. By this approach, the asymptotic functions are discarded, and only the displacement jump is included in the formulation. Propagation of a crack along an arbitrary path is made possible by the use of phantom nodes that initially have the exactly same coordinates than the real nodes and that are completely constrained to the real nodes up to damage initiation.

In Fig. 52, the highlighted element has nodes n_1–n_4. After being crossed by a crack at Γ_C, the element is partitioned in two sub-domains, Ω_A and Ω_B. The discontinuity in the displacements is made possible by adding phantom nodes ($\tilde{n}_1$–$\tilde{n}_4$) superimposed to the original nodes. When an element cracks, each one of the two sub elements will be formed by real nodes (the ones corresponding to the cracked part) and phantom nodes (the ones that no longer belong to the respective part of the original element). These two elements that have fully independent displacement fields replace the original one, constituted by the nodes $\tilde{n}_1$, $\tilde{n}_2$, n_3 and n_4 (Ω_A) and n_1, n_2, $\tilde{n}_3$ and $\tilde{n}_4$ (Ω_B). From this point, each pair of real/phantom node of the cracked element is allowed to separate according to a suitable cohesive law up to failure. At this stage, the real and phantom nodes are free to move unconstrained, simulating crack growth. In terms of damage initiation, Abaqus® allows the user to define initial cracks, but this is not mandatory. Regardless the choice taken, Abaqus® initiates and propagates damage during the simulation at regions experiencing principal stresses and/or strains greater than the corresponding limiting values specified in the traction–separation laws. Crack initiation/propagation will always take place orthogonally to the maximum principal stresses or strains.

2.5.2 Static Applications of the Extended Finite Element Method

XFEM applications to bonded joints are scarce and extremely recent in the literature, and this section actually describes the entire range of applications found
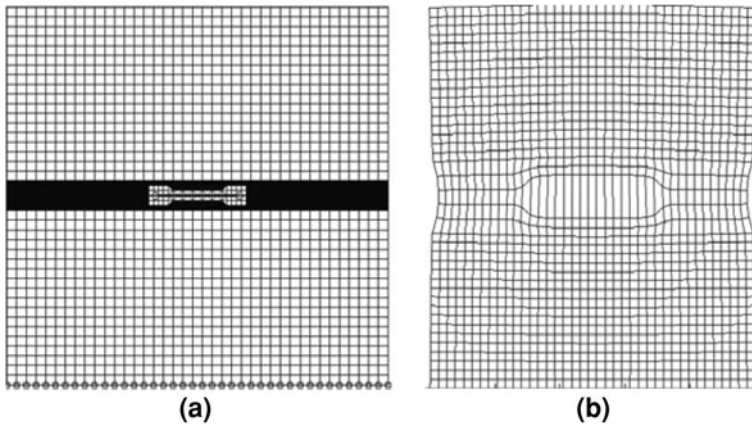
Fig. 53 Bonded joint geometry for stress intensity factor calculation by XFEM (**a**) and horizontal crack propagation after a pure tensile load (**b**) (Premchand and Sajikumar 2009)

while writing this work. Premchand and Sajikumar (2009) studied by the XFEM the variation of the tensile and shear stress intensity factors in adhesively bonded joints with different crack lengths, using the adhesive FM® 300-2 and aluminium adherends. The XFEM model, coupled to the conventional FE method, was implemented in a Matlab® code, for the geometry of Fig. 53a, in which the adhesive holds a flaw with the depicted shape. A series of analyses were carried out under tensile and shear loadings, giving estimations for stress intensity factors in both modes of loading. Figure 53b relates to the joint deformed shape after horizontal crack propagation induced by a pure tensile loading applied at the adherend edges.

The study by Campilho et al. (2011d) checked the XFEM feasibility to model crack propagation and to predict the fracture behaviour of a thin bond of two structural epoxy adhesives under tension by the DCB test using the XFEM, under varying restraining conditions: stiff and compliant adherends. The damage laws of the XFEM were built by experimental determination of G_n^c and t_n^0, by DCB and bulk tensile tests, respectively. Two DCB configurations were selected to check the suitability of the XFEM in simulating fracture in bonded joints. Configuration A corresponds to testing of a brittle epoxy adhesive (XN1244 by Nagase Chemtex) between stiff steel adherends, while in configuration B a ductile adhesive (Araldite® 2015) with compliant carbon-epoxy adherends was tested. Two methods were employed to evaluate G_n^c: the CCM and the CBT, including the effects of crack tip rotation and deflection by using a correction factor, since the formulation assumes clamped adherends at the crack tip. The 2D XFEM analysis was performed in Abaqus® and the damage laws were assumed as triangular, i.e., with linear softening after t_n^0, by using the properties obtained in the DCB and bulk tension tests.

The steel and composite adherends were regarded as elastic isotropic and elastic orthotropic, respectively, whilst the adhesive bond was modelled by the XFEM.
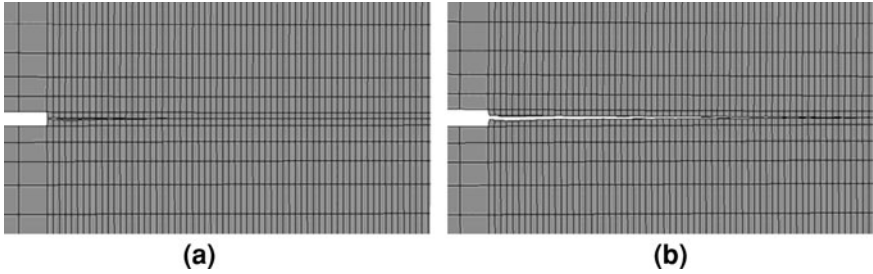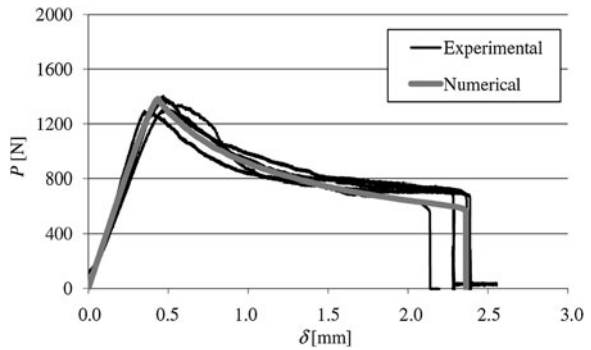
Fig. 54 Crack growth by the XFEM algorithm, initiating at the crack tip (**a**) and growing horizontally along the bondline (**b**) for configuration *A* (Campilho et al. 2011d)

Fig. 55 Experimental and XFEM *P–δ* curves comparison for the DCB specimens, considering configuration *A* (Campilho et al. 2011d)

Validation of the XFEM and the proposed laws was accomplished by comparison of the DCB experimental *P–δ* curves with the output of the XFEM simulations for the same geometry. Figure 54 depicts crack growth by the XFEM algorithm, initiating at the crack tip (a) and growing horizontally along the bondline (b) for configuration A. Figure 55 compares the experimental and XFEM *P–δ* curves of the DCB specimens for configuration A, showing the classical concave shape after the peak load corresponding to crack growth at a constant G_n^c value, and an accurate prediction of the specimens behaviour by using the XFEM with the previously characterized parameters.

For all conditions, the elastic stiffness, peak load, and load during propagation showed a good agreement, which testified the suitability of XFEM to simulate bonded structures for the conditions specified in the the analysis, i.e., pure tensile loading.

Campilho et al. (2011a) tested the CZM and XFEM formulations embedded in Abaqus® for the simulation of bonded single and double lap joints between aluminium adherends and bonded with a brittle adhesive (Araldite® AV138). Overlap lengths between 5 and 20 mm were tested. The adhesive was characterized under tension and shear, which allowed the determination of the XFEM damage parameters. The 2D XFEM analysis considered geometrical non-linearities, with plane strain solid elements. Figure 56a shows the failure process for a single lap joint with 20 mm overlap (detail at the overlap edge) using the principal strain
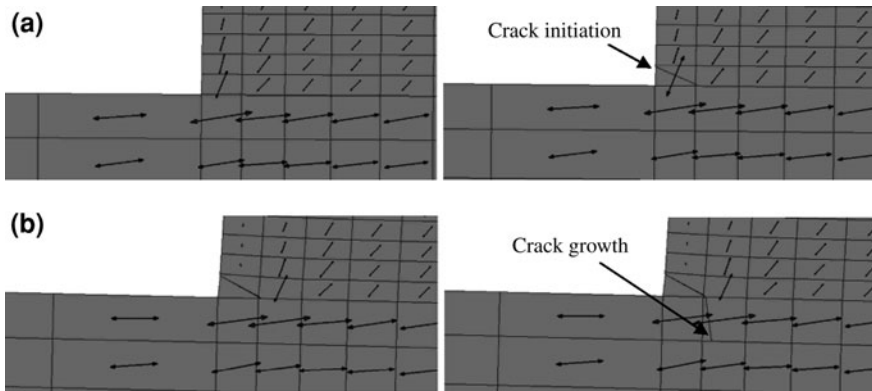
Fig. 56 Progressive failure of a single lap joint with 20 mm overlap using XFEM (the arrows represent the directions of maximum principal strain): damage initiation within the adhesive at the overlap edges (**a**) and damage growth to the aluminium adherend (**b**) (Campilho et al. 2011a)

criterion for the initiation of damage and estimation of crack growth direction. At this point, the direction of maximum strain led to propagation of damage towards the aluminium adherend.

When the crack front reached the adherend, damage propagated almost vertically due to the corresponding direction of principal strains at the crack tip (Fig. 56b), which clearly does not reflect the real behaviour of single lap joints. The authors concluded that damage propagation along the adhesive bond is thus rendered unfeasible with this technique, as it is currently implemented in Abaqus®, since the XFEM algorithm will always search for maximum stresses/strains at the crack tip, shifting the crack to the adherends, disregarding what happens within the adhesive bond and thus preventing damage propagation along the bondline. As a result of this handicap, a different solution was proposed by the authors, supported by the brittleness of the adhesive used. The joint strength was estimated by the initiation of cohesive cracking of the adhesive bond at the overlap edges, using the maximum principal strain criterion as it showed to be slightly less mesh sensitive than the maximum principal stress equivalent.

Figure 57 compares the experimental and XFEM data considering the maximum principal strain criterion, showing that the XFEM is moderately accurate in simulating these structures with brittle adhesives, which undergo a catastrophic failure when the maximum strain of the adhesive is attained anywhere in the structure. However, it was clarified that the chosen methodology was only acceptable due to the brittleness of the adhesive. If a ductile adhesive had been used instead, the predictions would clearly underestimate the experiments. Figure 58 shows the results of the presented mesh dependency study, by plotting the values of normalized peak load for element sizes at the overlap edges (equal length and height) between 0.05 and 0.2 mm, showing that, as expected, the predictions are extremely mesh dependent.

Fig. 57 Experimental and
XFEM strength comparison
as a function of the overlap
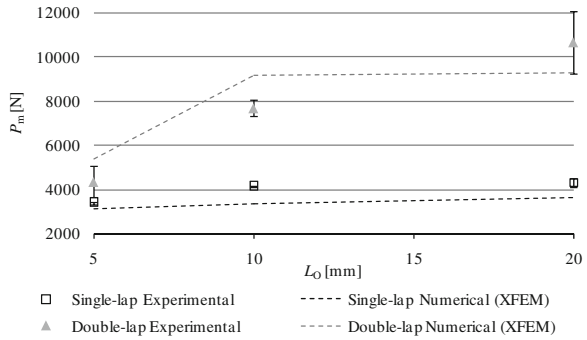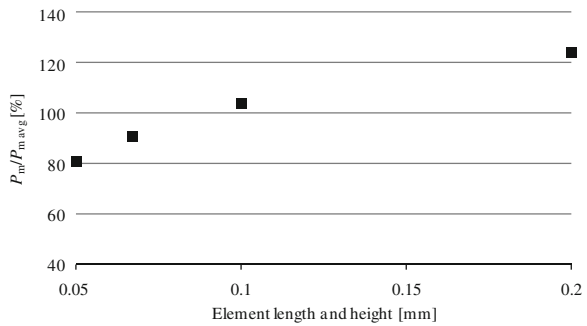length (Campilho et al.
2011a)

Fig. 58 XFEM mesh
dependency study for the
single lap joint with 20 mm
overlap (Campilho et al.
2011a)

Globally, the direct comparisons between the experimental data and the output
of the simulations revealed fair predictions by the XFEM using the proposed
simplification to the original formulation. However, the XFEM did not show to be
suited for damage propagation in bonded joints as it is currently implemented in
Abaqus®, since the direction of crack growth is ruled by the maximum principal
stresses/strains at the crack tip which, in bonded joints, typically leads to damage
growth towards and within the adherends.

2.5.3 Suitability of the Extended Finite Element Method for Bonded Joints

The limitation of CZM's is the requirement of the cohesive elements placement
along predefined paths where damage can occur, which can be hard to identify.
The XFEM allows overcoming this limitation, since it propagates cracks
arbitrarily within solid FE elements by using enrichment functions for the dis-
placements. However, the current XFEM implementation in Abaqus® is restricted
to only one value of maximum strength/strain leading to the initiation of damage
(by the maximum principal stress or strain criterion, respectively), which can be a
limitation as damage in thin adhesive bonds is not consistent with that of bulk
materials, due to the constraining effects imposed by the adherends (Xie and Waas
2006). This does not allow the separation of the adhesive behaviour into the tensile

and shear, which can be in some cases mandatory for the accuracy of the results if large constraining effects are present in the bond (Campilho et al. 2009a). This clearly does not reflect the behaviour of bonded joints and can be attributed to an algorithm for propagation not still suited to multi material structures as it does not search for failure points outside the crack tip nor following the interfaces between different materials. Thus, the separation of the adhesive behaviour into the tensile and shear components that is performed for CZM's is not possible to accomplish, which can be mandatory if large constraining effects exist (Campilho et al. 2009a). Apart from this feature, the current implementation of the method itself involves an even more important handicap. It is known that, if no initial cracks are introduced in the models, the XFEM algorithm will automatically search for the maximum principal stresses/strains in each one of the structure materials (in the present scenario, in both the adhesive and adherends), to initiate damage propagation in the first locus in which these stresses/strains surpass the respective material properties. During damage propagation, the XFEM algorithm continuously searches for the principal stress/strain direction at the crack tip, to specify the direction of subsequent crack growth (Moës et al. 1999; Moës and Belytschko 2002). For the specific case of single or double lap joints, cracking initiates in the adhesive bond orthogonally to the direction of principal stresses/stresses, growing up to the adhesive/adherend interface. Restriction of damage propagation only for the adhesive bond is also rendered unfeasible to surpass this limitation as crack propagation halts when the crack attains the aluminium (Campilho et al. 2011a).

As a result, under these conditions, slight inconsistencies between the predictions and experiments can occur. As a means to prevent this limitation of the current XFEM implementation in Abaqus®, a modification that could account for the distinction between tension and shear would increase the accuracy of the simulations (Campilho et al. 2011d). Concerning the mesh dependency, the XFEM behaves similarly to CZM's, i.e., it is almost mesh independent for the simulation of fracture propagation, due to the fact that G_n^c is averaged over a finite region. Thus, for a large range of mesh sizes, provided that a minimum refinement is used, all the relevant features of the failure process are accurately captured (Campilho et al. 2011a). However, the predictions of damage initiation load are mesh dependent, since the state of stress at a region with large stress concentrations largely depends on the mesh size. Apart from this, owing to the crack propagation method, i.e. orthogonally to the maximum stress/strain, mixed mode propagation is not allowed, although it is frequent in bonded joints. This will invariably lead to a wrong interpretation of the structures behaviour. Under these circumstances, assessment of the structures strength can be carried out by the initiation stress/strain criterion. However, this simplification is only expected to be sufficiently accurate for brittle adhesives that fail catastrophically when the peak stress/strain is achieved. For ductile adhesives, it will underestimate the structures strength, as the adhesive will endure plasticization and redistribution of stresses before colapsing. Nonetheless, the failure load predictions, using the described simplified technique, are expected to be mesh size dependent because of the stress/strain gradients at the sharp corners of bonded structures (Panigrahi and Pradhan 2007).

From this discussion it becomes clear that the XFEM, as it is currently implemented, is only suitable for the identification of the locus of damage initiation in adhesive bonds, by comparing the maximum principal stress/strain in each of the constituent materials to the respective maximum values. However, it does not show to be suited for the simulation of damage growth, as the principle for defining the crack direction (orthogonal to the maximum principal stress/strain) does not model accurately the propagation of damage in multi-material structures as it does not consider the initiation of damage outside the tip of the cracks that emerge from the structure boundaries nor does it take into account the prospect of damage growth along interfaces between different materials. For the specific case of bonded joints, a modification of the XFEM algorithm that would consider these possibilities would bring a significant breakthrough for the simulation of these structures, with the accuracy of CZM's but eliminating the major handicap of this method to follow the damage paths specified by the placement of the cohesive elements. Nonetheless, the XFEM is still a promising method that can be used in a large number of applications for the strength prediction of structures.

3 Boundary Element Method

The BE method is another frequently used and now well-established numerical method, especially for dealing with fracture mechanics problems. A few considerations about the BE method are first given and then applications of the BE method to adhesive joints are commented.

3.1 Simple Description

Vable (2008) explains why the BE method can be useful for analysing adhesive joints. Most of the methods of approximation convert a boundary value problem into a set of algebraic equations. This is usually accomplished by representing the field variable u (for example displacements in stress analysis) by a series

$$u = \sum_i^n c_i f_i, \tag{22}$$

where c_i are the constants to be determined, and f_i are an independent and complete set of n approximating functions. If there are no additional conditions on f_i, then three types of error will be generated: error in the differential equation (e_d) that is distributed in the domain Ω shown in Fig. 59, error in natural boundary conditions (e_n) distributed on the boundary (Γ_n) where natural boundary conditions (conditions on traction for example) are imposed, and error in essential boundary conditions (e_e) distributed on the boundary (Γ_e) where essential boundary conditions (conditions on displacements or temperature for example) are imposed.

Fig. 59 Homogeneous
body Ω
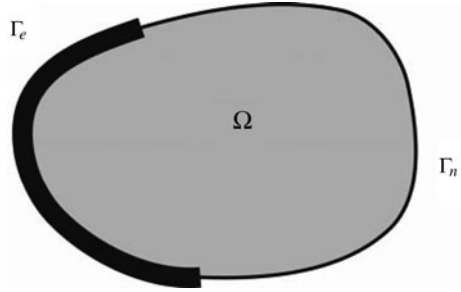
All three errors e_d, e_n, and e_e are zero for an analytical solution. In approximate
methods, at least one of the error is not zero. This non-zero error must be mini-
mized in some manner. The most general minimizing principle is the weighted
residue, in which the error is made orthogonal to a weighting function and can be
written in the general form

$$\int\limits_{\Omega} \int w_j^d e_d \mathrm{d}x\,\mathrm{d}y + \int\limits_{\Gamma_e} w_j^e e_e \mathrm{d}s + \int\limits_{\Gamma_n} w_j^n e_n \mathrm{d}s = 0, \qquad (23)$$

where w_j^d, w_j^e, and w_j^n are the weighting functions chosen by some criteria that
depends upon the approximate method, $\mathrm{d}s$ is an element on Γ and $x - y$ is the
coordinate system. In general, these weighting functions are related to the
approximating function f_i through the operators of the differential equation or
boundary conditions. On substituting the errors e_d, e_n, and e_e into Eq. 23, a linear
system of algebraic equations in the unknown constants c_i is obtained. In the
domain methods such as the FE and FD methods, the functions f_i are chosen such
that the error e_n or e_e is forced to be zero. For example, e_e is forced to zero in the
stiffness version of FE method and e_n is forced to zero in the flexibility version of
FE method. In either case, the integral evaluation over Ω must be performed,
requiring discretization of the domain. However, in boundary methods, such as BE
method, the functions f_i are chosen such that the error e_d is forced to zero, leaving
evaluation of integrals only over the boundary. Hence, in the BE method only the
boundary needs to be discretized, as shown in Fig. 60. As a direct result, the size of
the obtained system of equations can be much lower than in FE approaches.
Meshing and remeshing is significantly simpler in the BE method than in the FE
method (and other domain methods) for problems of shape optimisation or para-
metric studies (rounding, tapering or shaping of the adherend or adhesive fillet), in
which the boundary shape changes.

The discretization process converts the integrals in Eq. 23 to a sum of integrals
over the elements. Thus, in the FE method and domain methods, when the domain
integral is set over the element to zero in Eq. 23, it is implied that the differential
equation is satisfied in an average sense over the element. But in the BE method this

Fig. 60 Comparison between the general FE method and the BE method approach. **a** Structural model, **b** FE mesh, **c** BE mesh
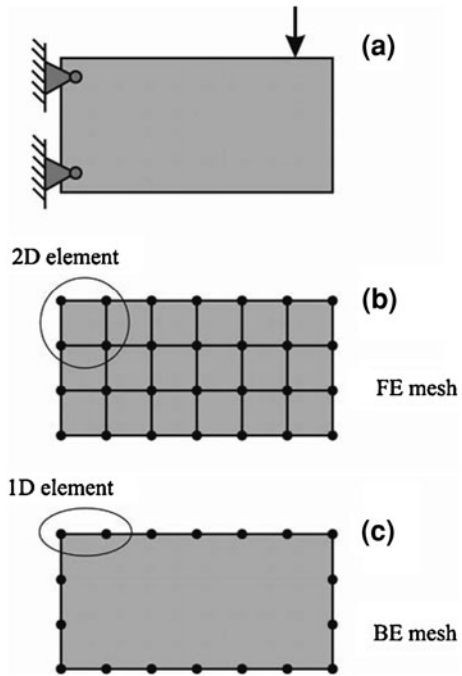
equation is satisfied exactly, as e_d is forced to zero. If there are stress gradients in the domain interior, then the BE method can potentially yield better resolution by choosing points of stress evaluation very close to each other, while in domain methods the resolution is dictated by the size of the elements. In the BE method, stresses are evaluated for example at the crack boundary and not at the integration points inside the element, as for the FE method. For this reason, the BE method has proven to have very good resolution of stress gradients for problems of stress concentration and fracture mechanics. Therefore, it can potentially give good resolution of stress gradients in the thickness direction of the adherend and the adhesive. However, if the stress gradients are along the boundary, as is the case on the adherend-adhesive interface, then the BE method like FE method requires a refined mesh. One research challenge for the application of the BE method to bonded joints is the development of a mesh refinement scheme for interface problems.

Another important feature is related to the treatment of infinite and semi-infinite boundaries. In the BE method, the functions f_i are the fundamental solutions of the differential equations, and therefore they implicitly satisfy the zero stress conditions at infinity. If there is a uniform stress at infinity then its value is simply added to the integral equations. For this reason, in the BE method, only the boundary of a hole in an infinite medium needs to be discretised contrarily to domain methods that require the discretization of the exterior. However, joints have boundaries that start at the adhesive end and extend to infinity. Such boundaries will need specialized infinite boundary elements.

3.2 Application to Adhesive Joints

Given the above potential advantages, one would expect an extensive use of the BE method in the analysis of bonded joints. However, the reality is that a very limited number of studies concerning the use of the BE method can be found in the literature. This is due to several disadvantages, described by Öchsner (2011). First of all, the derivation of the method is highly mathematical and the theoretical foundation is still not incorporated in many engineering degree courses. The stiffness matrix in the case of the BE method might be much smaller compared to the FE approach, but it is fully populated and many highly efficient equation solvers which take advantage of the band structure obtained with FE approaches cannot be used. In addition, domain integrals must be considered in the case of non-linearities, which requires at least a coarse mesh inside the domain. Thus, the advantage of the reduced mesh on the boundary disappears. Typical applications of the BE method in the context of adhesion technology are commonly found for the modelling of cracks (fracture mechanics) and other types of stress singularities. It has been widely used to analyse metallic structures repaired by composites. For example Young et al. (1988, 1992), Wen et al. (2002, 2003), Salgado and Aliabadi (1998), and Liu et al. (2009) used the BE method to analyse cracked sheets, in which the patch and the cracked sheet were modelled using boundary elements and the adhesive was simulated as shear springs. However, these studies are focussed on the cracked plate rather than on the adhesive bond. Ikeda et al. (1998) combined the FE and BE methods to analyse a butt joint with a crack in the adhesive. The FE method was used in the adhesive and the adherends were modelled with the BE method. Computer power can be saved but the use of the BE method for adhesive modelling is limited. Lee (1998) investigated the singular stresses at the interface corner between a viscoelastic adhesive and a rigid adherend subjected to a uniform transverse tensile strain using the time-domain BE method. The model is presented in Fig. 61. The BE analysis could capture the large stress gradients present at the interface corner and the stress singularity. Cavallini et al. (2006) presented a BE technique for modelling an adhesively bonded structural joint. The formulation allowed the analysis of general lay-up laminates such as Glare material. A simple model consisting of a layer of adhesive on aluminium showed good agreement with an analytical model. Vable and Maddi (2006) addressed specific problems (i.e., numerical modelling considerations which limited the application of the BE method in the past) related to bonded joints and BE simulation. In addition, numerical results of lap joints with isotropic elastic adherends and an elastic adhesive were presented, which demonstrated the potential of the BE method in analysis of bonded joints. The effect of several spew angles was also studied. Good agreements were found with a FE analysis. The authors pointed out that the BE method was a viable technique for stress analysis of bonded joints, since it had the potential of producing good resolution of stress gradients and it is robust enough for a parametric study of joint parameters. Further improvements in the resolution of stress gradients required development of a mesh refinement scheme for material
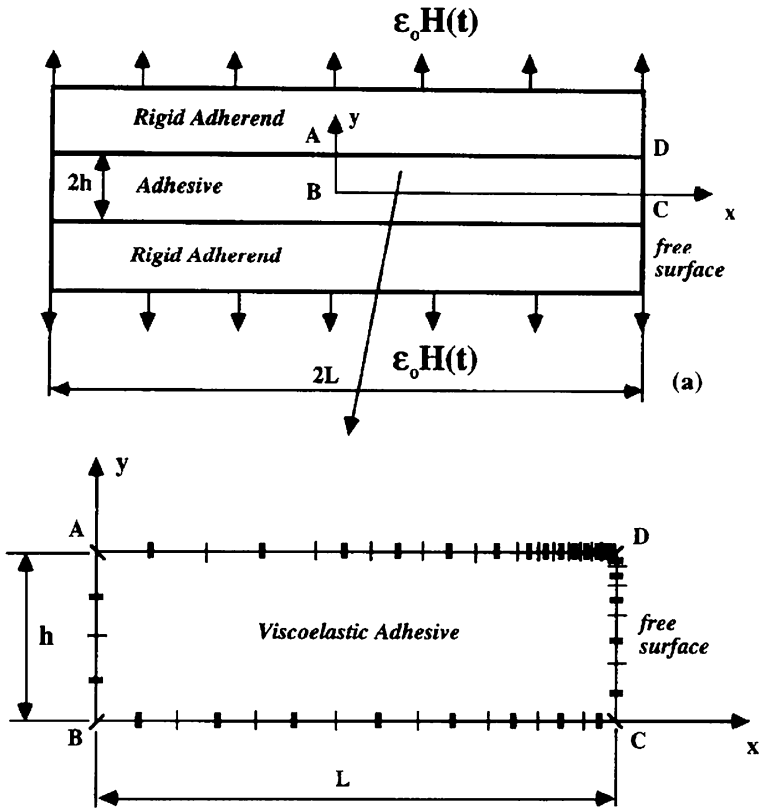
Fig. 61 Analysis model of Lee (1998) for determination of interface stresses developed in a visco-elastic adhesive layer

interfaces and development of infinite boundary elements for use with semi-analytical integration schemes. The authors referred that the design of mechanically fastened joints was facilitated by stress concentration factor curves, which are drawn as a function of various geometric parameters. If a similar design approach is to be developed with the concepts of stress intensity factors usage in bonded joints, then the BE method with its high accuracy and ease of modelling geometric features can well become a methodology of choice for stress analysis of bonded joints.

4 Finite Difference Method

The FD method is the first widely known approximation technique for partial differential equations. The method is described in detail in the works of Forsythe and Wasow (1960), Collatz (1966) and Mitchell and Griffiths (1980). A brief

Fig. 62 Illustration of the
approximation by the FD
method
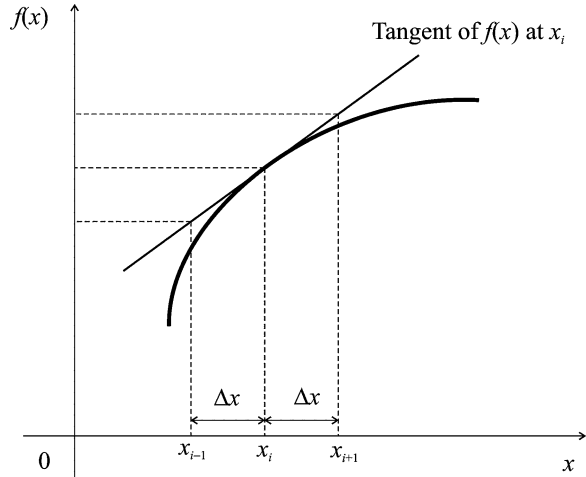
description of the FD method is firstly presented and then applications of the FD method to adhesive joints are given.

4.1 Simple Description

The FD method is a numerical technique for approximating the solutions to differential equations, by using FD equations to approximate derivatives. Physically, a derivative represents the rate of change of a physical quantity represented by a function $f(x)$ with respect to the change of its variable x. An example of a function $f(x)$ is graphically represented in Fig. 62. The differential $df(x)/dx$ is defined by:

$$\frac{df(x)}{dx} = \lim_{\Delta x \to 0} \frac{\Delta f}{\Delta x} \approx \frac{\Delta f}{\Delta x}. \tag{24}$$

Equation 24 depicts the principle of finite difference. The smaller the steps Δx the closer the values between the differential and difference of the rate change of the function. The two sources of error in the FD method are the round-off error (the loss of precision due to computer rounding of decimal quantities), and the truncation error or discretization error, i.e., the difference between the exact solution of the FD equation and the exact quantity.

To use a FD method to attempt to approximate the solution to a problem, one must first discretize the problem's domain. This is usually done by dividing the domain into a uniform grid (Fig. 63). In the case of the FE method, the domain must be discretized with elements (which are composed of nodes and boundaries, and which may have a distorted shape), whereas the FD method requires only the discretization of the grid points, which are not joined to elements. Therefore, for the case of the FD method, the results are only obtained at the grid points and not interpolated as in the case of the FE method. An interpolation

Fig. 63 Comparison between the FE method and the FD approach. **a** Structural model; **b** FE mesh; **c** FD grid points
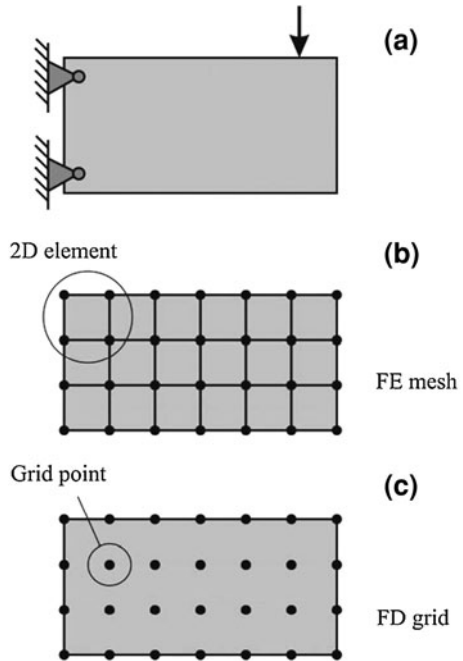
between the grid points might be obtained with additional formulation. Öchsner (2011) refers that the major advantage of the FD method is the simple computer implementation of the procedures. Therefore, in-house codes are easily implemented and new features are easy to add. The main disadvantages are the expected complications for the simulation of boundary conditions for complex shaped geometries and the difficult attainment of symmetry for the stiffness matrix. For these reasons, the FD method is only applied to simple geometries. However, these problems may be solved using the FD energy method developed by Bushnell et al. (1971).

4.2 Application to Adhesive Joints

Application of the FD method to the analysis of adhesively bonded joints is relatively limited due mainly to the availability of commercial FE programs that offer a large range of features and enable to include complex geometries and non-linear problems. For complex geometries and elaborate material models, a FE analysis is preferable. However, for a fast and easy answer, a closed-form analysis is more appropriate. Adhesive joints have been intensively investigated over the past 70 years and numerous analytical models have been proposed (da Silva et al. 2009a, b). The first model (Fig. 64) proposed by Volkersen (1938) assumes that the adhesive deforms only in shear and that the
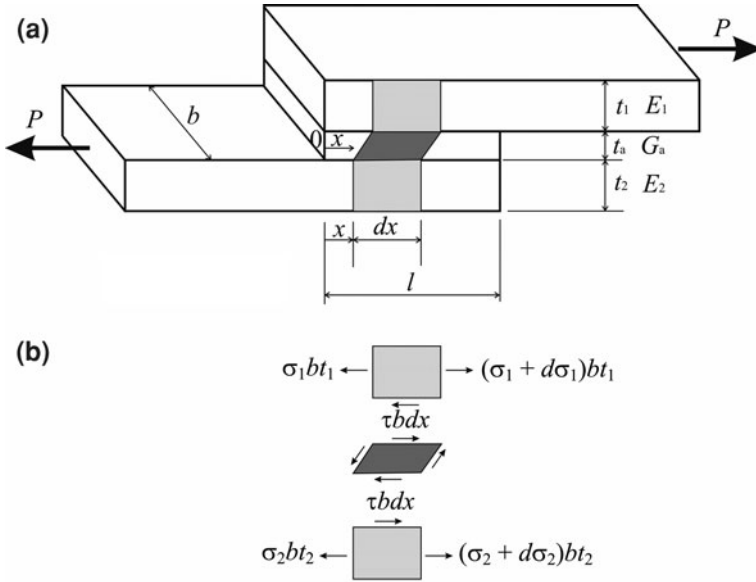
Fig. 64 Single lap joint analysed by Volkersen (1938)

adherends can deform in tension. The following partial differential equation is established

$$\frac{d^2\sigma_1}{dx^2} - \lambda^2\sigma_1 + C_0 = 0, \tag{25}$$

where $\lambda^2 = \frac{G_a}{t_a}\left(\frac{1}{E_1 t_1} + \frac{1}{E_2 t_2}\right)$, $C_0 = \frac{G_a}{t_a}\frac{P}{bE_2 t_2 t_1}$, G_a is the adhesive shear modulus and E_1 and E_2 are the adherends Young's modulus. This is a second order non-linear differential equation that has an algebraic solution of the form

$$\sigma_1 = A\cosh(\lambda x) + B\sinh(\lambda x) + \frac{C_0}{\lambda^2}, \tag{26}$$

where the two constants A and B are determined by the boundary conditions at the ends of the overlap.

The pioneering analytical models of adhesively bonded joints such as those of Vokersen (1938) and Goland and Reissner (1944) are described by differential equations that have an algebraic solution. However, many advanced adhesive joints analyses, such as those that include material nonlinearity (Bigwood and Crocombe 1990; Wang et al. 2003) and composite adherends (Srinivas 1975; Adams and Mallick 1992; Mortensen and Thomsen 2002), involve non-linear and non-homogeneous differential equations, and the solution of these equations is often beyond the reach of classical methods. Numerical solutions such as the FD method are then the only practical and viable ways to solve these differential equations. For example, the Crocombe and Bigwood

(1992) sandwich adherend-adhesive-adherend model can accommodate the non-linear stress response of both the adhesive and the adherends, and can also be subjected to several forms of loading. Numerical results were obtained by using a FD method to solve a set of six non-linear first-order differential equations. Wang et al. (2003) extended the work of Crocombe and Bigwood (1992) to account for shear deformation in the adherend to predict adhesive failure in arbitrary joints subjected to large scale adherend yielding. They also obtained a system of six non-linear first-order differential equations, which was solved by the double (precision) boundary value problem finite difference (DBVPFD) solver. The results obtained were in close agreement with a FE analysis, except for the localized stress and strain concentrations near the free edge. Additional models that solved the governing equations using FD methods are those of Kim and Kedward (2001) and Xu and Li (2010). Kim and Kedward (2001) developed a closed-form stress analysis of an adhesively bonded lap joint subjected to spatially varying in-plane shear loading. The solution, while similar to Volkersen's treatment of tension loaded lap joints, was inherently 2D and, in general, predicted a multi-component adhesive shear stress state. Stresses in adhesively bonded composite tubular joints, subjected to torsion, were investigated by Xu and Li (2010). The model resulted in a system of eighteen second-order partial differential equations and six linear equations with twenty-four unknowns, which were solved by a mathematical model based on the FD method.

5 Conclusions

The most recent trends in numerical modelling of adhesive joints have been discussed in this book. The three major numerical techniques, FE method, BE method and FD method were described. The following conclusions can be drawn.

The FE method is by far the most common numerical tool. In the continuum mechanics approach, the maximum values of stress, strain or strain energy, predicted by the FE analyses, are typically used in the failure criterion where they are compared with the corresponding material allowable values. However, it is known that these maximum predicted values are usually found very near to the singular points of the model (sharp corners or bi-material interfaces). Therefore, their magnitude strongly depends on how well the stress field around the singularity is modelled (i.e., mesh refinement). Additionally, the maximum critical values obtained by the FE analyses are also dependent on the proximity of the critical point from the stress or strain concentrator. In order to overcome this problem, a common approach used by many researchers is to use the same variables (stress, strain or energy) but this time at some arbitrary distance from the point of singularity, where the stress field is clear of any effects from the singular point. The critical distances must be usually calibrated from the FE results, and as a consequence, these critical values obtained can only be used for similar geometric and

material configurations. There is usually no physical explanation relating the critical distances with experimental observations. The average plastic density belongs to the same concept, but the use of this value gives a less sensitive result to the mesh size used.

Continuum mechanics assumes that the structure and its material are continuous. Defects or two materials with re-entrant corners obviously are not consistent with such an assumption. Cracks are the most common defects in structures, for which the method of fracture mechanics has been developed. Fracture mechanics can be used to predict joint strength or residual strength if there is a crack tip or a known and calibrated singularity. Fracture mechanics is more difficult to apply to strength predictions for joints bonded with ductile adhesives, since G^c is not independent of the joint geometry. This is mainly because the adherends restrict the development of the yield zone in the adhesive bond or they can cause fracture of the adhesive if the material yields.

Damage mechanics has been used to model the progressive damage and failure of a pre-defined crack path, or arbitrarily within a structure. This is an emerging field and the techniques for modelling damage can be divided into either local or continuum approaches. In the local approach, damage is confined to a zero thickness path (2D analyses) or surface (3D analyses). By the continuum approach, damage is modelled over a finite area (2D analyses) or volume (3D analyses). CZM's, which can be categorized under these two lines of analysis, simulate the macroscopic damage along this path by the specification of a traction–separation response between paired nodes on either sides of pre-defined crack paths. In most of the CZM's, the traction–separation relations for the interfaces are such that, with increasing interfacial separation, the traction across the interface reaches a maximum (crack initiation), then it decreases (softening), and finally the crack propagates, permitting a total de-bond. The whole failure response and crack propagation can thus be modelled. A CZM simulates the fracture process, extending the concept of continuum mechanics by including a zone of discontinuity modelled by cohesive zones, thus using both strength and energy parameters to characterize the debonding process. This allows the approach to be of much more general utility than conventional fracture mechanics. The method is also mesh insensitive, provided that enough integration points undergo softening simultaneously. It is similar to criteria where the stress or strain is averaged over a finite area so as to remove the singularity. Studies demonstrated that it is possible to experimentally determine the appropriate cohesive zone parameters of an adhesive bond, and to incorporate them into FE analyses for excellent predictive capabilities. However, CZM's present a limitation, as it is necessary to know beforehand the critical zones where damage is prone to occur, and to place the cohesive elements accordingly. Also, for ductile materials, the shape of the traction–separation law must be modified, which may give additional convergence problems.

The XFEM, expanding CZM by the allowance of crack propagation along arbitrary directions within solid continuum elements, is not suited for damage propagation in bonded joints as it is currently implemented in softwares, such as in

Abaqus®, since the direction of crack growth is ruled by the maximum principal stresses/strains at the crack tip which, in bonded joints, invariably leads to damage growth towards and within the adherends. This clearly does not reflect the behaviour of bonded joints and can be attributed to an algorithm for propagation not still suited to multi-material structures, as it does not search for failure points outside the crack tip nor following the interfaces between different materials. Restriction of damage propagation only for the adhesive bond is also rendered unfeasible to surpass this limitation as crack propagation halts when the crack attains the aluminium. Nonetheless, studies were made with some simplification hypotheses, which allowed fair approximations to the joints behaviour.

The BE method is still at an early stage of development concerning the analysis of adhesive joints. However, the inherent advantages of the method such as the easy modelling of cracks, stress singularities and large stress gradients justify its more intensive use in the context of adhesive joints.

The FD method is useful for solving differential equations derived in complex analytical models. It is generally used for own code development and solution of new analytical derivations for relatively simple geometries.

From the state-of-the-art description carried through in this book, it is clear that numerical methods have been largely exploited for some decades for the strength and fracture prediction of bonded joints by varying approaches, and with formulations tailored for different load scenarios. In the near future, further developments within this scope are expected, and a few research tendencies are proposed that can effectively expand the use of these powerful tools. CZM's will definitely be improved, beginning from easier and more efficient calibration tools. Regarding the analyses capabilities, further research on the residual strength of environmentally degraded joints is required, namely regarding degradation of the adhesive and interfacial regions because of extreme conditions that structures can be subjected to in industrial applications. Rate dependent damage formulations are still very incipient and need exploiting, and fatigue CZM's are very recent and need further validations and improvements for a widespread application to different geometries and load conditions. XFEM is also in the initial stages of development and it can be adjusted to be useful to bonded joints, if the aforementioned limitations of this method are surpassed.

References

Abaqus® Documentation (2009) Dassault Systèmes, Vélizy-Villacoublay

A. Abdul-Baqi, P.J.G. Schreurs, M.G.D. Geers, Fatigue damage modeling in solder interconnects using a cohesive zone approach. Int. J. Solids Struct. **42**, 927–942 (2005)

R.D. Adams, R. Davies, Strength of joints involving composites. J. Adhesion **59**, 171–182 (1996)

R.D. Adams, R. Davies, Strength of lap shear joints, in *The Mechanics of Adhesion*, ed. by D.A. Dillard, A.V. Pocius (Elsevier, Amsterdam, 2002)

R.D. Adams, J.A. Harris, Strength prediction of bonded single lap joints by nonlinear finite element methods. Int J Adhes Adhes **4**, 65–78 (1984)

R.D. Adams, J.A. Harris, The influence of local geometry on the strength of adhesive joints. Int. J. Adhes. Adhes. **7**, 69–80 (1987)

R.D. Adams, V. Mallick, A method for the stress analysis of lap joints. J. Adhesion **38**, 199–217 (1992)

R.D. Adams, N.A. Peppiatt, Effects of Poisson's ratio strains in adherend on stresses of an idealized lap joint. J. Strain Anal. **8**, 134–139 (1973)

R.D. Adams, N.A. Peppiatt, Stress analysis of adhesive-bonded lap joints. J. Strain Anal. **9**, 185–196 (1974)

R.D. Adams, R.W. Atkins, J.A. Harris, A.J. Kinloch, Stress analysis and failure properties of carbon-fibre-reinforced-plastic/steel double-lap joints. J. Adhesion **20**, 29–53 (1986)

R.D. Adams, J. Comyn, W.C. Wake, *Structural Adhesive Joints in Engineering*, 2nd edn. (Chapman & Hall, London, 1997)

G. Alfano, On the influence of the shape of the interface law on the application of cohesive-zone models. Compos. Sci. Technol. **66**, 723–730 (2006)

G. Alfano, M.A. Crisfield, Finite element interface models for the delamination analysis of laminated composites: mechanical and computational issues. Int. J. Numer. Methods Eng. **50**, 1701–1736 (2001)

O. Allix, A. Corigliano, Modeling and simulation of crack propagation in mixed-modes interlaminar fracture specimens. Int. J. Fract. **77**, 111–140 (1996)

T. Andersson, U. Stigh, The stress-elongation relation for an adhesive layer loaded in peel using equilibrium of energetic forces. Int. J. Solids Struct. **41**, 413–434 (2004)

I. Ashcroft, *Fatigue Load Conditions*, in *Handbook of Adhesion Technology*, ed. by L.M.F. da Silva, A. Öchsner, R.D. Adams (Springer, Heidelberg, 2011)

ASTM D3433-99 Standard, *Standard Test Method for Fracture Strength in Cleavage of Adhesives in Bonded Metal Joints*. ASTM International, West Conshohocken (2005)

ASTM D4501-01, *Standard Test Method for Shear Strength of Adhesive Bonds Between Rigid Substrates by The Block Shear Method* (ASTM International, West Conshohocken, 2009)

M.G. Bader, I. Hamerton, J.N. Hay, M. Kemp, S. Winchester, Double cantilever beam of repaired carbon fibre composites. Compos Part A **31**, 603–608 (2000)

M.D. Banea, L.F.M. da Silva, Adhesively bonded joints in composite materials: an overview. J. Mater. Design Appl. **223**, 1–18 (2009)

M.D. Banea, L.F.M. da Silva, R.D.S.G. Campilho, Temperature dependence of the fracture toughness of adhesively bonded joints. J. Adhesion Sci. Technol. **24**, 2011–2026 (2010)

M.D. Banea, L.F.M. da Silva, R.D.S.G. Campilho, Mode I fracture toughness of adhesively bonded joints as a function of temperature: experimental and numerical study. Int. J. Adhes. Adhes. **31**, 273–279 (2011)

G.I. Barenblatt, The formation of equilibrium cracks during brittle fracture. General ideas and hypothesis. Axisymmetrical cracks. J. Appl. Math. Mech. **23**, 622–636 (1959)

G.I. Barenblatt, The mathematical theory of equilibrium cracks in brittle fracture. Adv. Appl. Mech. **7**, 55–129 (1962)

W.D. Bascom, R.L. Cottingham, Effect of temperature on the adhesive fracture behavior of an elastomer–epoxy resin. J. Adhesion **7**, 333–346 (1976)

W.D. Bascom, R.L. Cottingham, R.L. Jones, P. Peyser, The fracture of epoxy- and elastomer-modified epoxy polymers in bulk and as adhesives. J. Appl. Polymer Sci. **19**, 2545–2562 (1975)

A.J. Bell, A.J. Kinlock, The effect of the substrate material on the value of the adhesive fracture energy, $G(c)$. J. Mater. Sci. Lett. **16**, 150–1453 (1997)

T. Belytschko, T. Black, Elastic crack growth in finite elements with minimal remeshing. Int. J. Fract. Mech. **45**, 601–620 (1999)

M.L. Benzeggagh, M. Kenane, Measurement of mixed-mode delamination fracture toughness of unidirectional glass/epoxy composites with mixed-mode bending apparatus. Compos. Sci. Technol. **56**, 439–449 (1996)

B. Bhattacharya, B. Ellingwood, Continuum damage mechanics analysis of fatigue crack initiation. Int. J. Fatigue **20**, 631–639 (1998)

A. Biel, Constitutive behaviour and fracture toughness of an adhesive layer. Licentiate of Engineering Dissertation, Chalmers University of Technology (2005)

A. Biel, U. Stigh, Effects of constitutive parameters on the accuracy of measured fracture energy using the DCB-specimen. Eng. Fract. Mech. **75**, 2968–2983 (2008)

D.A. Bigwood, A.D. Crocombe, Non linear adhesive bonded joint design analysis. Int. J. Adhes. Adhes. **10**, 31–41 (1990)

B.R.K. Blackman, H. Hadavinia, A.J. Kinloch, J.G. Williams, The use of a cohesive zone model to study the fracture of fibre composites and adhesively-bonded joints. Int. J. Fract. **119**, 25–46 (2003)

B.R.K. Blackman, A.J. Kinloch, M. Paraschi, The determination of the mode II adhesive fracture resistance, GIIC, of structural adhesive joints: an effective crack length approach. Eng. Fract. Mech. **72**, 877–897 (2005)

D. Bushnell, B.O. Almroth, F. Brogan, Finite-difference energy method for nonlinear shell analysis. Comput. Struct. **1**, 361–387 (1971)

R.D.S.G. Campilho, M.F.S.F. de Moura, J.J.M.S. Domingues, Modelling single and double-lap repairs on composite materials. Compos. Sci. Technol. **65**, 1948–1958 (2005)

R.D.S.G. Campilho, M.F.S.F. de Moura, J.J.M.S. Domingues, Stress and failure analyses of scarf repaired CFRP laminates using a cohesive damage model. J. Adhes. Sci. Technol. **21**, 855–970 (2007)

R.D.S.G. Campilho, M.F.S.F. de Moura, J.J.M.S. Domingues, Using a cohesive damage model to predict the tensile behaviour of CFRP single-strap repairs. Int. J. Solids Struct. **45**, 1497–1512 (2008a)

R.D.S.G. Campilho, M.F.S.F. de Moura, J.J.M.S. Domingues, J.J.L. Morais, Computational modelling of the residual strength of repaired composite laminates using a cohesive damage model. J. Adhes. Sci. Technol. **22**, 1565–1591 (2008b)

R.D.S.G. Campilho, M.F.S.F. de Moura, J.J.M.S. Domingues, Numerical prediction on the tensile residual strength of repaired CFRP under different geometric changes. Int. J. Adhes. Adhes. **29**, 195–205 (2009a)

R.D.S.G. Campilho, M.F.S.F. de Moura, A.M.G. Pinto, J.J.L. Morais, J.J.M.S. Domingues, Modelling the tensile fracture behaviour of CFRP scarf repairs. Compos. Part B **40**, 149–157 (2009b)

R.D.S.G. Campilho, M.F.S.F. de Moura, D.A. Ramantani, J.J.L. Morais, J.J.M.S. Domingues, Tensile behaviour of three-dimensional carbon-epoxy adhesively bonded single- and double-strap repairs. Int. J. Adhes. Adhes. **29**, 678–686 (2009c)

R.D.S.G. Campilho, M.F.S.F. de Moura, D.A. Ramantani, J.J.L. Morais, A.M.J.P. Barreto, J.J.M.S. Domingues, Adhesively-bonded repair proposal for wood members damaged by horizontal shear using carbon-epoxy patches. J. Adhesion **86**, 649–670 (2010)

R.D.S.G. Campilho, M.D. Banea, A.M.G. Pinto, L.F.M. da Silva, A.M.P. de Jesus, Strength prediction of single- and double-lap joints by standard and extended finite element modelling. Int. J. Adhes. Adhes. **31**, 363–372 (2011a)

R.D.S.G. Campilho, A.M.G. Pinto, M.D. Banea, L.F.M. da Silva, Optimization study of hybrid spot welded-bonded single-lap joints. Int. J. Adhes. Adhes. (2011b) (accepted)

R.D.S.G. Campilho, M.D. Banea, F.J.P. Chaves, L.F.M. da Silva, Modelling of single-lap joints using cohesive zones models: effect of the cohesive parameters on the output of the simulations. J. Adhesion (2011c) (accepted)

R.D.S.G. Campilho, M.D. Banea, F.J.P. Chaves, L.F.M. da Silva, eXtended Finite Element Method for fracture characterization of adhesive joints in pure mode I. Comput. Mater. Sci. **50**, 1543–1549 (2011d)

R.D.S.G. Campilho, Modelação da Execução de Reparações em Materiais Compósitos. M.Sc. Dissertation, Engineering Faculty of Porto University (2005)

R.D.S.G. Campilho, Repair of composite and wood structures. Ph.D. Dissertation, Engineering Faculty of Porto University (2009)

T. Carlberger, U. Stigh, An explicit FE-model of impact fracture in an adhesive joint. Eng. Fract. Mech. **74**, 2247–2262 (2007)

T. Carlberger, U. Stigh, Influence of layer thickness on cohesive properties of an epoxy-based adhesive—an experimental study. J. Adhesion **86**, 814–833 (2010)

T. Carlberger, A. Biel, U. Stigh, Influence of temperature and strain rate on cohesive properties of a structural epoxy adhesive. Int. J. Fract. **155**, 155–166 (2009)

M.N. Cavalli, M.D. Thouless, The effect of damage nucleation on the toughness of an adhesive joint. J. Adhesion **76**, 75–92 (2001)

G. Cavallini, G. Davi, A. Milazzo, Boundary element modeling and analysis of adhesive bonded structural joints. Electron. J. Bound Elem. **4**, 31–48 (2006)

H. Chai, Bond thickness effect in adhesive joints and its significance for mode I interlaminar fracture of composites. ASTM STP **893**, 209–231 (1986a)

H. Chai, On the correlation between the mode I failure of adhesive joints and laminated composites. Eng. Fract. Mech. **24**, 413–431 (1986b)

H. Chai, Shear fracture. Int. J. Fract. **37**, 137–159 (1988)

H. Chai, Experimental evaluation of mixed-mode fracture in adhesive bonds. Experimental Mech. **32**, 296–303 (1992)

N. Chandra, H. Li, C. Shet, H. Ghonem, Some issues in the application of cohesive zone models for metal–ceramic interfaces. Int. J. Solids Struct. **39**, 2827–2855 (2002)

M. Charalambides, A.J. Kinloch, Y. Wang, J.G. Williams, On the analysis of mixed mode failure. Int. J. Fracture **54**, 269–291 (1992)

J. Chen, Predicting progressive delamination of stiffened fibre-composite panel and by decohesion models. J. Thermopl. Compos. Mater. **15**, 429–441 (2002)

Z. Chen, R.D. Adams, L.F.M. da Silva, The use of the J-integral to analyse adhesive bonds with and without a crack. Int. J. Adhes. Adhes. **31**, 48–55 (2011a)

Z. Chen, R.D. Adams, L.F.M. da Silva, Prediction of crack initiation and propagation of adhesive lap joints using an energy failure criterion. Eng. Fract. Mech. **78**, 990–1007 (2011b)

P.T. Cheuk, L. Tong, A.N. Rider, J. Wang, Analysis of energy release rate for fatigue cracked metal-to-metal double-lap shear joints. Int. J. Adhes. Adhes. **25**, 181–191 (2005)

J.Y. Choi, H.J. Kim, J.K. Lim, Y.W. Mai, Numerical analysis of adhesive thickness effect on fracture toughness in adhesive-bonded joints. Key Eng. Mat. **270–273**, 1200–1205 (2004)

N. Choupani, Interfacial mixed-mode fracture characterization of adhesively bonded joints. Int. J. Adhes. Adhes. **28**, 267–282 (2008)

J.D. Clarke, I.J. Mcgregor, Ultimate tensile stress over a zone: a new failure criterion for adhesive joints. J. Adhes. **42**, 227–245 (1993)

L. Collatz, *The Numerical Treatment of Differential Equations* (Springer, Berlin, 1966)

R.D. Cook, *Finite Element Modeling for Stress Analysis* (Wiley, New York, 1995)

R. Courant, Variational methods for the solution of problems of equilibrium and vibrations. Bull. Am. Math. Soc. **49**, 1–23 (1943)

J.H. Crews, K.N. Shivakumar, I.S. Raju, Factors influencing elastic stresses in double cantilever beam specimens. ASTM STP **981**, 119–132 (1988)

A.D. Crocombe, Global yielding as a failure criteria for bonded joints. Int. J. Adhes. Adhes. **9**, 145–153 (1989)

A.D. Crocombe, R.D. Adams, Influence of the spew fillet and other parameters on the stress distribution in the single lap joint. J. Adhes. **13**, 141–155 (1981)

A.D. Crocombe, D.A. Bigwood, Development of a full elasto-plastic adhesive joint design. J. Strain Anal. Eng. Des. **27**, 211–218 (1992)

A.D. Crocombe, Y.X. Hua, W.K. Loh, M.A. Wahab, I.A. Ashcroft, Predicting the residual strength for environmentally degraded adhesive lap joints. Int. J. Adhes. Adhes. **26**, 325–336 (2006)

R.W. Clough, Second ASCE Conference on Electronic Computation, Pittsburgh, PA (1960)

W. Cui, M.R. Wisnom, A combined stress-based and fracture-mechanics-based model for predicting delamination in composites. Composites **24**, 467–474 (1993)

L.F.M. da Silva, G.W. Critchlow, M.A.V. Figueiredo, Parametric study of adhesively bonded single lap joints by the Taguchi method. J. Adhes. Sci. Technol. **22**(13), 1477–1494 (2008)

L.F.M. da Silva, R.J.C. Carbas, G.W. Critchlow, M.A.V. Figueiredo, K. Brown, Effect of material, geometry, surface treatment and environment on the shear strength of single lap joints. Int. J. Adhes. Adhes. 29, 621–632 (2009a)

L.F.M. da Silva, P.J.C. das Neves, R.D. Adams, J.K. Spelt, Analytical models of adhesively bonded joints—Part I: literature survey. Int. J. Adhes. Adhes. 29, 319–330 (2009b)

L.F.M. da Silva, P.J.C. das Neves, R.D. Adams, A. Wang, J.K. Spelt, Analytical models of adhesively bonded joints—part II: comparative study. Int. J. Adhes. Adhes. 29, 331–341 (2009c)

L.F.M. da Silva, R.F.T. Lima, R.M.S. Teixeira, Development of a software for the design of adhesive joints. J. Adhes. 85, 889–918 (2009d)

L.F.M. da Silva, A. Öchsner, R.D. Adams (eds.), Handbook of Adhesion Technology (Springer, Heidelberg, 2011)

L. Daudeville, P. Ladeveze, A damage mechanics tool for laminate delamination. Compos. Struct. 25, 547–555 (1993)

C. Daux, N. Moës, J. Dolbow, N. Sukumark, T. Belytschko, Arbitrary branched and intersecting cracks with the extended finite element method. Int. J. Numer. Meth. Eng. 48, 1741–1760 (2000)

M.F.S.F. de Moura, R.D.S.G. Campilho, J.P.M. Gonçalves, Crack equivalent concept applied to the fracture characterization of bonded joints under pure mode I loading. Compos. Sci. Technol. 68, 2224–2230 (2008)

M.F.S.F. de Moura, R.D.S.G. Campilho, J.P.M. Gonçalves, Pure mode II fracture characterization of composite bonded joints. Int. J. Solids Struct. 46, 1589–1595 (2009)

D.A. Dillard, H.K. Singh, D.J. Pohlit, Observations of decreased fracture toughness for mixed mode fracture testing of adhesively bonded joints. J. Adhes. Sci. Technol. 23, 515–1530 (2009)

J. Dolbow, N. Moës, T. Belytschko, An extended finite element method for modeling crack growth with frictional contact. Finite Elem. Anal. Des. 36, 235–260 (2000)

K. Duan, X.Z. Hu, F.H. Wittmann, Explanation of size effect in concrete fracture using non-uniform energy distribution. Mater. Struct. 35, 326–331 (2002)

K. Duan, X.Z. Hu, F.H. Wittmann, Boundary effect on concrete fracture and non-constant fracture energy distribution. Eng. Fract. Mech. 70, 2257–2268 (2003)

K. Duan, X. Hu, Y.W. Mai, Substrate constraint and adhesive thickness effects on fracture toughness of adhesive joints. J. Adhes. Sci. Technol. 18, 39–53 (2004)

P.A. DuBois, Crashworthiness Engineering Course Notes (Livermore Software Technology Corporation, Livermore, 2004)

F. Ducept, P. Davies, D. Gamby, Mixed mode failure criteria for a glass/epoxy composite and an adhesively bonded composite/composite joint. Int. J. Adhes. Adhes. 20, 233–244 (2000)

D.S. Dugdale, Yielding of steel sheets containing slits. J. Mech. Phys. Solids 8, 100–104 (1960)

T. Elguedj, A. Gravouil, A. Combescure, Appropriate extended functions for X-FEM simulation of plastic fracture mechanics. Comput. Methods Appl. Mech. Eng. 195, 501–515 (2006)

Engineering Sciences Data Unit, Inelastic shear stresses and strains in adhesive bonding lap joints loaded in tension or shear (Computer Program). Engineering Sciences Data Item Number 79016 (1979)

M. Fagerström, R. Larsson, Theory and numerics for finite deformation fracture modelling using strong discontinuities. Int. J. Numer. Methods Eng. 66, 911–948 (2006)

P. Feraren, H.M. Jensen, Cohesive zone modelling of interface fracture near flaws in adhesive joints. Eng. Fract. Mech. 71, 2125–2142 (2004)

G. Fernlund, J.K. Spelt, Failure load prediction. Int. J. Adhes. Adhes. 11, 213–227 (1991)

G. Fernlund, M. Papini, D. McCammond, J.K. Spelt, Fracture load predictions for adhesive joints. Compos. Sci. Technol. 51, 587–600 (1994)

D.B. Flinn, C.S. Lo, W.F. Zok, A.G. Evans, Fracture resistance characteristics of a metal-toughened ceramic. J. Am. Ceram. Soc. 76, 369–375 (1993)

G.E. Forsythe, W.R. Wasow, Finite-Difference Methods for Partial Differential Equations (Wiley, New York, 1960)

D.M. Gleich, M.J.L. Van Tooren, A. Beukers, Analysis and evaluation of bondline thickness effects on failure load in adhesively bonded structures. J. Adhes. Sci. Technol. **15**, 1091–1101 (2001)

M. Goland, E. Reissner, The stresses in cemented joints. J. Appl. Mech. **66**, A17–A27 (1944)

J.P.M. Gonçalves, M.F.S.F. de Moura, P.T. de Castro, A.T. Marques, Interface element including point-to-surface constraints for three-dimensional problems with damage propagation. Eng. Comput. **17**, 28–47 (2000)

J.P.M. Gonçalves, M.F.S.F. de Moura, P.M.S.T. de Castro, A three-dimensional finite element model for stress analysis of adhesive joints. Int. J. Adhes. Adhes. **22**, 357–365 (2002)

L. Greenwood, *The Strength of a Lap Joint*, in *Aspects of Adhesion-5*, ed. by D. Alner (University of London Press, London, 1969)

H.L. Groth, Stress singularities and fracture at interface corners in bonded joints. Int. J. Adhes. Adhes. **8**, 107–113 (1988)

A.L. Gurson, Continuum theory of ductile rupture by void nucleation and growth. Part I: yield criteria and flow rules for porous ductile media. J. Eng. Mater. Technol. **99**, 2–15 (1977)

L. Hamitouche, M. Tarfaoui, A. Vautrin, An interface debonding law subject to viscous regularization for avoiding instability: application to the delamination problems. Eng. Fract. Mech. **75**, 3084–3100 (2008)

L.J. Hart-Smith, Adhesive-bonded single-lap joints. NASA Contract Report, NASA CR-112236 (1973)

S. Hashemi, A.J. Kinloch, J.G. Williams, Corrections needed in double cantilever beam tests for assessing the interlaminar failure of fibre composites. J. Mater. Sci. Lett. **8**, 125–129 (1989)

J.L. Högberg, U. Stigh, Specimen proposals for mixed mode testing of adhesive layer. Eng. Fract. Mech. **73**, 2541–2556 (2006)

J.L. Högberg, B.F. Sørensen, U. Stigh, Constitutive behaviour of mixed mode loaded adhesive layer. Int. J. Solids Struct. **44**, 8335–8354 (2007)

M. Hojo, T. Ando, M. Tanaka, T. Adachi, S. Ochiai, Y. Endo, Modes I and II interlaminar fracture toughness and fatigue delamination of CF/epoxy laminates with self-same epoxy interleaf. Int. J. Fatigue **28**, 1154–1165 (2006)

Y. Hua, A.D. Crocombe, M.A. Wahab, I.A. Ashcroft, Continuum damage modelling of environmental degradation in joints bonded with EA9321 epoxy adhesive. Int. J. Adhes. Adhes. **28**, 302–313 (2008)

D.L. Hunston, A.J. Kinloch, S.J. Shaw, S.S. Wang, Characterization of fracture behavior of adhesive joints, in *Characteristics Formation Testing, Adhesive Joints*, ed. by K. Mittal (Plenum Press, New York, 1984)

D.L. Hunston, A.J. Kinloch, S.S. Wang, Micromechanics of fracture in structural adhesive bonds. J. Adhes. **28**, 103–114 (1989)

J.W. Hutchinson, Singular behavior at the end of a tensile crack in a hardening material. J. Mech. Phys. Solids **16**, 13–31 (1968)

T. Ikeda, A. Yamashita, N. Miyazaki, Elastic-plastic analysis of crack in adhesive joint by combination of boundary element and finite element methods. Comput. Mech. **21**, 533–539 (1998)

T. Ikeda, A. Yamashita, D. Lee, N. Miyazaki, Failure of a ductile adhesive layer constrained by hard adherends. J. Eng. Mater. Technol. **122**, 80–85 (2000)

K. Ikegami, T. Takeshita, K. Matsuo, T. Sugibayashi, Strength of adhesively bonded scarf joints between glass fibre-reinforced plastics and metal. Int. J. Adhes. Adhes. **10**, 199–206 (1990)

M. Imanaka, T. Hamano, A. Morimoto, R. Ashino, M. Kimoto, Fatigue damage evaluation of adhesively bonded butt joints with a rubber-modified epoxy adhesive. J. Adhes. Sci. Technol. **17**, 981–994 (2003)

G. Ji, Z. Ouyang, G. Li, S. Ibekwe, S.S. Pang, Effects of adhesive thickness on global and local Mode-I interfacial fracture of bonded joints. Int. J. Solids Struct. **47**, 2445–2458 (2010)

J. Jing, F. Gao, J. Johnson, F.Z. Liang, R.L. Williams, J. Qu, Simulation of dynamic fracture along solder-pad interfaces using a cohesive zone model. Eng. Failure Anal. **16**, 1579–1586 (2009)

S.J. John, A.J. Kinloch, F.L. Matthews, Measuring and predicting the durability of bonded fibre/epoxy composite joints. Composites **22**, 121–127 (1991)

A. Karac, B.R.K. Blackman, V. Cooper, A.J. Kinloch, S.R. Sanchez, W.S. Teo, A. Ivankovic, Modelling the fracture behavior of adhesively-bonded joints as a function of test rate. Eng. Fract. Mech. **78**, 973–989 (2011)

M.S. Kafkalidis, M.D. Thouless, The effects of geometry and material properties on the fracture of single lap-shear joints. Int. J. Solids Struct. **39**, 4367–4383 (2002)

P.I. Kattan, G.Z. Voyiadjis, *Damage Mechanics with Finite Elements* (Springer, Heidelberg, 2005)

A.R. Khoei, M. Nikbakht, Contact friction modeling with the extended finite element method (X-FEM). J. Mater. Process. Technol. **177**, 58–62 (2006)

H. Khoramishad, A.D. Crocombe, K.B. Katnam, I.A. Ashcroft, Predicting fatigue damage in adhesively bonded joints using a cohesive zone model. Int. J. Fatigue **32**, 1146–1158 (2010)

H. Kim, K.T. Kedward, Stress analysis of adhesively-bonded joints under in-plane shear loading. J. Adhesion **76**, 1–36 (2001)

A.J. Kinloch, *Adhesion and Adhesives: Science and Technology* (Chapman & Hall, London, 1987)

A.J. Kinloch, S.J. Shaw, The fracture resistance of a toughened epoxy adhesive. J. Adhesion **12**, 59–77 (1981)

A.J. Kinloch, J.G. Williams, Crack blunting mechanisms in polymers. J. Mater. Sci. **15**, 987–996 (1980)

A.J. Kinloch, R.J. Young, *Fracture Behaviour of Polymers* (Applied Science Publishers, London, 1983)

L. Lammerant, I. Verpoest, Modelling of the interaction between matrix cracks and delaminations during impact of composite plates. Compos. Sci. Technol. **56**, 1171–1178 (1996)

S.S. Lee, Boundary element analysis of the stress singularity at the interface corner of viscoelastic adhesive layers. Int. J. Solids Struct. **35**, 1385–1394 (1998)

S.J. Lee, D.G. Lee, Development of a failure model for the adhesively bonded tubular single lap joint. J. Adhes. **40**, 1–14 (1992)

D.B. Lee, T. Ikeda, N. Miyazaki, N.S. Choi, Fracture behavior around a crack tip in rubber-modified epoxy adhesive joint with various bond thicknesses. J. Mater. Sci. Lett. **22**, 229–233 (2003)

D.B. Lee, T. Ikeda, N. Miyazaki, N.S. Choi, Effect of bond thickness on the fracture toughness of adhesive joints. J. Eng. Mater. Technol. **126**, 14–18 (2004)

M.J. Lee, T.M. Cho, W.S. Kim, B.C. Lee, J.J. Lee, Determination of cohesive parameters for a mixed-mode cohesive zone model. Int. J. Adhes. Adhes. **30**, 322–328 (2010)

K. Leffler, K.S. Alfredsson, U. Stigh, Shear behaviour of adhesive layers. Int. J. Solids Struct. **44**, 530–545 (2007)

J. Lemaitre, Local approach of fracture. Eng. Fract. Mech. **25**, 523–537 (1986)

J. Lemaitre, J.M. Chaboche, *Mechanics of Solid Materials* (Cambridge University Press, Cambridge, 1985)

J. Lemaitre, R. Desmorat, *Engineering Damage Mechanics* (Springer, Heidelberg, 2005)

S. Li, M.D. Thouless, A.M. Waas, J.A. Schroeder, P.D. Zavattieri, Use of Mode-I cohesive-zone models to describe the fracture of an adhesively-bonded polymer–matrix composite. Compos. Sci. Technol. **65**, 281–293 (2005a)

S. Li, M.D. Thouless, A.M. Waas, J.A. Schroeder, P.D. Zavattieri, Use of a cohesive-zone model to analyze the fracture of a fiber reinforced polymer–matrix composite. Compos. Sci. Technol. **65**, 537–549 (2005b)

C.D.M. Liljedahl, A.D. Crocombe, M.A. Wahab, I.A. Ashcroft, Damage modelling of adhesively bonded joints. Int. J. Fract. **141**, 147–161 (2006)

X. Liu, G. Wang, Progressive failure analysis of bonded composite repairs. Compos. Struct. **81**, 331–340 (2007)

H. Liu, X.L. Zhao, R. Al-Mahaidi, Boundary element analysis of CFRP reinforced steel plates. Compos. Struct. **91**, 74–83 (2009)

A.G. Magalhães, M.F.S.F. de Moura, J.P.M. Gonçalves, Evaluation of stress concentration effects in single-lap bonded joints of laminate composite materials. Int. J. Adhes. Adhes. **25**, 313–319 (2005)

S. Maiti, P.H. Geubelle, A cohesive model for fatigue failure of polymers. Eng. Fract. Mech. **72**, 691–708 (2005)

A.V. Mello, K.M. Liechti, The effect of self-assembled monolayers on interfacial fracture. J. Appl. Mech. **73**, 860–870 (2006)

Y. Mi, M.A. Crisfield, G.A.O. Davies, H.B. Hellweg, Progressive delamination using interface elements. J. Compos. Mater. **32**, 1246–1272 (1998)

A.R. Mitchell, D.F. Griffiths, *The Finite Difference Method in Partial Differential Equations* (Wiley, New York, 1980)

N. Moës, T. Belytschko, Extended finite element method for cohesive crack growth. Eng. Fract. Mech. **69**, 813–833 (2002)

N. Moës, J. Dolbow, T. Belytschko, A finite element method for crack growth without remeshing. Int. J. Numer. Meth. Eng. **46**, 131–150 (1999)

S. Mohammadi, *Extended Finite Element Method for Fracture Analysis of Structures* (Blackwell Publishing, New Jersey, 2008)

F. Moroni, A. Pirondi, A procedure for the simulation of fatigue crack growth in adhesively bonded joints based on the cohesive zone model and different mixed-mode propagation criteria. Eng. Fract. Mech. **78**, 1808–1816 (2011)

F. Mortensen, O.T. Thomsen, Analysis of adhesive bonded joints: a unified approach. Compos. Sci. Technol. **62**, 1011–1031 (2002)

J.J. Munoz, U. Galvanetto, P. Robinson, On the numerical simulation of fatigue driven delamination with interface elements. Int. J. Fatigue **28**, 1136–1146 (2006)

J.A. Nairn, Energy release rate analysis for adhesive and laminate double cantilever beam specimens emphasizing the effect of residual stresses. Int. J. Adhes. Adhes. **20**, 59–70 (2000)

E.P. O'Brien, T.C. Ward, S. Guo, D.A. Dillard, Strain energy release rates of a pressure sensitive adhesive measured by the shaft-loaded blister test. J. Adhes. **79**, 69–97 (2003)

A. Öchsner, *Special Numerical Techniques*, in *Handbook of Adhesion Technology*, ed. by L.M.F. da Silva, A. Öchsner, R.D. Adams (Springer, Heidelberg, 2011)

K.C. Pandya, J.G. Williams, Measurement of cohesive zone parameters in tough polyethylene. Polymer Eng. Sci. **40**, 1765–1776 (2000)

S.K. Panigrahi, B. Pradhan, Three dimensional failure analysis and damage propagation behavior of adhesively bonded single lap joints in laminated FRP composites. J. Reinf. Plast. Compos. **26**, 183–201 (2007)

T. Pardoen, T. Ferracin, C.M. Landis, F. Delannay, Constraint effects in adhesive joint fracture. J. Mech. Phys. Solids **53**, 1951–1983 (2005)

A.B. Pereira, A.B. de Morais, Strength of adhesively bonded stainless steel joints. Int. J. Adhes. Adhes. **23**, 315–322 (2003)

Z. Petrossian, M.R. Wisnom, Prediction of delamination initiation and growth from discontinuous plies using interface elements. Compos. Part A **29**, 503–515 (1998)

A.M.G. Pinto, A.G. Magalhães, R.D.S.G. Campilho, M.F.S.F. de Moura, A.P.M. Baptista, Single-lap joints of similar and dissimilar adherends bonded with an acrylic adhesive. J. Adhes. **85**, 351–376 (2009)

V.P. Premchand, K.S. Sajikumar, Fracture analysis in adhesive bonded joints with centre crack. NCTT09 10th national conference on technological trends, Trivandrum, India (2009)

M. Quaresimin, M. Ricotta, Life prediction of bonded joints in composite materials. Int. J. Fatigue **28**, 1166–1176 (2006)

R.S. Raghava, R. Cadell, G.S.Y. Yeh, The macroscopic yield behavior of polymers. J. Mater. Sci. **8**, 225–232 (1973)

P.G.S. Raghavan, A continuum damage mechanics model for unidirectional composites undergoing interfacial de-bonding. Mech. Mater. **37**, 955–977 (2005)

J.R. Rice, G.F. Rosengren, Plane strain deformation near a crack tip in a powerlaw hardening material. J. Mech. Phys. Solids **16**, 1–12 (1968)

M. Ridha, V.B.C. Tan, T.E. Tay, Traction-separation laws for progressive failure of a bonded scarf repair of composite panel. Compos. Struct. **93**, 1239–1245 (2010)

P. Robinson, U. Galvanetto, D. Tumino, G. Bellucci, D. Violeau, Numerical simulation of fatigue-driven delamination using interface elements. Int. J. Numer. Methods Eng. **63**, 1824–1848 (2005)

K.L. Roe, T. Siegmund, An irreversible cohesive zone model for interface fatigue crack growth simulation. Eng. Fract. Mech. **70**, 209–232 (2003)

M. Sabsabi, E. Giner, F.J. Fuenmayor, Experimental fatigue testing of a fretting complete contact and numerical life correlation using X-FEM. Int. J. Fatigue **33**, 811–822 (2011)

N.K. Salgado, M.H. Aliabad, The boundary element analysis of cracked stiffened sheets, reinforced by adhesively bonded patches. Int. J. Numer. Meth. Eng. **42**, 195–217 (1998)

E.M. Sampaio, F.L. Bastian, H.S.C. Mattos, A simple continuum damage model for adhesively bonded butt joints. Mech. Res. Commun. **31**, 443–449 (2004)

C. Schuecker, B.D. Davidson, Effect of friction on the perceived mode II delamination toughness from three and four point bend end notched flexure tests. ASTM STP **1383**, 334–344 (2000)

K. Shahin, F. Taheri, The strain energy release rates in adhesively bonded balanced and unbalanced specimens and lap joints. Int. J. Solids Struct. **45**, 6284–6300 (2008)

V. Shenoy, I.A. Ashcroft, G.W. Critchlow, A.D. Crocombe, M.M. Abdel Wahab, An investigation into crack initiation and propagation behaviour of bonded single-lap joints using backface strain. Int. J. Adhes. Adhes. **29**, 361–371 (2009)

V. Shenoy, I.A. Ashcroft, G.W. Critchlow, A.D. Crocombe, Unified methodology for the prediction of the fatigue behavior of adhesively bonded joints. Int. J. Fatigue **32**, 1278–1288 (2010a)

V. Shenoy, I.A. Ashcroft, G.W. Critchlow, A.D. Crocombe, Fracture mechanics and damage mechanics based fatigue lifetime prediction of adhesively bonded joints subjected to variable amplitude fatigue. Eng. Fract. Mech. **77**, 1073–1090 (2010b)

A.G. Solana, A.D. Crocombe, I.A. Ashcroft, Fatigue life and backface strain predictions in adhesively bonded joints. Int. J. Adhes. Adhes. **30**, 36–42 (2010)

S.H. Song, G.H. Paulino, W.G. Buttlar, A bilinear cohesive zone model tailored for fracture of asphalt concrete considering viscoelastic bulk material. Eng. Fract. Mech. **73**, 2829–2848 (2006)

B.F. Sørensen, Cohesive law and notch sensitivity of adhesive joints. Acta Mater. **50**, 1053–1061 (2002)

B.F. Sørensen, T.K. Jacobsen, Determination of cohesive laws by the J integral approach. Eng. Fract. Mech. **70**, 1841–1858 (2003)

S. Srinivas (1975) Analysis of bonded joints. NASA Technical Note, NASA TN D-7855

N. Sukumar, J.H. Prevost, Modeling quasi-static crack growth with the extended finite element method part i: computer implementation. Int. J. Solids Struct. **40**, 7513–7537 (2003)

N. Sukumar, N. Moës, B. Moran, T. Belytschko, Extended finite element method for three-dimensional crack modeling. Int. J. Numer. Meth. Eng. **48**, 1549–1570 (2000)

V. Tamuzs, S. Tarasovs, U. Vilks, Delamination properties of translaminar-reinforced composites. Compos. Sci. Technol. **63**, 1423–1431 (2003)

D. Tumino, F. Cappello, Simulation of fatigue delamination growth in composites with different mode mixtures. J. Compos. Mater. **41**, 2415–2441 (2007)

M.J. Turner, R.W. Clough, H.C. Martin, J.L. Topp, Stiffness and deflection analysis of complex structures. J. Aerosp. Sci. **23**, 805–823 (1956)

A. Turon, J. Costa, P.P. Camanho, C.G. Dàvila, Simulation of delamination in composites under high-cycle fatigue. Compos. Part A **38**, 2270–2282 (2007a)

A. Turon, C.G. Dávila, P.P. Camanho, J. Costa, An engineering solution for mesh size effects in the simulation of delamination using cohesive zone models. Eng. Fract. Mech. **74**, 1665–1682 (2007b)

V. Tvergaard, J.W. Hutchinson, The relation between crack growth resistance and fracture process parameters in elastic-plastic solids. J. Mech. Phys. Solids **40**, 1377–1397 (1992)

V. Tvergaard, J.W. Hutchinson, The influence of plasticity on the mixed-mode interface toughness. J. Mech. Phys. Solids **41**, 1119–1135 (1993)

V.I. Tvergaard, A. Needleman, Analysis of cup one fracture in round tensile bar. Acta Metall. **32**, 157–169 (1984)

M. Vable, Stress analysis of bonded joints by boundary element method, in *Modeling of Adhesively Bonded Joints*, ed. by L.F.M. da Silva, A. Öchsner (Springer, Heidelberg, 2008)

M. Vable, J.R. Maddi, Boundary element analysis of adhesively bonded joints. Int. J. Adhes. Adhes. **26**, 133–144 (2006)

O. Volkersen, Die nietkraftoerteilung in zubeanspruchten nietverbindungen mit konstanten loschonquerschnitten. Luftfahrtforschung **15**, 41–47 (1938)

G.Z. Voyiadjis, P.I. Kattan, *Damage Mechanics* (Marcell Dekker, New York, 2005)

M.M.A. Wahab, I.A. Ashcroft, A.D. Crocombe, S.J. Shaw, Prediction of fatigue thresholds in adhesively bonded joints using damage mechanics and fracture mechanics. J. Adhes. Sci. Technol. **15**, 763–781 (2001)

M.M.A. Wahab, I.A. Ashcroft, A.D. Crocombe, P.A. Smith, Numerical prediction of fatigue crack propagation lifetime in adhesively bonded structures. Int. J. Fatigue **24**, 705–709 (2002)

R.X. Wang, J. Cui, A.N. Sinclair, J.K. Spelt, Strength of adhesive joints with adherend yielding: I. Analytical model. J. Adhes. **79**, 23–48 (2003)

Y. Wei, J.W. Hutchinson, Nonlinear delamination mechanics for thin films. J. Mech. Phys. Solids **45**, 1137–1159 (1997)

Y. Wei, J.W. Hutchinson, Interface strength, work of adhesion and plasticity in the peel test. Int. J. Fract. **93**, 315–333 (1999)

P.H. Wen, M.H. Aliabadi, A. Young, Boundary element analysis of flat cracked panels with adhesively bonded patches. Eng. Fract. Mech. **69**, 2129–2146 (2002)

P.H. Wen, M.H. Aliabadi, A. Young, Boundary element analysis of curved cracked panels with adhesively bonded patches. Int. J. Numer. Methods Eng. **58**, 43–61 (2003)

M.L. Williams, The stresses around a fault or crack in dissimilar media. Bull. Seism. Soc. Am. **49**, 199–204 (1959)

D. Xie, A.M. Waas, Discrete cohesive zone model for mixed-mode fracture using finite element analysis. Eng. Fract. Mech. **73**, 1783–1796 (2006)

D. Xie, A.G. Salvi, C. Sun, A.M. Waas, A. Caliskan, Discrete cohesive zone model to simulate static fracture in 2D triaxially braided carbon fiber composites. J. Compos. Mater. **40**, 2025–2046 (2006)

W. Xu, G. Li, Finite difference three-dimensional solution of stresses in adhesively bonded composite tubular joint subjected to torsion. Int. J. Adhes. Adhes. **30**, 191–199 (2010)

Y. Xu, H. Yuan, Computational analysis of mixed-mode fatigue crack growth in quasi-brittle materials using extended finite element methods. Eng. Fract. Mech. **76**, 165–181 (2009)

J.Q. Xu, Y.H. Liu, X.G. Wang, Numerical methods for the determination of multiple stress singularities and related stress intensity coefficients. Eng. Fract. Mech. **63**, 775–790 (1999)

C. Yan, Y.W. Mai, L. Ye, Effect of bond thickness on fracture behaviour in adhesive joints. J. Adhes. **75**, 27–44 (2001a)

C. Yan, Y.W. Mai, Q. Yuan, L. Ye, J. Sun, Effects of substrate materials on fracture toughness measurement in adhesive joints. Int. J. Mech. Sci. **43**, 2091–2102 (2001b)

Q.D. Yang, M.D. Thouless, Mixed-mode fracture analyses of plastically deforming adhesive joints. Int. J. Fract. **110**, 175–187 (2001)

Q.D. Yang, M.D. Thouless, S.M. Ward, Numerical simulations of adhesively-bonded beams failing with extensive plastic deformation. J. Mech. Phys. Solids **47**, 1337–1353 (1999)

Q.D. Yang, M.D. Thouless, S.M. Ward, Analysis of the symmetrical 90° peel test with extensive plastic deformation. J. Adhes. **72**, 115–132 (2000)

Q.D. Yang, M.D. Thouless, S.M. Ward, Elastic-plastic mode-II fracture of adhesive joints. Int. J. Solids Struct. **38**, 3251–3262 (2001)

H. Yoshihara, Simple estimation of critical stress intensity factors of wood by tests with double cantilever beam and three-point end-notched flexure. Holzforschung **61**, 182–189 (2007)

A. Young, D.J. Cartwright, D.P. Rooke, Boundary element method for analysing repair patches on cracked finite sheets. Aeronaut. J. **92**, 416–421 (1988)

A. Young, D.P. Rooke, D.J. Cartwright, Analysis of patched and stiffened cracked panels using the boundary element method. Int. J. Solids Struct. **29**, 2201–2216 (1992)

X. Zhao, R.D. Adams, L.F.M. da Silva, Single lap joints with rounded adherend corners: Stress and strain analysis. J. Adhes. Sci. Technol. **25**, 819–836 (2011a)

X. Zhao, R.D. Adams, L.F.M. da Silva, Single lap joints with rounded adherend corners: experimental results and strength prediction. J. Adhes. Sci. Technol. **25**, 837–856 (2011b)

Y. Zhu, K.M. Liechti, K. Ravi-Chandar, Direct extraction of rate-dependent traction-separation laws for polyurea/steel interfaces. Int. J. Solids Struct. **46**, 31–51 (2009)

O.C. Zienkiewicz, Y.K. Cheung, *The Finite Element Method in Structural and Continuum Mechanics* (McGraw-Hill, London, 1967)

O.C. Zienkiewicz, R. Taylor, *The Finite Element Method: Vol 2, Solid Mechanics*, 5th edn. (Butterworth-Heinemann, Oxford, 2001)

G.P. Zou, K. Shalin, F. Taheri, An analytical solution for the analysis of symmetric composite adhesively bonded joints. Compos. Struct. **65**, 499–510 (2004)